

A doctoral thesis

Development of temperature-responsive
polysaccharide microparticles for pulmonary drug
delivery

Takumi SATO

Tokyo University of Agriculture and Technology

<u>Chapter 1</u>	
<u>Introduction of pulmonary drug delivery and drug carriers</u>	1
1. General methods for drug administration	1
1.1. Oral administration	1
1.2. Intravenous administration	2
1.3. Transdermal administration	2
1.4. Pulmonary administration	2
2. Drug carriers	3
2.1. Microparticles	3
2.2. Nanocarriers	4
2.3. Materials for drug carriers	5
<i>2.3.1. Hydrophilic polymers</i>	5
<i>2.3.2. Synthetic polymers</i>	8
<i>2.3.3. Inorganic materials</i>	9
3. Drug carriers for pulmonary administration	10
3.1. Requirements for drug carriers for pulmonary administration	10
3.2. Preparation techniques of drug carriers for pulmonary administration	11
<i>3.2.1. Emulsion-solvent evaporation technique</i>	11
<i>3.2.2. Spray-drying technique</i>	13
<i>3.2.3. Spray-freeze-drying technique</i>	15
4. Stimuli-responsive drug carriers	17
4.1. Temperature-responsive drug carriers	18
4.2. Photo-responsive drug carriers	19
4.3. pH-responsive drug carriers	20
5. The aim of this thesis	22
6. References	24
<u>Chapter 2</u>	
<u>Temperature-Responsive Polysaccharide Particles for Pulmonary Drug Delivery: Preparation of Particles and Evaluation of Temperature-responsiveness and Aerosol-dispersion Performance</u>	35

1. Introduction	35
2. Materials and Methods	36
2.1. Materials	36
2.2. Effect of surfactants on the formation and stability of s/o (solid-in-oil) suspension	36
2.3. Preparation of κ -carrageenan (κ -CRG) particles and observation of their surface morphology	38
2.4. Evaluation of the temperature-responsiveness of the κ -CRG particles	38
2.5. <i>In vitro</i> aerosol-dispersion performance of κ -CRG particles	38
3. Results and Discussion	41
3.1. Effect of surfactants on the formation and stability of s/o suspension	41
3.2. Preparation of κ -CRG particles and observation of their surface morphology	43
3.3. Evaluation of the temperature-responsiveness of the κ -CRG particles	46
3.4. <i>In vitro</i> aerosol-dispersion performance of κ -CRG particles	49
4. Conclusions	52
5. References	54
<u>Chapter 3</u>	
<u>Temperature-Responsive Polysaccharide Particles for Pulmonary Drug Delivery: Control of Dissolution and Release Properties</u>	58
1. Introduction	58
2. Material and Methods	59
2.1. Materials	59
2.2. Evaluation of the effect of the composition of the block copolymers on their melting point using DSC (differential scanning calorimetry)	61
2.3. Preparation of κ -CRG, λ -CRG and mixed κ,λ -CRG particles with or without methylene blue (Mb) and observation of their surface morphology	61
2.4. Evaluation of the temperature-responsiveness of the CRG particles	61
2.5. Evaluation of profiles depicting the release of Mb from the CRG particles	61

3. Results and Discussion	62
3.1. Determination of the effect of the compositions of polymeric surfactants on their melting point using DSC	62
3.2. Surface morphology of κ -CRG particles	64
3.3. Evaluation of the temperature-responsiveness of the κ -CRG particles	65
3.4. Observation of the surface morphology of the κ -CRG particles containing Mb and evaluation of their release behavior	68
3.5. Observation of the surface morphology of the mixed κ, ι -CRG particles containing Mb and evaluation of their release behavior	72
4. Conclusion	75
5 References	76

Chapter 4

Temperature-Responsive Nanoparticle-Decorated Polysaccharide Microparticles for Pulmonary Drug Delivery: The Release of Multiple Cationic/Anionic Compounds **80**

1. Introduction	80
2. Material and Methods	81
2.1. Materials	81
2.2. Preparing CS(Ns) and PLL(Ns) nanoparticles	82
2.3. Preparing CRG(CS(Ns), Mb) and CRG(PLL(Ns), Mb) microparticles	82
2.4. Characterizing nanoparticles and microparticles	84
3. Results and Discussion	84
3.1. Preparing and characterizing the CS(Ns) and PLL(Ns) nanoparticles	84
3.2. Ns-release profiles for CS(Ns) and PLL(Ns) nanoparticles	88
3.3. Evaluation of the profile depicting the release of the Ns from the CS(Ns) and PLL(Ns) nanoparticles	89
3.4. Inclusions of nanoparticles in microparticles	91
3.5. Ns- and Mb-release profiles of CRG(CS(Ns), Mb) and CRG(PLL(Ns), Mb) microparticles	95
4. Conclusion	97

5 References	98
---------------------	-----------

<u>Chapter 5</u>	
<u>General conclusion of this thesis</u>	103

<u>Acknowledgement</u>	106
-------------------------------	------------

Chapter 1

Introduction of pulmonary drug delivery and drug carriers

This doctoral thesis is a study to develop polysaccharide-based temperature-responsive microparticles and to evaluate the feasibility application of these microparticles in pulmonary administration. In chapter 1, general methods for drug administration and drug carriers are introduced and possibility of applying novel drug carriers to pulmonary administration are described.

1. General methods for drug administration

There are a variety of drug-administration methods, including oral, intravenous, transdermal, and pulmonary administrations. The pharmacological effects in the body and the duration of drug effect vary greatly depending on the method of administration. Because each of these administration methods has its own advantages and challenges, it is necessary to select the administration method that is appropriate for the patient's situation. In section 1, general methods for drug administration are introduced.

1.1. Oral administration^[1-5]

The oral administration is advantageous owing to its simple administration form and low cost. A number of oral administration formulations have been developed to achieve therapeutic effects at home. There are various forms of orally administered materials such as liquid tablets, capsules, pills, and chewable tablets. However, drugs are exposed to the environments at a wide range of pH levels and come into significant contact with both digestive enzymes and gastrointestinal-tract contents. Therefore, in oral administration, drugs may exhibit insufficient pharmacological effects because of their denaturation, and furthermore, drugs can require considerable time before their pharmacological effects take hold in the body. Most of the orally administered drug is eliminated from the body due to poor absorption of the drug from the intestinal wall and metabolism in the liver (first pass metabolism). Oral administration may not be effective for urgent diseases because of the long time required for the onset of drug effect after oral administration.

1.2. Intravenous administration ^[6–10]

Intravenous administration is a fast-acting method because drugs are administered directly into blood vessels. Intravenous administration has the great advantage of avoiding the first pass metabolism in the liver and maximizing drug efficacy without denaturing the drug. In contrast, it is very difficult for patients to inject themselves at home, and specialized equipment and techniques are essential. Therefore, the problem with intravenous administration is the heavy burden on the patient. Because the drug effect occurs immediately after the drug is administered into blood vessels, the amount of drug administered to patients should be carefully determined, and attention should be paid to the occurrence of side effects and anaphylactic shock in patients.

1.3. Transdermal administration ^[11–15]

In transdermal administration, drugs are delivered into the body by penetrating through skin. The major advantage of transdermal administration is that it avoids the reduction of drug efficacy due to the first pass metabolism. In addition, a sheet-like material can be used to intensively administer drugs on the target tissue (local administration). In contrast, transdermal administration is limited by the rate at which drugs penetrate skin. The problem with transdermal administration is that adhesives and patch materials (drug absorption enhancer) contained in sheet-like materials can cause irritation to the skin.

1.4. Pulmonary administration ^[16–23]

Pulmonary administration is a method of inhaling drugs and absorbing them into the body via the lungs. The method has many advantages, three of which are highly prominent: (1) a simple administration (inhalation), (2) highly efficient absorption^[24–26] due to both an enormous surface area (100 m²) and a highly permeable membrane (0.1–1 μm in thickness) in alveoli, and (3) no denaturation owing to the absence of digestive enzymes in the alveoli^[26]. However, the problem with pulmonary administration is that it is difficult to deliver drugs to the alveoli due to the size and density of drugs. Currently, inhalation drugs approved in Japan include drugs for chronic obstructive pulmonary disease (COPD) (Symbicort[®], Advair[®]) and influenza (Relenza[®], Inavir[®]), which exhibit drug effects in the bronchi. The pulmonary administration method requires efficient drug delivery to the deep lungs.

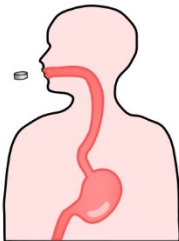
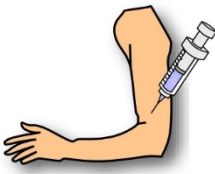
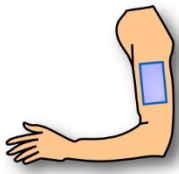
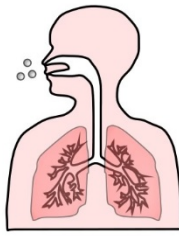
	Administration route			
	Oral	Intravenous	Transdermal	Pulmonary
Characteristics				
Simplicity	Simple	Complicated	Simple	Simple
Invasiveness	None	Existent	Existent	None
Bioavailability	Low	High	Medium	High
Time for absorption	Variable	Immediate	Quick	Immediate
Delivery to absorption sites	Medium	High	Medium	Low

Fig. 1-1 General methods for drug administration and their characteristics.

2. Drug carriers

In drug administration, drug carriers have been developed to deliver drugs only to the target tissues, known as drug delivery system (DDS), because administration of only drugs causes drug denaturation and side effects^[27-30]. In section 2, I describe two types of drug carriers with different sizes and the advantages of each type of drug carrier. In addition, I will discuss the materials that are currently used to form drug carriers.

2.1. Microparticles^[27,31-39]

Drug carriers with a size greater than 1 μm are defined as microparticles^[34]. Microparticles are commonly applied in oral and pulmonary administration. Drugs are encapsulated in microparticles, which has the advantages of (1) to (5). (1) Drug denaturation is inhibited because drugs avoid the direct effects of pH changes and enzymes^[31,34,36]. (2) The odor and bitterness of the drugs are suppressed^[32,38]. (3) Drugs are delivered only to the target tissue^[34]. (4) The release of drugs from microparticles is sustained for a certain time period, reducing the frequency of drug administration^[33,36,37]. (5) Reproducibility of drug efficacy is high because the drug is uniformly dispersed inside the microparticles and the amount of drug delivered is constant^[34].

These microparticles are formed by mixing and stirring of solvents and are inexpensive to form^[31]. Inside the microparticles, various interactions occur such as chemical bonds, entanglement of molecular chains, and electrostatic interactions^[31,39].

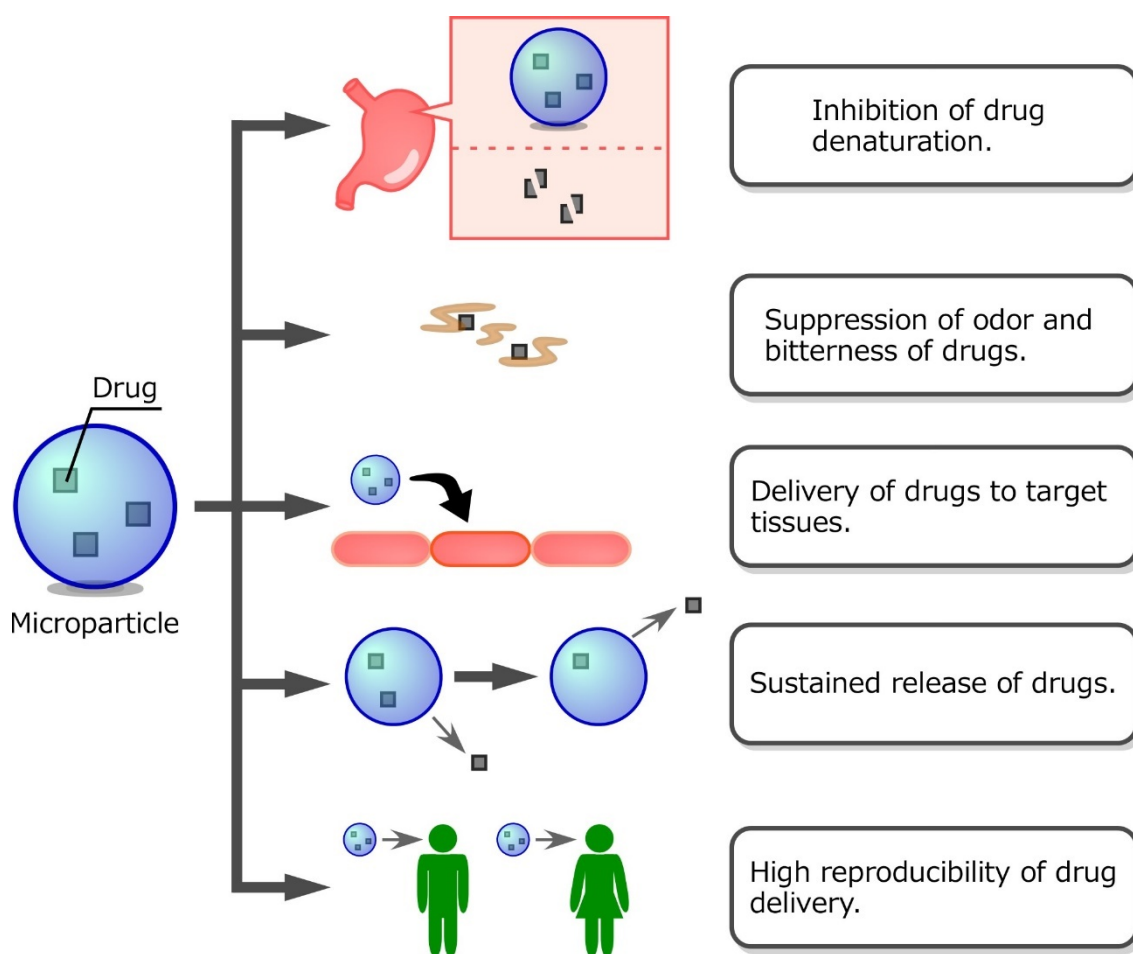


Fig. 1-2 Advantages of microparticles in DDS (drug delivery system).

2.2. Nanocarriers^[27,36,40–52]

Nanocarriers have diameters ranging from several nanometer to several hundred nanometer. Nanocarriers are often utilized for oral and intravenous administration. Nanocarriers can take the form of (1) to (3): (1) nanoparticles^[36,40–43] with an inorganic or polysaccharide core, (2) polymeric micelles^[44–49] with a self-assembled surfactant (block copolymer), and (3) liposomes^[27,50–52], which are spherical vesicles with a lipid bilayer. These nanoparticles accumulate in tumor tissues via enhanced permeation and retention (EPR) effect in blood vessels, and can release drugs only to tumor tissues. Therefore, the nanocarriers have low toxicity to cells other than the tumor tissue and are expected to reduce side effects.

Nanoparticles with inorganic and polysaccharide cores have particle diameters ranging from tens to hundreds of nanometers^[36,40–43]. These nanoparticles are formed by chemical bonding, electrostatic interaction, and physical interaction between molecules. Nanoparticles do not form spontaneously; they are formed but by applying external forces such as heating, homogenization, or sonication. Nanoparticles can encapsulate hydrophilic or hydrophobic drugs, and the nanoparticles themselves often have unique properties such as antimicrobial properties, electrical charge, and magnetism. The unique properties of nanoparticles are based on the properties of the excipients (inorganics and polysaccharides) that form the nanoparticles.

Polymeric micelles are formed by self-assembly of polymeric surfactants and are several to several tens of nanometers in diameter^[44-49]. Because the core of polymeric micelles is hydrophobic, polymeric micelles preferentially encapsulate hydrophobic drugs such as anticancer agents and anti-inflammatory agents via hydrophobic interactions. Therefore, polymeric micelles can efficiently deliver hydrophobic drugs to tumor tissues. The release rate of encapsulated drugs can be controlled by the composition of polymeric surfactants^[49].

Liposomes^[27,50-52] are spherical vesicles with a phospholipid bilayer and have a diameter of approximately 100-200 nm. Because the central core of liposomes is hydrophilic, they can encapsulate hydrophilic substances such as proteins and biologically active agents. Furthermore, liposomes can encapsulate both hydrophilic and hydrophobic substances because hydrophobic substances are encapsulated in a lipid bilayer. However, unlike polymeric micelles, it is difficult to form liposomes by self-assembly, and liposomes are formed by sonication.

These nanocarriers will be material forms that can achieve DDS to preferentially deliver drugs to target tissues in blood vessels.

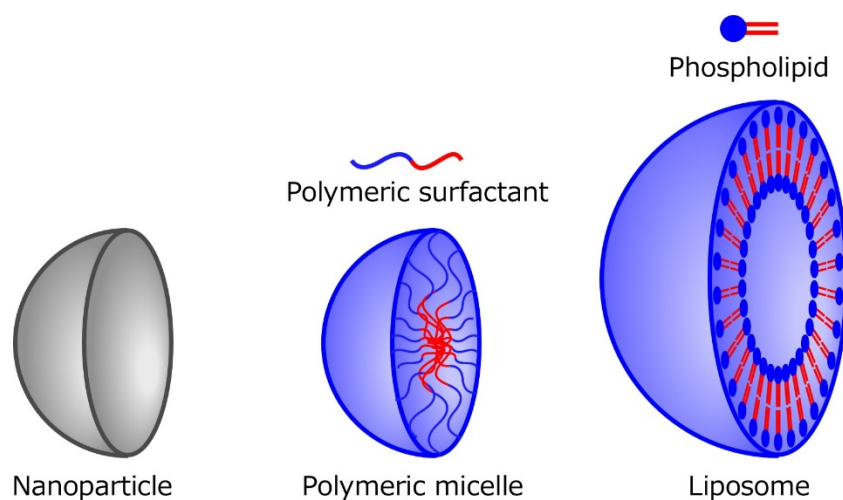


Fig. 1-3 Structure of nanocarriers.

2.3. Materials for drug carriers

2.3.1 Hydrophilic polymers

Hydrophilic polymers for drug carriers include polysaccharides (e.g., carrageenan (CRG), chitosan (CS), hyaluronic acid (HA), alginate) or polypeptides (e.g., poly-L-lysine, polyarginine).

CRG, a linear sulfated polysaccharide that is extracted from red algae seaweed, is an anionic natural polymer in which 3,6-anhydro-D-galactose alternately repeats α -1,3 and β -1,4 glycosidic linkages^[53-58]. As shown in Fig. 1-4, depending on the number of sulfone groups and the presence or absence of an anhydro bond, CRG falls into one of three classes: κ , ι , and λ . Co-existing metal salts and proteins greatly affect the physical properties of CRG. Furthermore, novel physical properties of CRG become manifest when the polymer is mixed with other polysaccharides. These properties have made CRG a widely popular component of gelling, thickening, and stabilizing agents in the food and medical industries^[59,60]. In addition, aqueous solutions of polysaccharides form a gel at

appropriate temperatures (sol-gel transition), where a coil-helix transition occurs and a subsequent aggregation of helices forms physically crosslinked domains^[59,60].

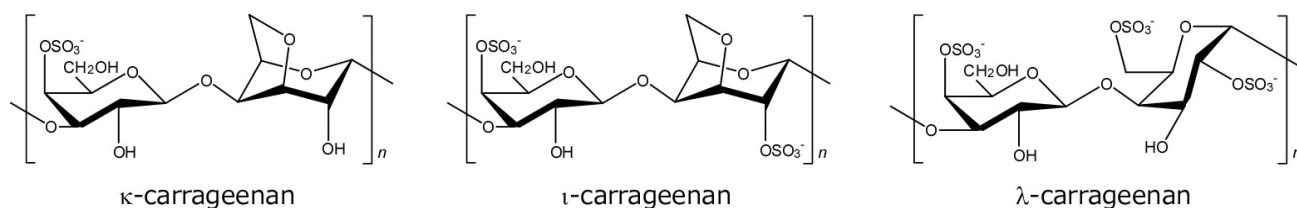


Fig. 1-4 Chemical structure of carrageenan (CRG).

To date, several CRG-based drug carriers have been reported^[53,58,61-63]. Among them, as shown in Fig. 1-5, Obaidat *et al.* prepared CRG microparticles with diameters of approximately 15-40 μm ^[53]. After the preparation of CRG microparticles, ibuprofen, which is an anti-inflammatory analgesic, was encapsulated in the microparticles in supercritical carbon dioxide. The CRG particles rapidly released ibuprofen and were expected to be applied for oral administration.

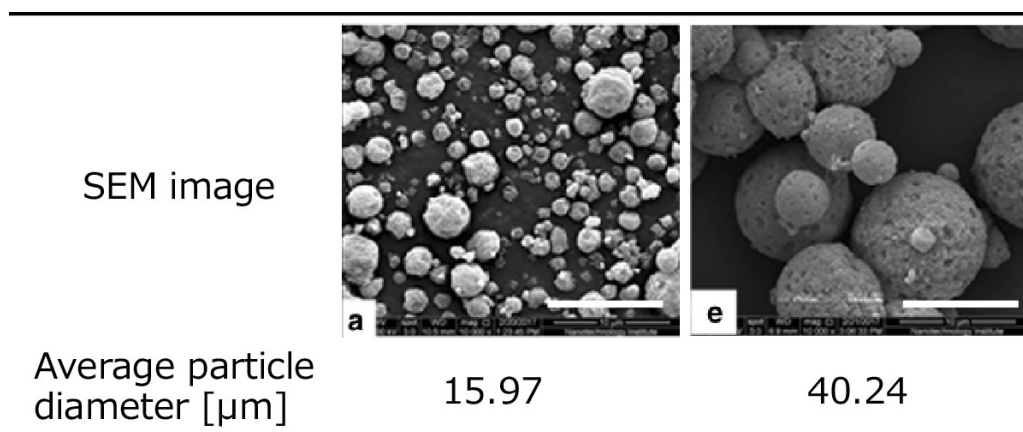


Fig.1-5 Scanning electron microscope (SEM) images (bar: 10 μm) and average diameter of CRG particles^[53].

CS is a linear polymer prepared by deacetylating natural chitin, which is obtained from crustaceans, such as shrimp and crab^[36,64-66]. CS has been reported to have antibacterial properties due to its intramolecular amino groups^[36,64]. CS interacts with mucins on the surface of body tissues, so drug carriers based on CS exhibit adhesion to body tissues (e.g., oral and intestinal walls)^[67]. CS has also been reported to improve the membrane permeability of the intestinal wall^[65,68]. Due to these advantages, CS-based drug carriers have high performance in drug delivery.

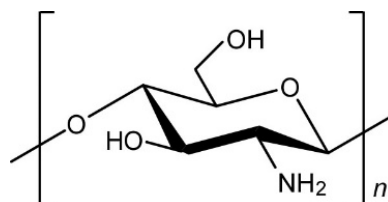


Fig. 1-6 Chemical structure of chitosan (CS).

CS has been applied to micro and nanoparticles^[65,66,69-71]. Among them, Antoniou *et al.* prepared nanoparticles with diameters of 100-200 nm by electrostatic interaction between CS and tripolyphosphate (TPP)^[69].

A diameter of nanoparticles formed by CS and TPP was controlled by CS concentration, pH change, and salt concentration. The diameter of the nanoparticles is directly related to the efficiency of accumulation in tumor tissues by EPR effect and membrane permeability, and localized accumulation of the nanoparticles can be expected by controlling the diameter of the nanoparticles.

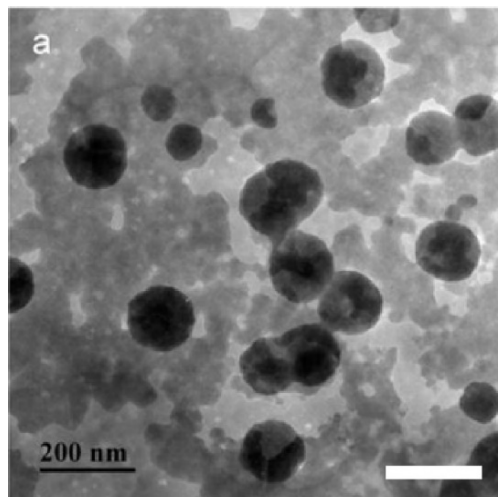


Fig. 1-7 A transmission electron microscope (TEM) image of CS nanoparticles (bar: 200 nm)^[69].

As shown in Fig. 1-8, poly-L-lysine is a polymer produced by the fermentation of lysine by *Streptomyces albulus*^[72-75]. Poly-L-lysine also has a positive charge due to its intramolecular amino group, and is expected to be applied as antibacterial and anticancer agents^[72-74].

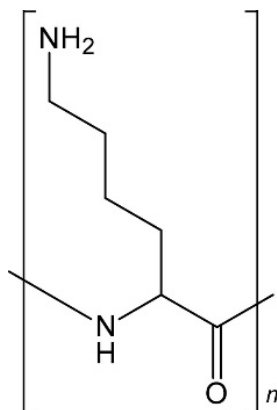


Fig. 1-8 Chemical structure of poly-L-lysine.

Drug carriers based on poly-L-lysine were developed^[36,76-79]. Among them, as shown in Fig. 1-9, Agazzi *et al.* prepared nanoparticles with diameters of approximately 200 nm formed from dendrigraft poly-L-lysine (DGL) and TPP^[76]. DGL-TPP nanoparticle with diameters of approximately 200 nm was formed by the electrostatic interaction between the nanoparticles of a few nm formed from DGL and TPP. The DGL-TPP nanoparticles were disassembled by decreasing the electrostatic interaction between DGL and TPP due to pH change, and then DGL was disintegrated by the enzyme (trypsin) encapsulated in the DGL-TPP nanoparticles. Therefore, drugs were released from DGL-TPP nanoparticles in two steps.

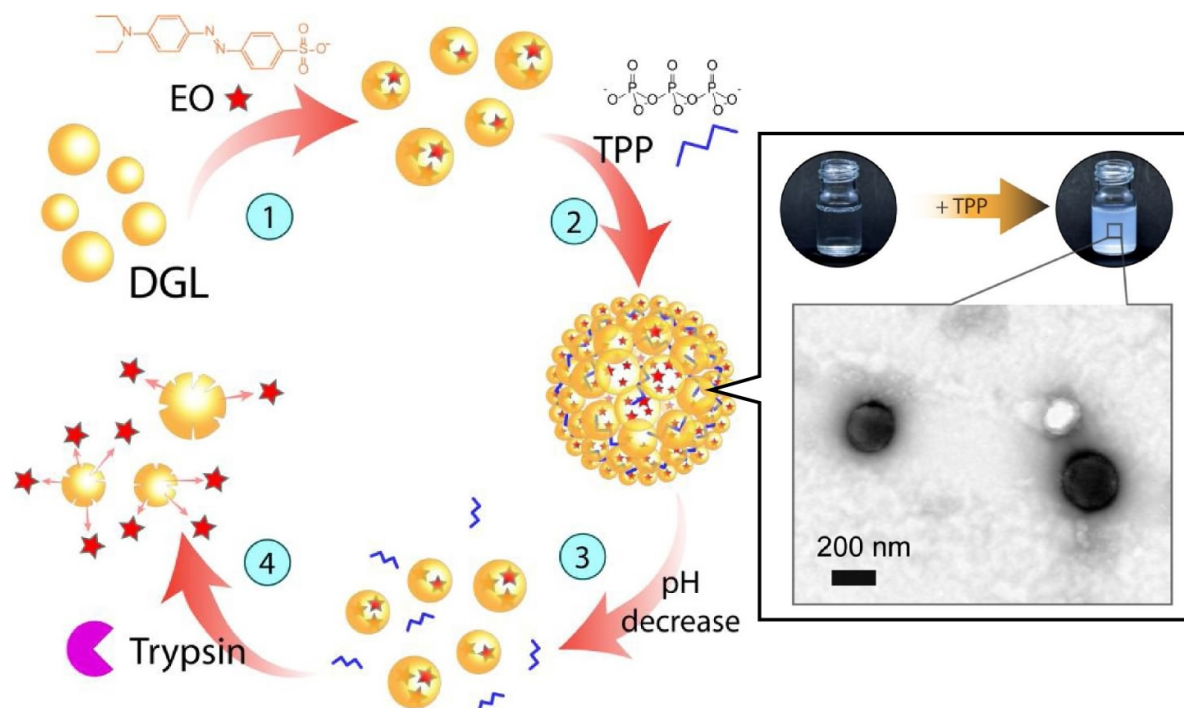


Fig. 1-9 Drug release behavior and TEM image of DGL-TPP nanoparticles^[76].

2.3.2 Synthetic polymer

Synthetic polymers for drug carriers are, e.g., PLGA (poly(lactic-*co*-glycolic acid)), PLA (polylactide), and PCL (poly(ϵ -caprolactone))^[36,80–87]. These synthetic polymers are biocompatible and biodegradable, and their molecular weight is controlled. The synthetic polymers have a lower polydispersity index than natural polymers^[83,86]. Therefore, the synthetic polymers are often utilized as excipients for DDS carriers, and they have high reproducibility of carrier formation^[87]. Drug carriers based on synthetic polymers have been reported to have controlled long-term drug release characteristics ranging from one week to 60 days, depending on the composition of the synthetic polymer^[80,82,86].

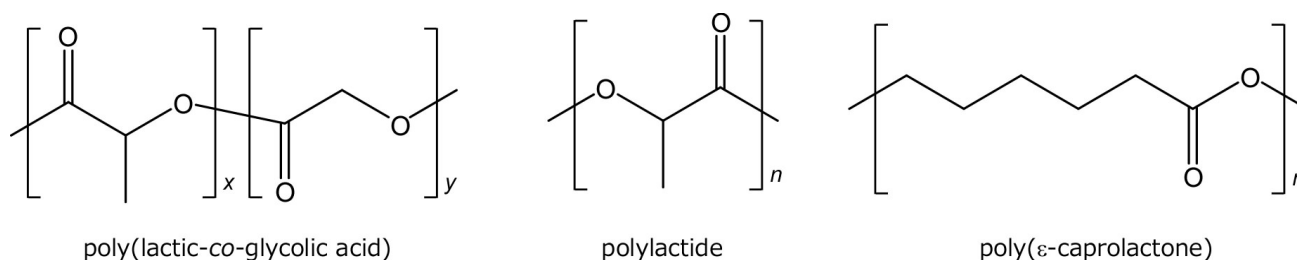
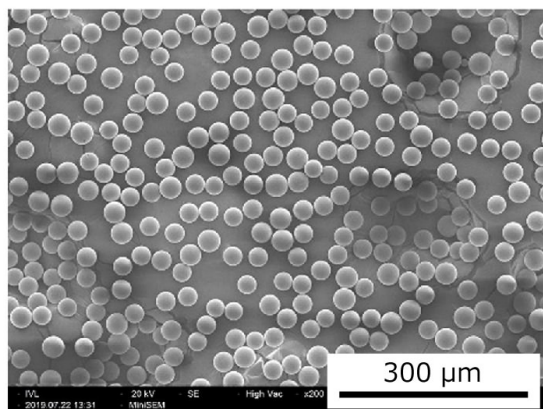


Fig. 1-10 Chemical structure of PLGA (poly(lactic-*co*-glycolic acid)), PLA (polylactide), and PCL (poly(ϵ -caprolactone)).

Finasteride-loaded microspheres



Extended drug release (Beagles)

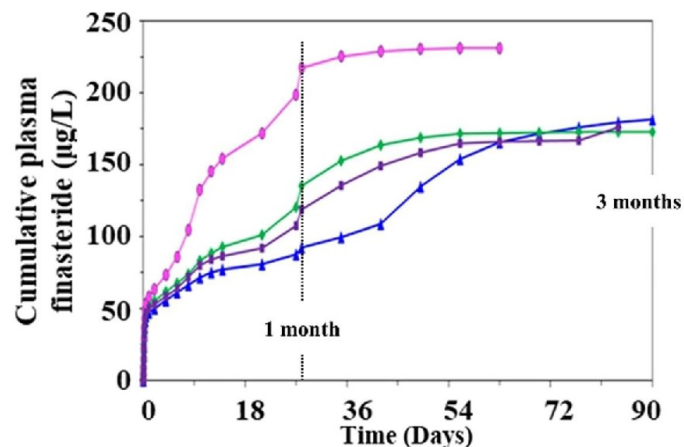


Fig. 1-11 SEM image (bar: 300 μm) and release behavior of drug form PLGA particles^[81].

As shown in Fig. 1-11, Kim *et al.* prepared microparticles with a diameter of approximately 40 μm from PLGA. Drugs were released from PLGA microparticles into the body of beagle dogs for three months^[81]. It was shown that the release rate of drugs could be controlled by the composition of lactic acid and glycolic acid in PLGA.

2.3.3 Inorganic materials

Inorganic materials for drug carriers are, e.g., silica^[88–95] and metals^[96–101].

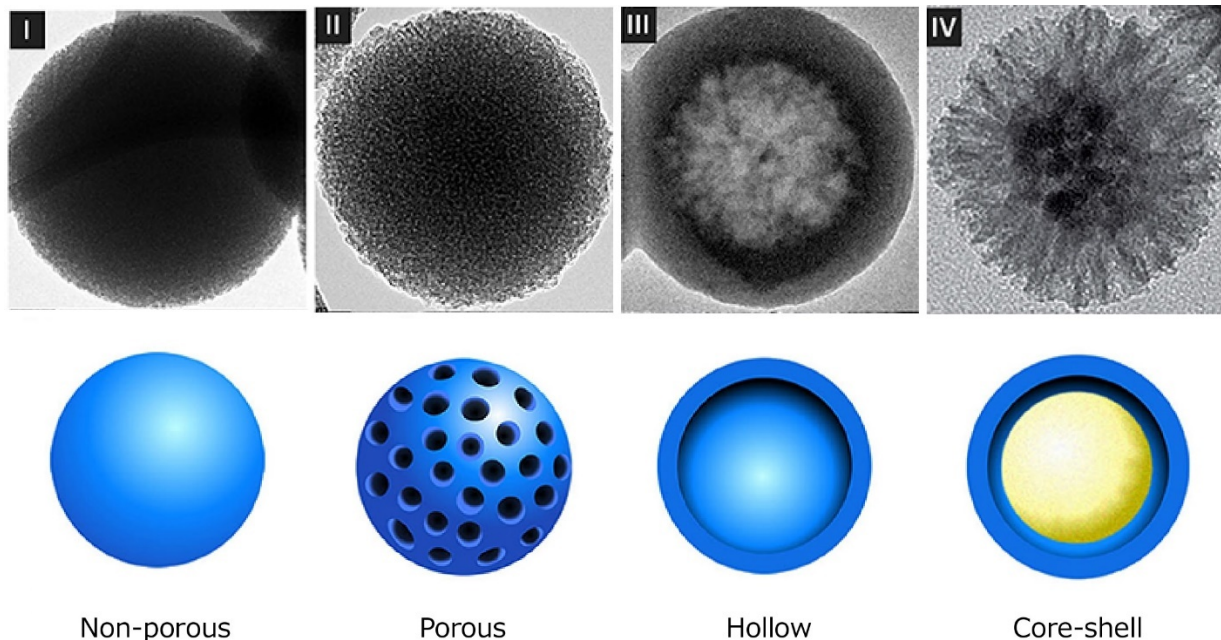


Fig. 1-12 Shape of silica particles^[90–95].

As shown in Fig. 1-12, silica particles are formed by siloxane bonds, and preparation methods of silica particles have a great influence on their shapes^[90–95]. It has been reported that particles with various shapes can be

formed from the same material (silica), e.g., non-porous^[90,91], porous^[90,93-95], hollow^[90,94], and core-shell^[92].

Drug carriers formed from metals often have unique properties of the metals themselves. Among them, magnetic nanoparticles have been prepared from magnetite, iron, nickel, and cobalt^[96-101]. The magnetic nanoparticles are applied in thermotherapy and medical diagnostic devices. By accumulating magnetic nanoparticles in tumor tissue by the EPR effect and then changing the magnetic field, the magnetic nanoparticles generate heat from magnetic energy and actively destroy the tumor tissue^[96,97]. By NMR imaging, magnetic nanoparticles can enhance contrast in images between normal and tumor tissues and visualize organ function and blood flow^[98,99].

3. Drug carriers for pulmonary administration

Pulmonary administration is very useful as the next generation drug administration route in the super-aging society because it exhibits high therapeutic efficacy at home. Drug carriers for pulmonary administration have more detailed requirements than drug carriers utilized for other medications. In section 3, I describe the requirements for drug carriers for pulmonary administration and the current preparation techniques of drug carriers for pulmonary administration.

3.1. Requirements for drug carriers for pulmonary administration

The drug carriers used for the pulmonary administration need to satisfy the following (1) to (4) conditions for the delivery of drugs to alveoli: (1) biocompatibility^[102], (2) proper control of the size of the carriers (1–5 μm in an aerodynamic diameter)^[103-107], (3) an ability to avoid the immune system^[102,107-109], and (4) rapid release of drugs^[110]. When the drug carriers exhibit poor biocompatibility, the drug carriers will be eliminated from the body by the immune system before the drugs are released from the carriers. When the diameter of the drug carriers is larger than 5 μm , it is difficult for the drug carriers to deliver to the alveoli due to deposition in organs prior to the alveoli. In addition, the drug carriers smaller than 1 μm (nanocarriers) may be expelled from the body by exhalation^[103]. The diameter of the drug carriers is an important factor for pulmonary delivery capacity, and their diameter should be finely controlled. The alveoli in the lungs contain alveolar macrophages as an immune system. The phagocytosis of alveolar macrophages is most active in the range of 1-3 μm ^[109], and the diameter of the drug carriers delivered to the lung overlaps with the phagocytic range of alveolar macrophages. Therefore, it is necessary to select materials and modify the surface of the drug carriers to avoid phagocytosis from alveolar macrophages. Pulmonary administration is suitable for the delivery of drugs with immediate effect because the absorption efficiency of drugs is very high. Thus, the drug carrier should release the drug rapidly.

Requirements for drug carriers for pulmonary administration

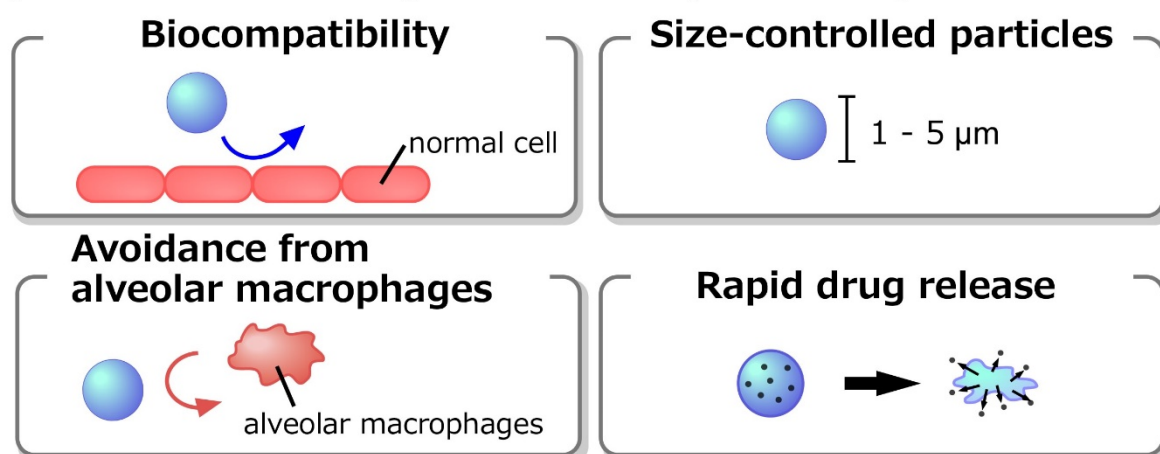


Fig. 1-13 Requirements for drug carriers for pulmonary administration.

3.2. Preparation techniques of drug carriers for pulmonary administration

3.2.1. Emulsion-solvent evaporation technique

Emulsions are systems where stable small droplets (the dispersed phase) suspend in another immiscible solution (the continuous phase), e.g., dressings, mayonnaise^[111–114] Emulsions are formed by applying external force (mechanical homogenization or sonication) to a mixture of two incompatible solvents^[115–118]. The formation of o/w (oil-in-water) emulsion, in which oil droplets are dispersed in water, and w/o (water-in-oil) emulsion, in which water droplets are dispersed in oil, is affected by the volume ratio of the solvent and the nature of the mixed surfactants (hydrophilic and hydrophobic). In the emulsion-solvent evaporation technique, the dispersed phase of the emulsion forms the drug carriers. For this reason, o/w emulsions with highly volatile organic solvents as the dispersed phase are often used.

Silva *et al.* prepared lipid microparticles for pulmonary administration of o/w emulsions by emulsion-solvent evaporation technique^[119]. The lipid microparticles (glyceryl trimyristate and glyceryl behenate microparticles) exhibit biocompatibility and can predominantly encapsulate lipophilic drugs. The glyceryl trimyristate microparticles had a diameter of $6.84 \pm 0.92 \mu\text{m}$, a Span value of 2.56 ± 1.04 indicating the dispersion of the particles, and a density of $0.24 \pm 0.002 \text{ g/cm}^3$. The glyceryl behenate microparticles had a diameter of $25.62 \pm 1.30 \mu\text{m}$, a span value of 2.94 ± 0.90 , and a density of $0.227 \pm 0.007 \text{ g/cm}^3$.

Edwards *et al.* prepared non-porous particles (diameter: $3.5 \mu\text{m}$, density: 0.8 g/cm^3) and porous particles (diameter: $8.5 \mu\text{m}$, density: 0.1 g/cm^3) from PLGA and PLAL-Lys (poly(lactic acid-*co*-lysine-*graft*-lysine))^[120]. The inhalable fraction of these particles was $20.5 \pm 2.5\%$ for the non-porous particles and $50 \pm 10\%$ for the porous particles. Interestingly, the porous particles with an unsuitable particle diameter for pulmonary administration were more delivered to the deep lung than the non-porous particles with a suitable particle diameter for pulmonary administration.

The advantage of the emulsion-solvent evaporation method is that it can produce spherical particles with a narrow diameter distribution.

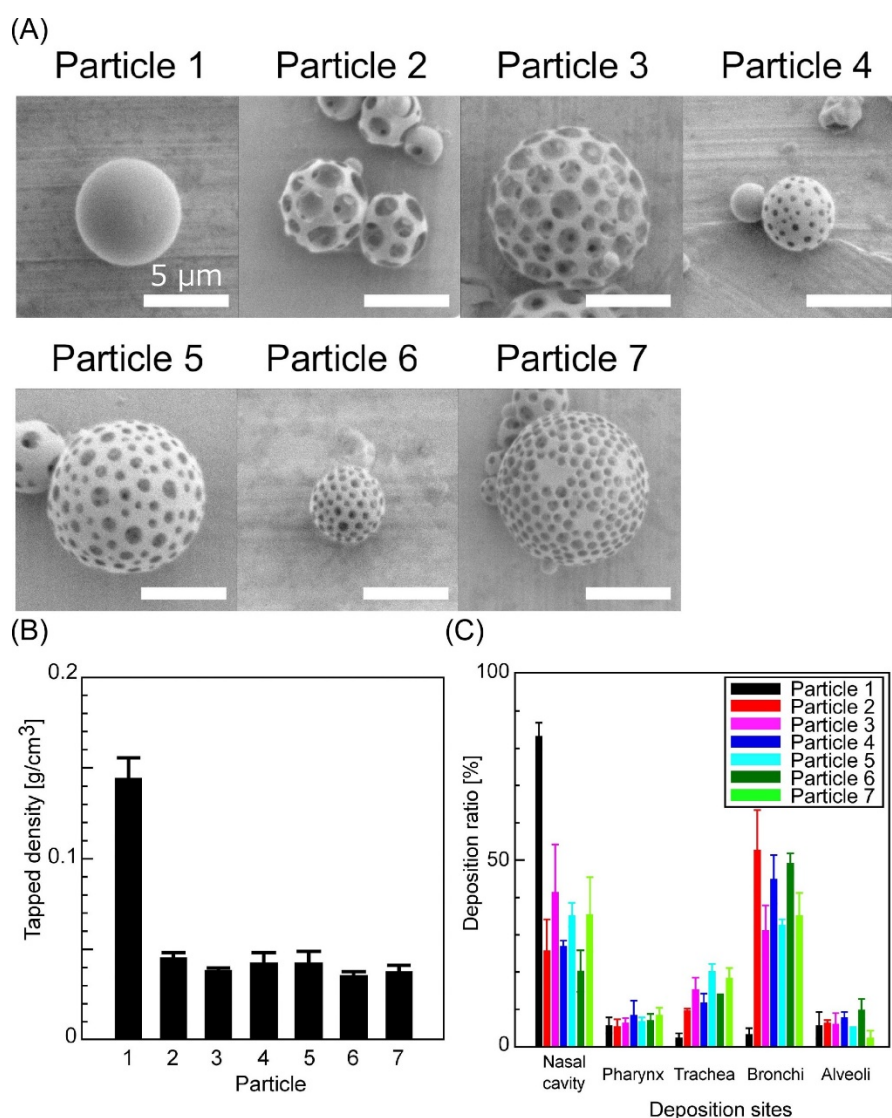


Fig. 1-14 Porous particles based on PLGA for pulmonary administration, (A) SEM images (bar: 5 μm), (B) tapped density, and (C) aerosol-dispersion performance^[121].

W/o/w (water-in-oil-in-water) emulsions and o/w/o (oil-in-water-in-oil) emulsions are formed when w/o and o/w emulsions are used as the dispersed phase. Particles formed from these w/o/w and o/w/o emulsions have a unique surface morphology compared to particles formed from w/o and o/w emulsions. As shown in Fig. 1-14, Nishimura and Takami *et al.* developed porous particles from w/o/w emulsions^[121,122]. The PLGA particles formed from w/o/w emulsions become porous on the surface and inside of the particles due to evaporation of internal water droplets of the w/o/w emulsion by freeze-drying. Therefore, the porous particles have a very low density (0.05 g/cm³) compared to non-porous particles (average density is 0.1-0.5 g/cm³). The surface morphology of the PLGA particles was successfully controlled from the emulsification conditions and surfactant composition, and high aerosol-dispersion performance was achieved even at a particle diameter of approximately 10 μm , which is unfavorable for pulmonary delivery.

From the above reports, it is very important to control the particle properties (surface morphology, diameter, and density) for pulmonary administration.

3.2.2. Spray-drying technique

Particles are formed when a liquid or a mixture of solid and liquid is sprayed into a gas and dried rapidly by heating, which is the spray-drying technique. The particles are prepared by a spray dryer (Fig. 1-15). The diameter of the particles prepared by spray drying depends on the nozzle diameter of a spray dryer and solution conditions (e.g., drying and spraying rate, concentration, and pH). To date, the particles with diameters ranging from tens of nanometer to hundreds of micrometer have been prepared^[20,123–125]. Surface morphology of the particles is also affected by drying rates and additives in solutions^[126–128].



Fig. 1-15 Appearance of a spray dryer (Mini Spray Dryer B-290, Nihon BUCHI K.K.).

	HBCD particles containing INH	HBCD particles containing RFP	Lactose particles containing INH and RFP	Sucrose particles containing INH and RFP	Maltose particles containing INH and RFP
SEM image					
Deposition rate of the particles in the treatment sites [%]	3.13±1.3	38.3±3.1	31.8±2.3	25.9±3.2	42.3±3.2
	β-CD particles containing INH and RFP	Mβ-CD particles containing INH and RFP	HBCD particles containing INH and RFP	PLGA particles containing RFP	PLGA particles containing RFP prepared with leucine
SEM image					
Deposition rate of the particles in the treatment sites [%]	33.0±3.9	34.4±4.7	53.1±5.2	6.3±4.0	43.4±5.7

Fig. 1-16 Effect of drugs encapsulated in particles, particle excipients, and additives to solvents on surface morphology and aerosol-dispersion performance of spray-drying based particles^[20,123].

As shown in Fig. 1-16, Kadota *et al.* prepared particles by spray-drying a polysaccharide, highly Branched cyclic dextrin (HBCD). The HBCD particles have been successfully encapsulated with both rifanmpicin (RFP), which is a hydrophobic drug used in the treatment of pulmonary tuberculosis, and isoniazid (INH), which is a

hydrophilic drug^[123]. They also prepared the particles with various surface morphologies from saccharides (lactose, sucrose, maltose, β -cyclodextrin (β -CD), methyl β -cyclodextrin (M β -CD)).

Takeuchi *et al.* prepared particles of PLGA encapsulating RFP and reported that the surface morphology of the particles changed significantly depending on the concentration of leucine^[20]. Furthermore, they showed that the surface morphology of these particles was greatly affected by (1) to (3): (1) the drugs encapsulated in the particles, (2) the polymers that formed the particles, and (3) the additives to the solution. The particles with dimpled surfaces were more likely to be delivered to the deep lung than particles with non-porous surfaces, and the deposition rate of the particles in the treatment area for non-porous surface particles was 3-6%, while that for dimpled particles was 30-55%. These results indicated that dimpled particles achieve higher aerosol-dispersion performance compared to non-porous particles.

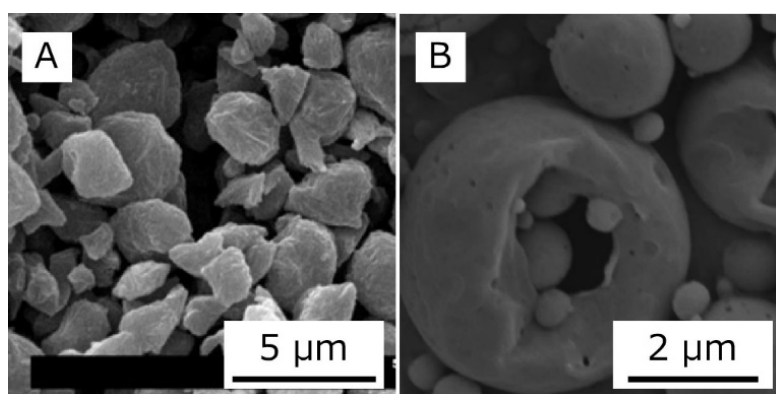


Fig. 1-17 SEM images of microparticles containing nanoparticles (A: mannitol microparticles containing nanoparticles formed from tadalafil, B: PEG-modified CS microparticles containing PLGA nanoparticles)^[129,130].

In recent years, nanoparticles have been investigated for delivery to the deep lung, but it is difficult to deliver only nanoparticles to the deep lung due to the particles' diameter. Therefore, the administration of nanoparticles to the deep lung has been investigated by (1) preparation of microparticles containing nanoparticles formed by spray-drying an aqueous solution of dispersed nanoparticles, and (2) inhalation of a dispersion of nanoparticles in an aqueous solution. As shown in Fig. 1-17, Rad *et al.* prepared microparticles by spray-drying a mixture of nanoparticles formed from tadalafil, which is a drug for pulmonary hypertension, and an aqueous solution of mannitol (Man), which is a sugar alcohol^[129]. El-Sherbiny *et al.* prepared PEG-modified CS microparticles containing PLGA nanoparticles^[130]. The deposition rates of these particles in the treatment area were 64.2% for the mannitol microparticles and 30.2% for the PEG-modified CS microparticles, indicating that the nanoparticles were delivered to the deep lung with high efficiency by the contained microparticles.

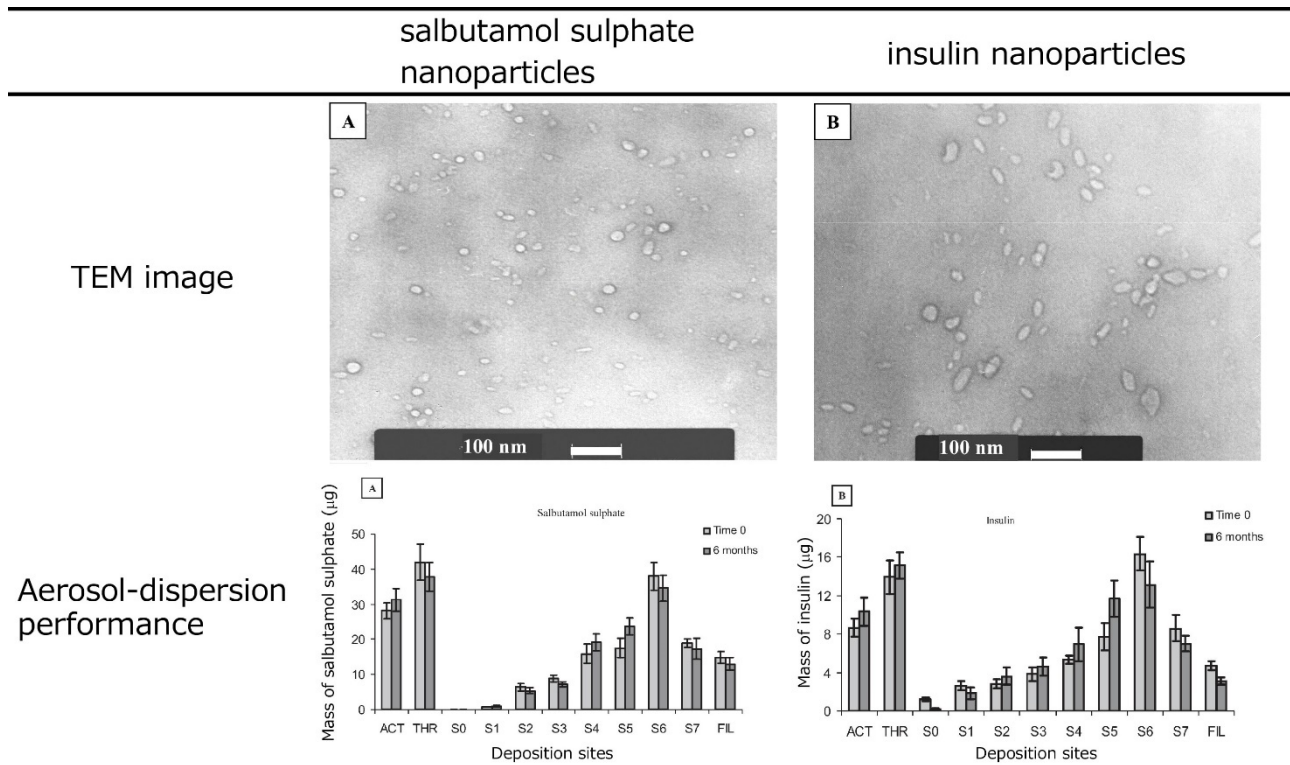


Fig. 1-18 TEM images (bar: 100 nm) and aerosol-dispersion performance of particles formed by spray-drying w/o emulsion^[131].

As shown in Fig. 1-18, Li *et al.* dissolved salbutamol sulfate, which is a bronchodilator, and insulin, which is a blood glucose suppressor, in lactose solution and dispersed each in isooctane to form w/o emulsions. The nanoparticles of less than 100 nm were prepared by spray-drying the w/o emulsions^[131]. When the prepared nanoparticles were dispersed in an aerosol solution and inhaled, the deposition rates of salbutamol sulfate particles and insulin particles in the treatment area were $62.9 \pm 1.5\%$ and $65.1 \pm 1.0\%$, respectively, showing very high values. In some cases, the nanoparticles are prepared by both emulsion and spray-drying techniques.

3.2.3. Spray-freeze-drying technique^[132–138]

The particles are formed by spraying an aqueous solution containing the drug in liquid nitrogen vapor and freeze-drying, which is the spray-freeze-drying technique. In spray freeze-drying technology, the particles are mainly formed by aqueous solutions, and freeze-drying removes the water, resulting in low-density particles with internal pores^[132–134]. The diameter of the particles depends on a diameter of a dryer nozzle, flow rate of a atomizing gas, and viscosity and concentration of aqueous solutions^[133,134,138]. Furthermore, a major advantages of the spray-freeze-drying technique is that proteins and nucleic acids, which are denatured by external forces (heat, mechanical homogenization, sonication), can be encapsulated in the particles without denaturation^[134–138]. It would be one of techniques to prepare high-performance particles with high therapeutic effect.

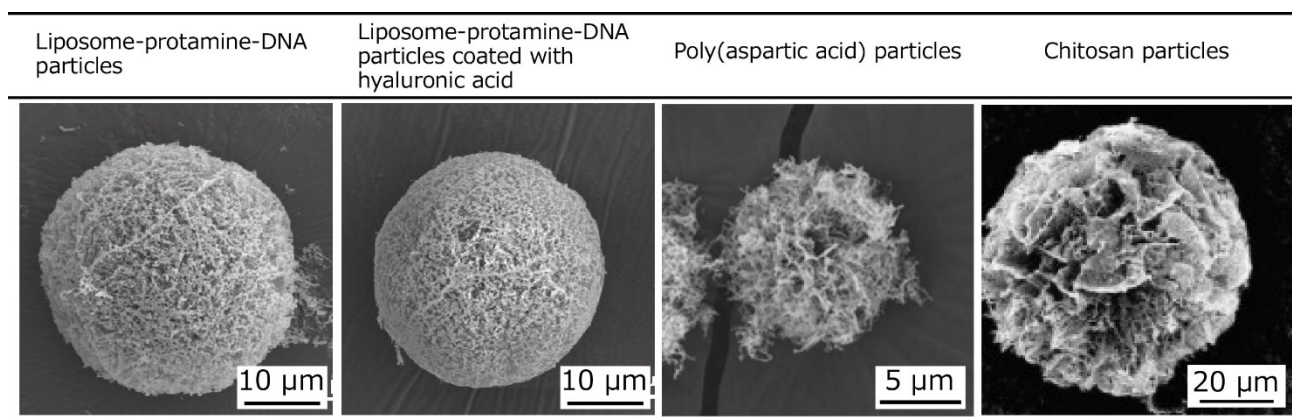


Fig. 1-19 SEM images of particles formed by spray-freeze-drying^[135-137].

As shown in Fig. 1-19, Fukushige *et al.* prepared porous microparticles for deliver nucleic acids to the lung (LPD-SFDP) by spray freeze-drying a complex (LPD) of liposomes, protamine (protein), DNA, and small interfering RNA (siRNA) with mannitol solution^[135]. Furthermore, porous particles with enhanced cell uptake (LPDH-SFDP) were prepared by coating LPD with hyaluronic acid (HA) and then spray freeze-drying. The HA coating of the particles resulted in (1) no difference in the surface morphology of the particles, (2) a deposition rate of 30-40% in the treatment area, and (3) a twofold increase in cellular uptake.

Okuda *et al.* prepared porous microparticles that delivered Plasmid DNA (pDNA) formed from polyaspartic acid (PAsp) and mannitol^[136]. The deposition rate of the particles in the treatment area was $51.3 \pm 6.2\%$. The formation of particles from PAsp enhanced the uptake of pDNA by the cells.

Mohri *et al.* prepared microparticles that delivered pDNA formed from CS and mannitol^[137]. The containing of CS in the microparticles reduced the physicochemical stress on pDNA inside the microparticles, indicating the possibility of delivering pDNA to the deep lung without denaturation.

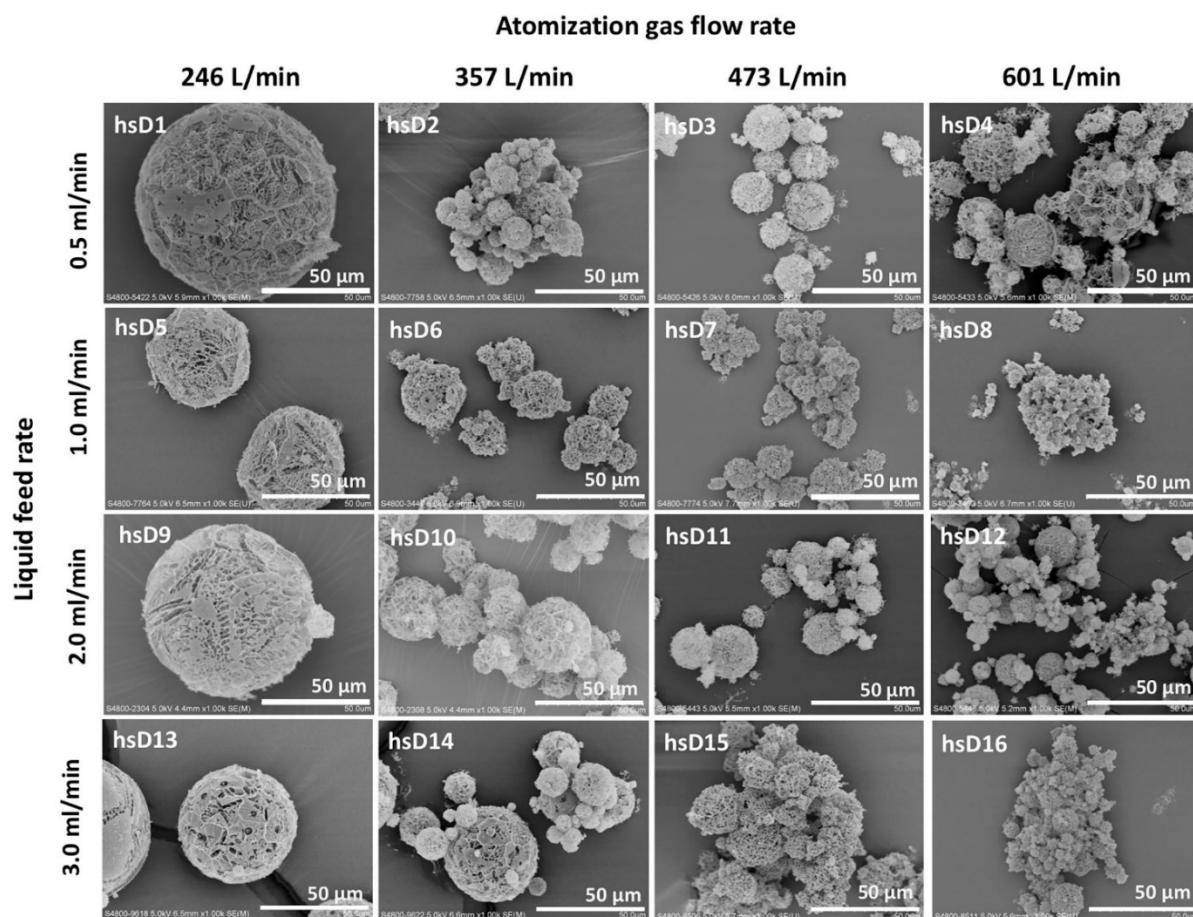


Fig. 1-20 Effect of atomization gas flow rate on particle diameter (bar: 50 μm)^[138].

As shown in Fig. 1-20, Liang *et al.* prepared porous microparticles by spray-freeze-drying a mixture of mannitol solution and siRNA or herring sperm DNA (hsDNA)^[138]. They showed that flow rate of atomizing gas affected only a diameter of the particles, without affecting the surface morphology on the particles. Mannitol is widely used as an excipient for particles in spray-freeze-drying technique. Mannitol is biocompatible, has low hygroscopicity, and crystallizes easily during the freezing process, which enhances the structural stability of particles^[139–141]. In other words, substances with a slow crystal nucleation or crystal growth rate during spray freeze drying are unsuitable as excipients for particles.

4. Stimuli-responsive drug carriers

Drug carriers are expected to release drugs only at the target site. In addition to the drug carriers listed above, drug carriers that respond to external stimuli have been investigated. In stimuli-responsive drug carriers, the microstructure of the drug carriers changes rapidly in response to stimuli from the external environment, resulting in dissolution or deformation of the drug carriers. The control of drug release behavior utilizing these state changes has been investigated. In section 4, I will describe the advantages of "temperature," "light", and "pH" responsive drug carriers among stimuli-responsive drug carriers.

4.1. Temperature-responsive drug carriers

The temperature-responsive drug carriers release the encapsulated drugs by changing the steric configuration and physical properties of the molecules forming the carrier in response to temperature. Drug carriers based on sol-gel transition at lower critical solution temperature (LCST) and upper critical solution temperature (UCST) have been reported^[142–149].

At below LCST, hydrogen bonding between the polymer and water causes the polymer to form random coils and dissolve. At above LCST, when the hydrogen bond between the polymer and water weakens and dehydration occurs from the hydrophobic part of the polymer, the polymer chains form aggregates^[142–149]. Polymers that exhibit LCST include poly(*N*-Isopropylacrylamide) and methyl cellulose. UCST exhibits a phase transition in contrast to LCST. At below UCST, betaine type (amphoteric ion type) polymers form aggregates due to aggregation between polymers driven by intramolecular electrostatic interactions^[144,145]. However, at above UCST, molecular motility increases and dissolves rather than the intramolecular electrostatic interaction.

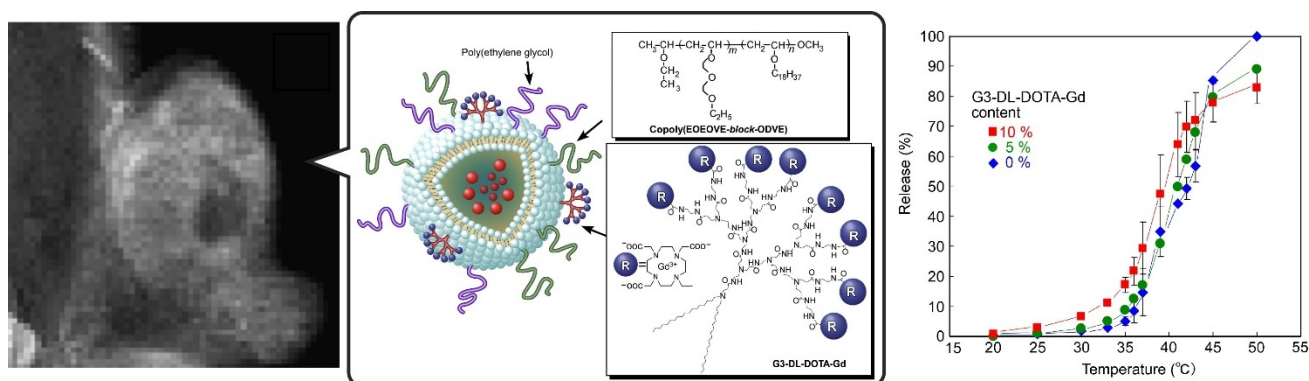


Fig. 1-21 A magnetic resonance imaging and drugs (doxorubicin) release behavior of temperature-responsive liposomes^[148].

As shown in Fig. 1-21, Kono *et al.* prepared temperature-responsive liposomes with a diameter of approximately 110 nm by grafting poly(2-(2-ethoxy)ethoxyethyl vinyl ether-*b*-octadecyl vinyl ether) (EOEVE-*b*-ODVE), which is a temperature-responsive polymer, onto the surface of the liposomes^[148]. EOEVE-*b*-ODVE showed LCST at approximately 40°C. At body temperature (approximately 37°C), EOEVE-*b*-ODVE was hydrophilic and thus had a high affinity with liposomes and stabilized the surface structure of the liposomes. However, above the LCST, EOEVE-*b*-ODVE became hydrophobic, which destabilized the surface structure of the liposomes and resulted the liposome to disintegrate. Thus, the drugs (doxorubicin) encapsulated in the liposome was released. Therefore, drugs were locally administered from liposomes by local heating (hyperthermia therapy) in the body^[150,151].

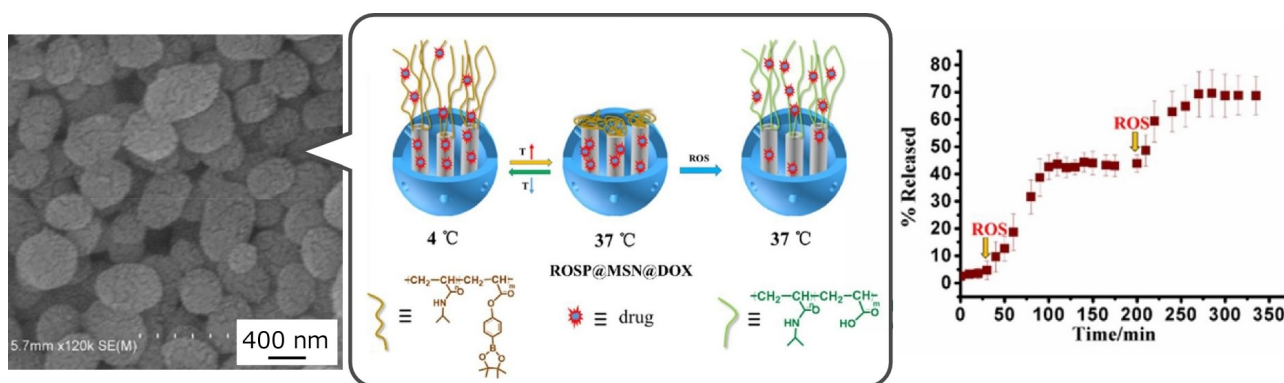


Fig. 1-22 SEM image (bar: 400 nm) and a drug (doxorubicin) release behavior of particles in response to temperature and reactive oxygen species^[149].

As shown in Fig. 1-22, Yu *et al.* prepared nanoparticles with a diameter of approximately 240 nm that react with temperature and active enzymes by grafting poly(*N*-isopropylacrylamide-*co*-4-(benzyl acrylate) phenylboronic acid pinacol ester) (poly(NIPAM-*co*-BAPAE)) onto the surface of porous silica particles^[149]. The nanoparticles encapsulated the drug (doxorubicin) by concentration gradient below LCST (37°C) and inhibited the release of the drug by hydrophobic interaction above the LCST. Thus, the release and internalization of drugs in stimuli-responsive carriers are greatly affected by temperature. Furthermore, reactive oxygen species (ROS) changed the conformation of molecular chains and accelerated the release rate of the drug from the nanoparticles. In the body, local release of the drug was expected to occur at sites where the amount of ROS was high (tumor tissue and inflammation sites).

4.2. Photo-responsive drug carriers

In photo-responsive drug carriers, the encapsulated drugs are released when the structure of the molecules forming the carriers is altered by light irradiation (e.g., light-induced structural change of molecules via *cis-trans* isomerization reactions^[152–154]). In addition, substances that convert light into heat are used to form photo-responsive drug carriers^[152,155–159].

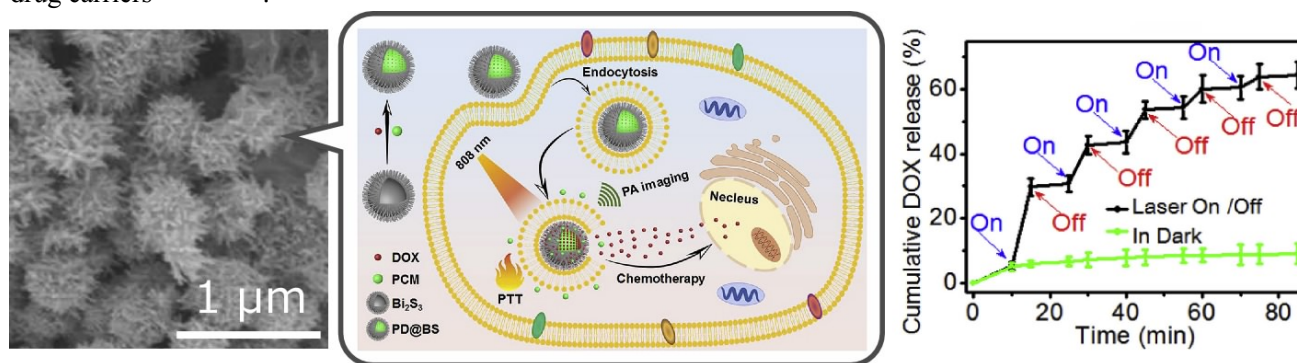


Fig. 1-23 SEM image (bar: 1 μm) and drugs (doxorubicin) release behavior of photo-responsive particles thermally generated by near-infrared light^[158].

As shown in Fig. 1-23, Zhang *et al.* prepared urchin-like hollow microparticles formed from ZnS microparticles and Bi_2S_3 ^[158]. The hollow microparticles were encapsulated with 1-tetradecanol (phase change

material, PCM) which exhibits phase change at 38°C and drugs (doxorubicin). When the hollow microparticles were irradiated with near-infrared light at 808 nm, Bi₂S₃ absorbed the light and generated heat. As a result, the hollow microparticles destroyed the cells and the 1-tetradecanol inside the hollow microparticles changed phase and accelerated the release rate of the drugs. The drug was released from the hollow particles only while light was irradiated, and the release of the drugs was switched by light. Tumor tissues are reported to have less dilated blood vessels and are more vulnerable to heat than normal cells, and efficient treatment of tumor tissues can be expected by converting light into heat^[150]. Because shorter wavelengths of irradiated light increase toxicity to cells, near-infrared light has been widely used in recent years^{[152][160]}.

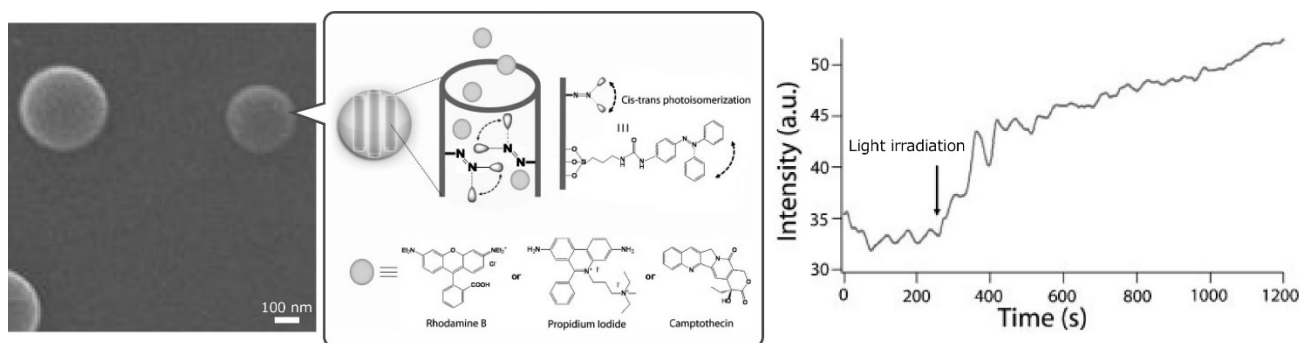


Fig. 1-24 SEM image (bar: 100 nm) and a fluorescent substance (rhodamine B) release behavior of mesoporous silica particles by cis-trans isomerization reaction.

As shown in Fig. 1-24, Lu et al. prepared mesoporous silica particles with a diameter of approximately 300 nm that released a fluorescent substance (Rhodamine B) by light-induced cis-trans isomerization reaction^[159]. By modifying the pores of mesoporous silica particles with an azobenzene derivative, rhodamine B was rapidly released from the particles upon light irradiation at 413 nm.

4.3. pH-responsive drug carriers

In pH-responsive drug carriers, the encapsulated drugs are released when the structure of the molecules forming the carriers or their intermolecular interactions change due to pH changes in the environment. pH-responsive drug carriers are formed from polymers with intramolecular amino groups and are affected by the pK_a of the polymer. When the pH becomes lower than pK_a , polymers change from hydrophobic to positively charged hydrophilic and this change in aqueous solubility has a significant effect on the release behavior of drugs from the drug carriers^[76,161,162]. In tumor tissues, it is known that the pH is weakly acidic by substances, such as lactic acid and glutathione, produced during the metabolic process, and drugs can be released locally into the tumor in response to such changes^[163,164]. In addition, during endocytosis, the pH changes to approximately 5-6, and drugs are released from the carriers in response to the pH change^[163-165].

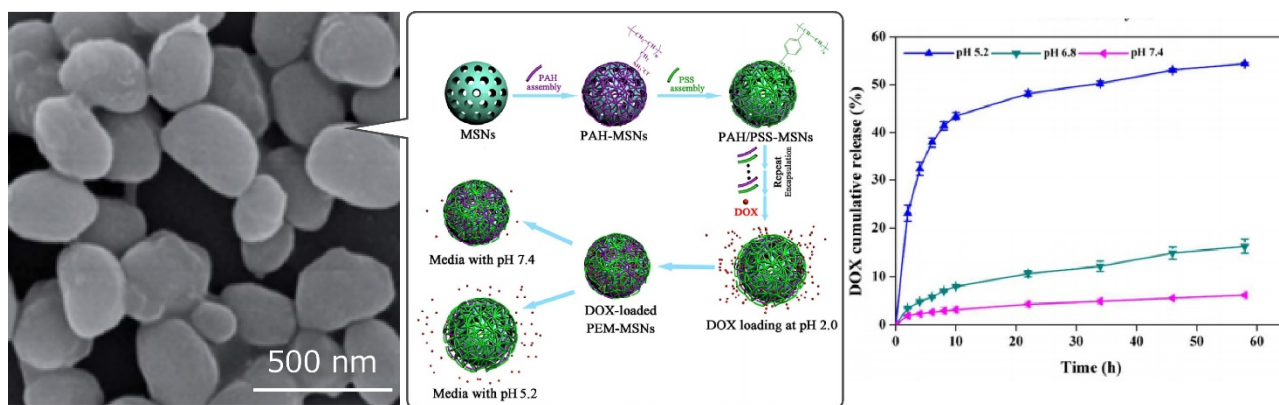


Fig. 1-25 SEM image (bar: 500 nm) and drugs (doxorubicin) release behavior of pH-responsive nanoparticles^[166].

As shown in Fig. 1-25, Feng *et al.* prepared pH-responsive nanoparticles by grafting poly (allylamine hydrochloride) (PAH) and sodium poly(styrene sulfonate) (PSS) onto the surface of porous silica nanoparticles^[166]. The nanoparticles rapidly released the drugs (doxorubicin) by desorption of PAH and PSS from the particle surface under weakly acidic conditions. Evaluation of histology showed that nanoparticles have lower systemic toxicity than free drugs, which could reduce side effects.

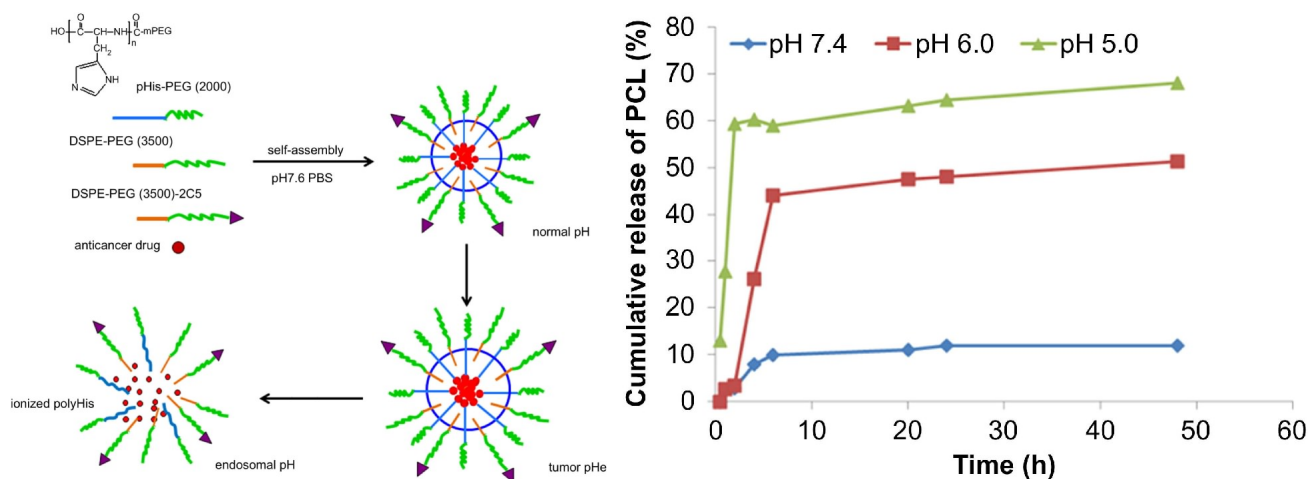


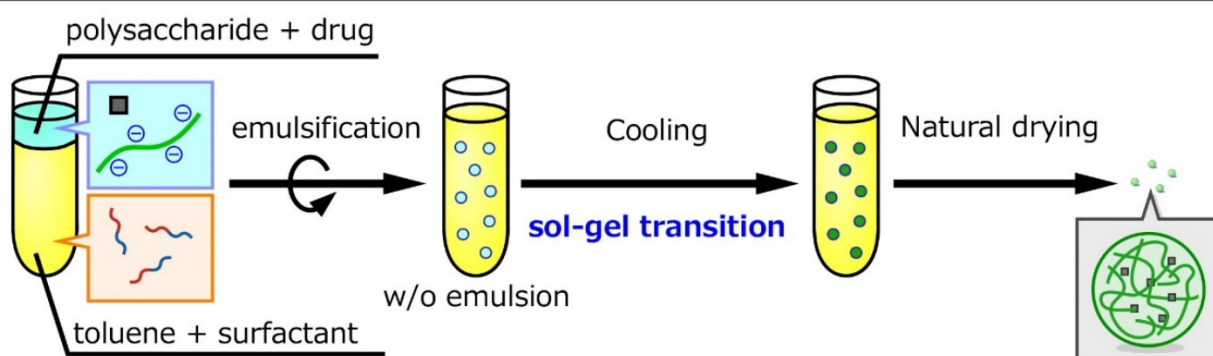
Fig. 1-26 Release behavior of drugs (paclitaxel) in pH-responsive polymeric micelles formed from three different polymers^[46].

As shown in Fig. 1-26, Wu *et al.* prepared pH-responsive polymeric micelles with a diameter of approximately 110 nm from three different polymers, poly(ethylene glycol)-grafted histidine (PHIS-PEG), 1,2-distearoyl-*sn*-glycero-3-phosphoethanolamine-polyethylene glycol-2000 (DSPE-PEG2000), and antinucleosome antibody (mAb 2C5)-modified DSPE-PEG3400 (DSPE-PEG3400-2C5)^[46]. At pH=7.5, polymeric micelles were formed with the hydrophobic part of histidine as the core, but when the pH changed to acidic, the histidine protonated and the polymeric micelles disintegrated, thereby releasing the drugs (paclitaxel).

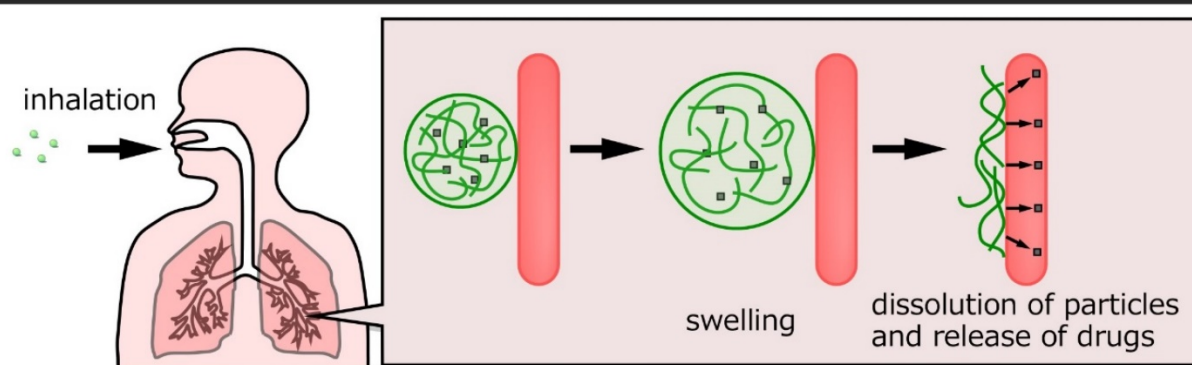
5. The aim of this thesis

In this doctoral thesis, I aim to develop "temperature-responsive microparticles" that rapidly release drugs in the body by an emulsion method utilizing the sol-gel transition phenomenon of polysaccharide. By emulsifying an organic solvent in which a surfactant is dissolved and an aqueous polysaccharide solution, a w/o emulsion is formed. When the resulted w/o emulsion is cooled, the polysaccharide performs the sol-gel transition and gel particles are formed. The resulted gel particles are then dried to form microparticles. The diameter of the microparticles depends on the emulsification rate and emulsification time, so the microparticles with diameters suitable for pulmonary administration are prepared. I have selected CRG to form a drug carrier. The formation of microparticles for pulmonary administration from CRG provides the advantages of (1) to (5). (1) κ - and ι -type CRGs are highly biocompatible in the lungs^[56]. (2) The physical properties (surface morphology and rigidity) of the microparticles can be changed based on the unique properties of κ - and ι -type CRGs. (3) The encapsulation and release of positively charged compounds can be controlled by the electrostatic interaction of sulfate groups in the CRG molecule. (4) Because CRG swells by absorbing water, the microparticles swell by absorbing body fluids, which will increase the diameter of the microparticles and may avoid phagocytosis from alveolar macrophages. (5) After the microparticles are delivered to the lungs, the drugs are released from the microparticles by body temperature without any special heating. Thus, the CRG microparticles to be developed in this doctoral thesis (1) are simple to administer, (2) are fast-acting drug carriers that respond to body temperature and release drugs, and (3) have a high potential advantage in urgent diseases such as seizures and abnormal increases of blood glucose levels. As aging populations around the world grow, the CRG microparticles will be the next generation of drug carriers that can be administered by patients themselves to provide highly effective home treatment (Fig. 1-27).

Preparation of carrageenan microparticles



Carrageenan microparticles for pulmonary delivery



Development of temperature-responsive polysaccharide microparticles for pulmonary drug delivery

Fig. 1-27 The aim of this thesis.

In chapter 2, I tried to prepare CRG particles having a proper diameter, show their temperature-responsive behavior, and aerodynamic properties in order to achieve a highly efficient delivery of the particles to the lungs. I evaluated both of the factors affecting the preparation of the CRG particles and their *in vitro* aerosol-dispersion performance. In chapter 3, I reported (1) the development of temperature-responsive carrageenan particles by changing the melting point of the polymeric surfactants (amphiphilic block copolymers that stabilize emulsions) used in particle formation by varying the composition of the block copolymers and using the melting of the surfactants oriented on the particle surface as the driving force for particle dissolution, and (2) the investigation of the release properties of the particles. In chapter 4, based on the knowledge of chapters 2 and 3, I challenged the encapsulation of cationic nanoparticles with the CRG particles by electrostatic interaction between the sulfate groups of CRG and the cationic nanoparticles to enhance the functionality of CRG particles. I evaluated the release properties of multiple inclusions from the CRG particles for application as a drug carrier for pulmonary administration with improved drug selectivity and the ability to deliver more than two different drugs.

6. Reference

- [1] Schenk, M., Mueller, C., The mucosal immune system at the gastrointestinal barrier., *Best Pract. Res. Clin. Gastroenterol.*, **22**, 391–409, (2008)
- [2] Yoshida, H., Lehr, C. M., Kok, W., Junginger, H. E., Verhoef, J. C., Bouwstra, J. A., Niosomes for oral delivery of peptide drugs., *J. Control. Release*, **21**, 145–153, (1992)
- [3] Zhang, L., Wang, S., Zhang, M., Sun, J., Nanocarriers for oral drug delivery., *J. Drug Target.*, **21**, 515–527, (2013)
- [4] Griffin, B. T., Guo, J., Presas, E., Donovan, M. D., Alonso, M. J., O’Driscoll, C. M., Pharmacokinetic, pharmacodynamic and biodistribution following oral administration of nanocarriers containing peptide and protein drugs., *Adv. Drug Deliv. Rev.*, **106**, 367–380, (2016)
- [5] Sastry, S. V., Nyshadham, J. R., Fix, J. A., Recent technological advances in oral drug delivery - A review., *Pharm. Sci. Technol. Today*, **3**, 138–145, (2000)
- [6] Kuppens, I. E. L. M., Beijnen, J. H., Schellens, J. H. M., Topoisomerase I inhibitors in the treatment of gastrointestinal cancer: From intravenous to oral administration., *Clin. Colorectal Cancer*, **4**, 163–180, (2004)
- [7] De Jong, W. H., Hagens, W. I., Krystek, P., Burger, M. C., Sips, A. J. A. M., Geertsma, R. E., Particle size-dependent organ distribution of gold nanoparticles after intravenous administration., *Biomaterials*, **29**, 1912–1919, (2008)
- [8] Raskin, P., Holcombe, J. H., Tamborlane, W. V., Malone, J. I., Strowig, S., Ahern, J. A., Lavent, F., A comparison of insulin lispro and buffered regular human insulin administered via continuous subcutaneous insulin infusion pump., *J. Diabetes Complications*, **15**, 295–300, (2001)
- [9] Intravenous, C., Intravenous Drug Administration., *Handb. Behav. Neurosci.*, **12**, 5–22, (1994)
- [10] Laizure, S. C., *Chapter 10: Clinical Pharmacokinetics.*, *The Complete PCOA ® Review*, (Elsevier Ltd, 2020), doi:10.21019/9781582123417.ch10
- [11] Prausnitz, M. R., Mitragotri, S., Langer, R., Current status and future potential of transdermal drug delivery., *Nat. Rev. Drug Discov.*, **3**, 115–124, (2004)
- [12] Alkilani, A. Z., McCrudden, M. T. C., Donnelly, R. F., Transdermal drug delivery: Innovative pharmaceutical developments based on disruption of the barrier properties of the stratum corneum., *Pharmaceutics*, **7**, 438–470, (2015)
- [13] Szunerits, S., Boukherroub, R., Heat: A highly efficient skin enhancer for transdermal drug delivery., *Front. Bioeng. Biotechnol.*, **6**, 1–13, (2018)
- [14] Jeong, W. Y., Kwon, M., Choi, H. E., Kim, K. S., Recent advances in transdermal drug delivery systems: a review., *Biomater. Res.*, **25**, 1–15, (2021)
- [15] Bird, D., Ravindra, N. M., Transdermal drug delivery and patches—An overview., *Med. Devices Sensors*, **3**, 1–15, (2020)
- [16] Patton, J. S., Byron, P. R., Inhaling medicines: Delivering drugs to the body through the lungs., *Nat. Rev. Drug Discov.*, **6**, 67–74, (2007)

- [17] d'Angelo, I., Conte, C., La Rotonda, M. I., Miro, A., Quaglia, F., Ungaro, F., Improving the efficacy of inhaled drugs in cystic fibrosis: Challenges and emerging drug delivery strategies., *Adv. Drug Deliv. Rev.*, **75**, 92–111, (2014)
- [18] Bangyozova, M., Jordanova, A., Tsanova, A., Stoyanova, V., Tasheva, E., Ivanova, K., Todorov, R., Hristova, E., Lalchev, Z., Application of axisymmetric drop shape analysis and brewster angle microscopy for assessment of clinical samples from prematurely born infants with NRDS., *Colloids Surfaces A Physicochem. Eng. Asp.*, **519**, 187–191, (2017)
- [19] Takeuchi, I., Tetsuka, Y., Nii, T., Shinogase, M., Makino, K., Inhalable nanocomposite particles using amino acids with improved drug content and humidity resistance., *Colloids Surfaces A Physicochem. Eng. Asp.*, **529**, 387–393, (2017)
- [20] Takeuchi, I., Taniguchi, Y., Tamura, Y., Ochiai, K., Makino, K., Effects of L-leucine on PLGA microparticles for pulmonary administration prepared using spray drying: Fine particle fraction and phagocytotic ratio of alveolar macrophages., *Colloids Surfaces A Physicochem. Eng. Asp.*, **537**, 411–417, (2018)
- [21] Gonçalves, A., Nikmaram, N., Roohinejad, S., Estevinho, B. N., Rocha, F., Greiner, R., McClements, D. J., Production, properties, and applications of solid self-emulsifying delivery systems (S-SEDS) in the food and pharmaceutical industries., *Colloids Surfaces A Physicochem. Eng. Asp.*, **538**, 108–126, (2018)
- [22] Jain, H., Bairagi, A., Srivastava, S., Singh, S. B., Mehra, N. K., Recent advances in the development of microparticles for pulmonary administration., *Drug Discov. Today*, **25**, 1865–1872, (2020)
- [23] Loira-Pastoriza, C., Todoroff, J., Vanbever, R., Delivery strategies for sustained drug release in the lungs., *Adv. Drug Deliv. Rev.*, **75**, 81–91, (2014)
- [24] Bosquillon, C., Lombry, C., Pr eat, V., Vanbever, R., Influence of formulation excipients and physical characteristics of inhalation dry powders on their aerosolization performance., *J. Control. Release*, **70**, 329–339, (2001)
- [25] Wall, D. A., Pulmonary absorption of peptides and proteins., *Drug Deliv.*, **2**, 1–20, (1995)
- [26] Agu, R. U., Ugwoke, M. I., Armand, M., Kinget, R., Verbeke, N., Agu - 2001 - Lung as a route for peptide administration., (2001)
- [27] Tiwari, G., Tiwari, R., Bannerjee, S., Bhati, L., Pandey, S., Pandey, P., Sriwastawa, B., Drug delivery systems: An updated review., *Int. J. Pharm. Investig.*, **2**, 2, (2012)
- [28] Patra, J. K., Das, G., Fraceto, L. F., Campos, E. V. R., Rodriguez-Torres, M. D. P., Acosta-Torres, L. S., Diaz-Torres, L. A., Grillo, R., Swamy, M. K., Sharma, S., *et al.*, Nano based drug delivery systems: Recent developments and future prospects 10 Technology 1007 Nanotechnology 03 Chemical Sciences 0306 Physical Chemistry (incl. Structural) 03 Chemical Sciences 0303 Macromolecular and Materials Chemistry 11 Medical and He., *J. Nanobiotechnology*, **16**, 1–33, (2018)
- [29] Trucillo, P., and Industrial Approach., *Processes*, **9**, 1–18, (2021)
- [30] Vega-V asquez, P., Mosier, N. S., Irudayaraj, J., Nanoscale Drug Delivery Systems: From Medicine to Agriculture., *Front. Bioeng. Biotechnol.*, **8**, 1–16, (2020)
- [31] Barclay, T. G., Day, C. M., Petrovsky, N., Garg, S., Review of polysaccharide particle-based functional drug delivery., *Carbohydr. Polym.*, **221**, 94–112, (2019)

- [32] Obeidat, W., Recent Patents Review in Microencapsulation of Pharmaceuticals Using the Emulsion Solvent Removal Methods., *Recent Pat. Drug Deliv. Formul.*, **3**, 178–192, (2009)
- [33] Abdellatif, A. A., Microparticles Formulation as a Targeting Drug Delivery System., *J. Nanomedicine Res.*, **6**, 2–5, (2017)
- [34] Lengyel, M., Kállai-Szabó, N., Antal, V., Laki, A. J., Antal, I., Microparticles, microspheres, and microcapsules for advanced drug delivery., *Sci. Pharm.*, **87**, (2019)
- [35] Uyen, N. T. T., Hamid, Z. A. A., Tram, N. X. T., Ahmad, N., Fabrication of alginate microspheres for drug delivery: A review., *Int. J. Biol. Macromol.*, **153**, 1035–1046, (2020)
- [36] Jana, P., Shyam, M., Singh, S., Jayaprakash, V., Dev, A., Biodegradable polymers in drug delivery and oral vaccination., *Eur. Polym. J.*, **142**, 110155, (2021)
- [37] Bee, S. L., Hamid, Z. A. A., Mariatti, M., Yahaya, B. H., Lim, K., Bee, S. T., Sin, L. T., Approaches to Improve Therapeutic Efficacy of Biodegradable PLA/PLGA Microspheres: A Review., *Polym. Rev.*, **58**, 495–536, (2018)
- [38] Zheng, X., Wu, F., Hong, Y., Shen, L., Lin, X., Feng, Y., Developments in taste-masking techniques for traditional Chinese medicines., *Pharmaceutics*, **10**, 1–22, (2018)
- [39] Han, F. Y., Thurecht, K. J., Whittaker, A. K., Smith, M. T., Bioerodable PLGA-based microparticles for producing sustained-release drug formulations and strategies for improving drug loading., *Front. Pharmacol.*, **7**, 1–11, (2016)
- [40] Sreekumar, S., Goycoolea, F. M., Moerschbacher, B. M., Rivera-Rodriguez, G. R., Parameters influencing the size of chitosan-TPP nano- and microparticles., *Sci. Rep.*, **8**, 1–11, (2018)
- [41] Sarcina, L., García-Manrique, P., Gutiérrez, G., Ditaranto, N., Cioffi, N., Matos, M., Blanco-López, M. D. C., Cu nanoparticle-loaded nanovesicles with antibiofilm properties. Part i: Synthesis of new hybrid nanostructures., *Nanomaterials*, **10**, 1–14, (2020)
- [42] Lazaridou, M., Christodoulou, E., Nerantzaki, M., Kostoglou, M., Lambropoulou, D. A., Katsarou, A., Pantopoulos, K., Bikiaris, D. N., Formulation and in-vitro characterization of chitosan-nanoparticles loaded with the iron chelator deferoxamine mesylate (DFO)., *Pharmaceutics*, **12**, (2020)
- [43] Liu, Z., Jiao, Y., Wang, Y., Zhou, C., Zhang, Z., Polysaccharides-based nanoparticles as drug delivery systems., *Adv. Drug Deliv. Rev.*, **60**, 1650–1662, (2008)
- [44] Uchida, Y., Murakami, Y., Colloids and Surfaces B : Biointerfaces Trilayered polymeric micelle : A newly developed macromolecular assembly that can incorporate hydrophilic compounds., *Colloids Surfaces B Biointerfaces*, **79**, 198–204, (2010)
- [45] Uchida, Y., Murakami, Y., Successful preferential formation of a novel macromolecular assembly-Trilayered polymeric micelle-That can incorporate hydrophilic compounds: The optimization of factors affecting the micelle formation from amphiphilic block copolymers., *Colloids Surfaces B Biointerfaces*, **84**, 346–353, (2011)
- [46] Wu, H., Zhu, L., Torchilin, V. P., PH-sensitive poly(histidine)-PEG/DSPE-PEG co-polymer micelles for cytosolic drug delivery., *Biomaterials*, **34**, 1213–1222, (2013)
- [47] Kedar, U., Phutane, P., Shidhaye, S., Kadam, V., Advances in polymeric micelles for drug delivery and tumor targeting., *Nanomedicine Nanotechnology, Biol. Med.*, **6**, 714–729, (2010)
- [48] Kataoka, K., Harada, A., Nagasaki, Y., Block copolymer micelles for drug delivery: Design, characterization and

- biological significance., *Adv. Drug Deliv. Rev.*, **64**, 37–48, (2012)
- [49] Moroishi, H., Sonotaki, S., Murakami, Y., PLA- and PLA/PLGA-emulsion composite biomaterial sheets for the controllable sustained release of hydrophilic compounds., *Materials (Basel)*, **11**, 1–12, (2018)
- [50] Bonicelli, M. G., Giansanti, L., Ierino, M., Mancini, G., Interaction of cationic liposomes with cell membrane models., *J. Colloid Interface Sci.*, **355**, 1–8, (2011)
- [51] Sercombe, L., Veerati, T., Moheimani, F., Wu, S. Y., Sood, A. K., Hua, S., Advances and challenges of liposome assisted drug delivery., *Front. Pharmacol.*, **6**, 1–13, (2015)
- [52] Guan, T., Miao, Y., Xu, L., Yang, S., Wang, J., He, H., Tang, X., Cai, C., Xu, H., Injectable nimodipine-loaded nanoliposomes: Preparation, lyophilization and characteristics., *Int. J. Pharm.*, **410**, 180–187, (2011)
- [53] Obaidat, R. M., Alnaief, M., Mashaqbeh, H., Investigation of Carrageenan Aerogel Microparticles as a Potential Drug Carrier., *AAPS PharmSciTech*, **19**, 2226–2236, (2018)
- [54] Alnaief, M., Obaidat, R., Mashaqbeh, H., Effect of processing parameters on preparation of carrageenan aerogel microparticles., *Carbohydr. Polym.*, **180**, 264–275, (2018)
- [55] Valente, S. A., Silva, L. M., Lopes, G. R., Sarmiento, B., Coimbra, M. A., Passos, C. P., Polysaccharide-based formulations as potential carriers for pulmonary delivery – A review of their properties and fates., *Carbohydr. Polym.*, 118784, (2021), doi:10.1016/j.carbpol.2021.118784
- [56] Yamada, K., Kamada, N., Odomi, M., Okada, N., Nabe, T., Fujita, T., Kohno, S., Yamamoto, A., Carrageenans can regulate the pulmonary absorption of antiasthmatic drugs and their retention in the rat lung tissues without any membrane damage., *Int. J. Pharm.*, **293**, 63–72, (2005)
- [57] Pacheco-Quito, E. M., Ruiz-Caro, R., Veiga, M. D., Carrageenan: Drug Delivery Systems and Other Biomedical Applications., *Mar. Drugs*, **18**, (2020)
- [58] Khan, A. K., Saba, A. U., Nawazish, S., Akhtar, F., Rashid, R., Mir, S., Nasir, B., Iqbal, F., Afzal, S., Pervaiz, F., *et al.*, Carrageenan based bionanocomposites as drug delivery tool with special emphasis on the influence of ferromagnetic nanoparticles., *Oxid. Med. Cell. Longev.*, **2017**, (2017)
- [59] Yegappan, R., Selvaprithviraj, V., Amirthalingam, S., Jayakumar, R., Carrageenan based hydrogels for drug delivery, tissue engineering and wound healing., *Carbohydr. Polym.*, **198**, 385–400, (2018)
- [60] Li, L., Ni, R., Shao, Y., Mao, S., Carrageenan and its applications in drug delivery., *Carbohydr. Polym.*, **103**, 1–11, (2014)
- [61] Leong, K. H., Chung, L. Y., Noordin, M. I., Mohamad, K., Nishikawa, M., Onuki, Y., Morishita, M., Takayama, K., Carboxymethylation of kappa-carrageenan for intestinal-targeted delivery of bioactive macromolecules., *Carbohydr. Polym.*, **83**, 1507–1515, (2011)
- [62] Grenha, A., Gomes, M. E., Rodrigues, M., Santo, V. E., Mano, J. F., Neves, N. M., Reis, R. L., Development of new chitosan/carrageenan nanoparticles for drug delivery applications., *J. Biomed. Mater. Res. - Part A*, **92**, 1265–1272, (2010)
- [63] Alnaief, M., Obaidat, R., Mashaqbeh, H., Effect of processing parameters on preparation of carrageenan aerogel microparticles., *Carbohydr. Polym.*, **180**, 264–275, (2018)
- [64] Samal, S. K., Dash, M., Vlierberghe, S. Van, Kaplan, D. L., Chiellini, E., Blitterswijk, C. van, Moroni, L., Dubruel, P., Cationic polymers and their therapeutic potential., *Chem. Soc. Rev.*, **41**, 7147–7194, (2012)

- [65] Mohammed, M. A., Syeda, J. T. M., Wasan, K. M., Wasan, E. K., An overview of chitosan nanoparticles and its application in non-parenteral drug delivery., *Pharmaceutics*, **9**, (2017)
- [66] Li, J., Cai, C., Li, J., Li, J., Li, J., Sun, T., Wang, L., Wu, H., Yu, G., Chitosan-based nanomaterials for drug delivery., *Molecules*, **23**, 1–26, (2018)
- [67] Yeh, T. H., Hsu, L. W., Tseng, M. T., Lee, P. L., Sonjae, K., Ho, Y. C., Sung, H. W., Mechanism and consequence of chitosan-mediated reversible epithelial tight junction opening., *Biomaterials*, **32**, 6164–6173, (2011)
- [68] Bowman, K., Bowman y Leung ., **1**, 117–128, (2006)
- [69] Antoniou, J., Liu, F., Majeed, H., Qi, J., Yokoyama, W., Zhong, F., Physicochemical and morphological properties of size-controlled chitosan-tripolyphosphate nanoparticles., *Colloids Surfaces A Physicochem. Eng. Asp.*, **465**, 137–146, (2015)
- [70] Dyer, A. M., Hinchcliffe, M., Watts, P., Castile, J., Jabbal-Gill, I., Nankervis, R., Smith, A., Illum, L., Nasal delivery of insulin using novel chitosan based formulations: A comparative study in two animal models between simple chitosan formulations and chitosan nanoparticles., *Pharm. Res.*, **19**, 998–1008, (2002)
- [71] Yuan, Q., Shah, J., Hein, S., Misra, R. D. K., Controlled and extended drug release behavior of chitosan-based nanoparticle carrier., *Acta Biomater.*, **6**, 1140–1148, (2010)
- [72] Gaul, R., Ramsey, J. M., Heise, A., Cryan, S. A., Greene, C. M., *Nanotechnology approaches to pulmonary drug delivery: Targeted delivery of small molecule and gene-based therapeutics to the lung.*, *Design of Nanostructures for Versatile Therapeutic Applications*, (Elsevier Inc., 2018)., doi:10.1016/B978-0-12-813667-6.00006-1
- [73] Shukla, S. C., Singh, A., Pandey, A. K., Mishra, A., Review on production and medical applications of ε-polylysine., *Biochem. Eng. J.*, **65**, 70–81, (2012)
- [74] Rodrigues, B., Morais, T. P., Zaini, P. A., Campos, C. S., Almeida-Souza, H. O., Dandekar, A. M., Nascimento, R., Goulart, L. R., Antimicrobial activity of Epsilon-Poly-L-lysine against phytopathogenic bacteria., *Sci. Rep.*, **10**, 1–9, (2020)
- [75] Chen, S., Huang, S., Li, Y., Zhou, C., Recent Advances in Epsilon-Poly-L-Lysine and L-Lysine-Based Dendrimer Synthesis, Modification, and Biomedical Applications., *Front. Chem.*, **9**, 1–14, (2021)
- [76] Agazzi, M. L., Herrera, S. E., Cortez, M. L., Marmisollé, W. A., Azzaroni, O., Self-assembled peptide dendrigraft supraparticles with potential application in pH/enzyme-triggered multistage drug release., *Colloids Surfaces B Biointerfaces*, **190**, 110895, (2020)
- [77] Tripathi, P. K., Tripathi, S., *Dendrimers for anticancer drug delivery.*, *Pharmaceutical Applications of Dendrimers*, (Elsevier Inc., 2019)., doi:10.1016/B978-0-12-814527-2.00006-8
- [78] Yang, D. H., Kim, H. J., Park, K., Kim, J. K., Chun, H. J., Preparation of poly-L-lysine-based nanoparticles with pH-sensitive release of Curcumin for targeted imaging and therapy of liver cancer in vitro and in vivo., *Drug Deliv.*, **25**, 950–960, (2018)
- [79] Patil, N. A., Kandasubramanian, B., Functionalized polylysine biomaterials for advanced medical applications: A review., *Eur. Polym. J.*, **146**, 110248, (2021)
- [80] Legaz, S., Gilbert, S. C., Paul, S., Poly (lactic acid) and poly (lactic- co -glycolic acid) particles as versatile carrier platforms for vaccine delivery., **9**, 2703–2718, (2014)

- [81] Kim, J. H., Ryu, C. H., Chon, C. H., Kim, S., Lee, S., Maharjan, R., Kim, N. A., Jeong, S. H., Three months extended-release microspheres prepared by multi-microchannel microfluidics in beagle dog models., *Int. J. Pharm.*, **608**, 121039, (2021)
- [82] Park, K., Skidmore, S., Hadar, J., Garner, J., Park, H., Otte, A., Soh, B. K., Yoon, G., Yu, D., Yun, Y., *et al.*, Injectable, long-acting PLGA formulations: Analyzing PLGA and understanding microparticle formation., *J. Control. Release*, **304**, 125–134, (2019)
- [83] Danhier, F., Ansorena, E., Silva, J. M., Coco, R., Le Breton, A., Pr eat, V., PLGA-based nanoparticles: An overview of biomedical applications., *J. Control. Release*, **161**, 505–522, (2012)
- [84] Li, X., Jiang, X., Microfluidics for producing poly (lactic-co-glycolic acid)-based pharmaceutical nanoparticles., *Adv. Drug Deliv. Rev.*, **128**, 101–114, (2018)
- [85] Lagreca, E., Onesto, V., Di Natale, C., La Manna, S., Netti, P. A., Vecchione, R., Recent advances in the formulation of PLGA microparticles for controlled drug delivery., *Prog. Biomater.*, **9**, 153–174, (2020)
- [86] Xu, Y., Kim, C. S., Saylor, D. M., Koo, D., Polymer degradation and drug delivery in PLGA-based drug–polymer applications: A review of experiments and theories., *J. Biomed. Mater. Res. - Part B Appl. Biomater.*, **105**, 1692–1716, (2017)
- [87] Haque, S., Boyd, B. J., McIntosh, M. P., Pouton, C. W., Kaminskas, L. M., Whittaker, M., Suggested Procedures for the Reproducible Synthesis of Poly(d,l-lactide-co-glycolide) Nanoparticles Using the Emulsification Solvent Diffusion Platform., *Curr. Nanosci.*, **14**, 448–453, (2018)
- [88] Selvarajan, V., Obuobi, S., Ee, P. L. R., Silica Nanoparticles—A Versatile Tool for the Treatment of Bacterial Infections., *Front. Chem.*, **8**, 1–16, (2020)
- [89] Jeelani, P. G., Mulay, P., Venkat, R., Ramalingam, C., Multifaceted Application of Silica Nanoparticles. A Review., *Silicon*, **12**, 1337–1354, (2020)
- [90] Bao, Y., Wang, T., Kang, Q., Shi, C., Ma, J., Micelle-template synthesis of hollow silica spheres for improving water vapor permeability of waterborne polyurethane membrane., *Sci. Rep.*, **7**, 1–14, (2017)
- [91] Zhao, Y., Wang, Y., Ran, F., Cui, Y., Liu, C., Zhao, Q., Gao, Y., Wang, D., Wang, S., A comparison between sphere and rod nanoparticles regarding their in vivo biological behavior and pharmacokinetics., *Sci. Rep.*, **7**, 1–11, (2017)
- [92] Xiong, L., Bi, J., Tang, Y., Qiao, S. Z., Magnetic Core-Shell Silica Nanoparticles with Large Radial Mesopores for siRNA Delivery., *Small*, **12**, 4735–4742, (2016)
- [93] Zhang, K., Xu, L. L., Jiang, J. G., Calin, N., Lam, K. F., Zhang, S. J., Wu, H. H., Wu, G. D., Albela, B., Bonneviot, L., *et al.*, Facile large-scale synthesis of monodisperse mesoporous silica nanospheres with tunable pore structure., *J. Am. Chem. Soc.*, **135**, 2427–2430, (2013)
- [94] Huang, X., Young, N. P., Townley, H. E., Characterization and comparison of mesoporous silica particles for optimized drug delivery., *Nanomater. Nanotechnol.*, **4**, 1–15, (2014)
- [95] Moon, D., Lee, J., Langmuir **28** (2012) 12341–12347.pdf., (2012)
- [96] Arruebo, M., Fern andez-Pacheco, R., Ibarra, M. R., Santamar a, J., Magnetic nanoparticles for drug delivery The potential of magnetic NPs stems from the intrinsic properties of their magnetic cores combined with their drug loading capability and the biochemical properties that can be bestowed on them by means of a suitab., **2**, 22–32,

- (2007)
- [97] Green, M., Organometallic based strategies for metal nanocrystal synthesis., *Chem. Commun.*, 3002–3011, (2005), doi:10.1039/b501835h
- [98] Dubuisson, J., Fehlmann, A., Petignat, P., Management of presumed benign giant ovarian cysts: A minimally invasive technique using the alexis laparoscopic system., *J. Minim. Invasive Gynecol.*, **22**, 540, (2015)
- [99] Anderson, S. D., Gwenin, V. V., Gwenin, C. D., Magnetic Functionalized Nanoparticles for Biomedical, Drug Delivery and Imaging Applications., *Nanoscale Res. Lett.*, **14**, (2019)
- [100] McBain, S. C., Yiu, H. H. P., Dobson, J., Magnetic nanoparticles for gene and drug delivery., *Int. J. Nanomedicine*, **3**, 169–180, (2008)
- [101] Price, P. M., Mahmoud, W. E., Al-Ghamdi, A. A., Bronstein, L. M., Magnetic drug delivery: Where the field is going., *Front. Chem.*, **6**, 1–7, (2018)
- [102] Nair, L. S., Laurencin, C. T., Biodegradable polymers as biomaterials., *Prog. Polym. Sci.*, **32**, 762–798, (2007)
- [103] Yang, W., Peters, J. I., Williams, R. O., Inhaled nanoparticles-A current review., *Int. J. Pharm.*, **356**, 239–247, (2008)
- [104] Ungaro, F., d’Emmanuele di Villa Bianca, R., Giovino, C., Miro, A., Sorrentino, R., Quaglia, F., La Rotonda, M. I., Insulin-loaded PLGA/cyclodextrin large porous particles with improved aerosolization properties: In vivo deposition and hypoglycaemic activity after delivery to rat lungs., *J. Control. Release*, **135**, 25–34, (2009)
- [105] Kleinstreuer, C., Zhang, Z., Li, Z., Modeling airflow and particle transport/deposition in pulmonary airways., *Respir. Physiol. Neurobiol.*, **163**, 128–138, (2008)
- [106] Park, S. S., Wexler, A. S., Size-dependent deposition of particles in the human lung at steady-state breathing., *J. Aerosol Sci.*, **39**, 266–276, (2008)
- [107] Duong, T., López-Iglesias, C., Szewczyk, P. K., Stachewicz, U., Barros, J., Alvarez-Lorenzo, C., Alnaief, M., García-González, C. A., A Pathway From Porous Particle Technology Toward Tailoring Aerogels for Pulmonary Drug Administration., *Front. Bioeng. Biotechnol.*, **9**, 1–16, (2021)
- [108] Patel, B., Gupta, N., Ahsan, F., Particle engineering to enhance or lessen particle uptake by alveolar macrophages and to influence the therapeutic outcome., *Eur. J. Pharm. Biopharm.*, **89**, 163–174, (2015)
- [109] Champion, J. A., Walker, A., Mitragotri, S., Role of particle size in phagocytosis of polymeric microspheres., *Pharm. Res.*, **25**, 1815–1821, (2008)
- [110] Gehr, P., Geiser, M., Im Hof, V., Schuerch, S., Cruz-Orive, L. M., Stereological estimation of particle retention and clearance in the intrapulmonary conducting airways of the hamster lungs., *J. Aerosol Sci.*, **21**, 75–88, (1990)
- [111] Moroishi, H., Yoshida, C., Murakami, Y., A free-standing, sheet-shaped, ‘hydrophobic’ biomaterial containing polymeric micelles formed from poly(ethylene glycol)-poly(lactic acid) block copolymer for possible incorporation/release of ‘hydrophilic’ compounds., *Colloids Surfaces B Biointerfaces*, **102**, 597–603, (2013)
- [112] Murakoshi, H., Saotome, T., Fujii, Y., Ozeki, T., Takashima, Y., Yuasa, H., Okada, H., Effect of physical properties of carrier particles on drug emission from a dry powder inhaler device., *J. Drug Deliv. Sci. Technol.*, **15**, 223–226, (2005)
- [113] Ohba, N., Hydrophile-Lipophile Balance Values for O/W Emulsions Stabilized by Nonionic Surfactants. II. “Required Hydrophile-Lipophile Balance Values” of the Oil Mixture., *Bull. Chem. Soc. Jpn.*, **35**, 1021–1025,

(1962)

- [114] Todo, H., Okamoto, H., Iida, K., Danjo, K., Improvement of stability and absorbability of dry insulin powder for inhalation by powder-combination technique., *Int. J. Pharm.*, **271**, 41–52, (2004)
- [115] Hirata, M., Ishimine, T., Hirata, A., Development of Novel Method for Enzymatic Peptide Synthesis Utilizing Extractive Reaction., *J. Chem. Eng. JAPAN*, **30**, 467–477, (1997)
- [116] Silva, B. F. B., Rodríguez-Abreu, C., Vilanova, N., Recent advances in multiple emulsions and their application as templates., *Curr. Opin. Colloid Interface Sci.*, **25**, 98–108, (2016)
- [117] Harman, C. L. G., Patel, M. A., Guldin, S., Davies, G. L., Recent developments in Pickering emulsions for biomedical applications., *Curr. Opin. Colloid Interface Sci.*, **39**, 173–189, (2019)
- [118] Murakami, Y., Hirata, A., Continuous enzymatic synthesis of aspartame precursor at low pH using an extractive reaction., *J. Ferment. Bioeng.*, **84**, 264–267, (1997)
- [119] Silva, L. F. C., Kasten, G., de Campos, C. E. M., Chinelatto, A. L., Lemos-Senna, E., Preparation and characterization of quercetin-loaded solid lipid microparticles for pulmonary delivery., *Powder Technol.*, **239**, 183–192, (2013)
- [120] Edwards, D. A., Hanes, J., Caponetti, G., Hrkach, J., Ben-Jebria, A., Eskew, M. Lou, Mintzes, J., Deaver, D., Lotan, N., Langer, R., Large Porous Particles for Pulmonary Drug Delivery., *Science (80-)*, **276**, 1868–1872, (1997)
- [121] Nishimura, S., Takami, T., Murakami, Y., Porous PLGA microparticles formed by “one-step” emulsification for pulmonary drug delivery: The surface morphology and the aerodynamic properties., *Colloids Surfaces B Biointerfaces*, **159**, 318–326, (2017)
- [122] Takami, T., Murakami, Y., Unexpected and successful ‘one-step’ formation of porous polymeric particles only by mixing organic solvent and water under ‘low-energy-input’ conditions., *Langmuir*, **30**, 3329–3336, (2014)
- [123] Kadota, K., Senda, A., Tagishi, H., Ayorinde, J. O., Tozuka, Y., Evaluation of highly branched cyclic dextrin in inhalable particles of combined antibiotics for the pulmonary delivery of anti-tuberculosis drugs., *Int. J. Pharm.*, **517**, 8–18, (2017)
- [124] Alhaji, N., O’Reilly, N. J., Cathcart, H., Designing enhanced spray dried particles for inhalation: A review of the impact of excipients and processing parameters on particle properties., *Powder Technol.*, **384**, 313–331, (2021)
- [125] Toro-Sierra, J., Schumann, J., Kulozik, U., Impact of spray-drying conditions on the particle size of microparticulated whey protein fractions., *Dairy Sci. Technol.*, **93**, 487–503, (2013)
- [126] Lintingre, E., Lequeux, F., Talini, L., Tsapis, N., Control of particle morphology in the spray drying of colloidal suspensions., *Soft Matter*, **12**, 7435–7444, (2016)
- [127] Ekdahl, A., Mudie, D., Malewski, D., Amidon, G., Goodwin, A., Effect of Spray-Dried Particle Morphology on Mechanical and Flow Properties of Felodipine in PVP VA Amorphous Solid Dispersions., *J. Pharm. Sci.*, **108**, 3657–3666, (2019)
- [128] Both, E. M., *Powder morphology development during spray drying.*, (2019).
- [129] Teymouri Rad, R., Dadashzadeh, S., Vatanara, A., Alavi, S., Ghasemian, E., Mortazavi, S. A., Tadalafil nanocomposites as a dry powder formulation for inhalation, a new strategy for pulmonary arterial hypertension treatment., *Eur. J. Pharm. Sci.*, **133**, 275–286, (2019)

- [130] El-Sherbiny, I. M., Smyth, H. D. C., Controlled release pulmonary administration of curcumin using swellable biocompatible microparticles., *Mol. Pharm.*, **9**, 269–280, (2012)
- [131] Li, H. Y., Xu, E. Y., Innovative pMDI formulations of spray-dried nanoparticles for efficient pulmonary drug delivery., *Int. J. Pharm.*, **530**, 12–20, (2017)
- [132] Otake, H., Okuda, T., Okamoto, H., Development of spray-freeze-dried powders for inhalation with high inhalation performance and antihygroscopic property., *Chem. Pharm. Bull.*, **64**, 239–245, (2016)
- [133] Adali, M. B., Barresi, A. A., Boccardo, G., Pisano, R., Spray freeze-drying as a solution to continuous manufacturing of pharmaceutical products in bulk., *Processes*, **8**, (2020)
- [134] Wanning, S., Süverkrüp, R., Lamprecht, A., Pharmaceutical spray freeze drying., *Int. J. Pharm.*, **488**, 136–153, (2015)
- [135] Fukushige, K., Tagami, T., Naito, M., Goto, E., Hirai, S., Hatayama, N., Yokota, H., Yasui, T., Baba, Y., Ozeki, T., Developing spray-freeze-dried particles containing a hyaluronic acid-coated liposome–protamine–DNA complex for pulmonary inhalation., *Int. J. Pharm.*, **583**, 119338, (2020)
- [136] Okuda, T., Suzuki, Y., Kobayashi, Y., Ishii, T., Uchida, S., Itaka, K., Kataoka, K., Okamoto, H., Development of biodegradable polycation-based inhalable dry gene powders by spray freeze drying., *Pharmaceutics*, **7**, 233–254, (2015)
- [137] Mohri, K., Okuda, T., Mori, A., Danjo, K., Okamoto, H., Optimized pulmonary gene transfection in mice by spray-freeze dried powder inhalation., *J. Control. Release*, **144**, 221–226, (2010)
- [138] Liang, W., Chow, M. Y. T., Chow, S. F., Chan, H. K., Kwok, P. C. L., Lam, J. K. W., Using two-fluid nozzle for spray freeze drying to produce porous powder formulation of naked siRNA for inhalation., *Int. J. Pharm.*, **552**, 67–75, (2018)
- [139] Kaialy, W., Nokhodchi, A., Freeze-dried mannitol for superior pulmonary drug delivery via dry powder inhaler., *Pharm. Res.*, **30**, 458–477, (2013)
- [140] Hottot, A., Nakagawa, K., Andrieu, J., Effect of ultrasound-controlled nucleation on structural and morphological properties of freeze-dried mannitol solutions., *Chem. Eng. Res. Des.*, **86**, 193–200, (2008)
- [141] Mehta, M., Bhardwaj, S. P., Suryanarayanan, R., Controlling the physical form of mannitol in freeze-dried systems., *Eur. J. Pharm. Biopharm.*, **85**, 207–213, (2013)
- [142] Luo, Y. L., Yang, X. L., Xu, F., Chen, Y. S., Zhang, B., Thermosensitive PNIPAM-b-HTPB block copolymer micelles: Molecular architectures and camptothecin drug release., *Colloids Surfaces B Biointerfaces*, **114**, 150–157, (2014)
- [143] Park, J. S., Yang, H. N., Woo, D. G., Jeon, S. Y., Park, K. H., Poly(N-isopropylacrylamide-co-acrylic acid) nanogels for tracing and delivering genes to human mesenchymal stem cells., *Biomaterials*, **34**, 8819–8834, (2013)
- [144] Schmaljohann, D., Thermo- and pH-responsive polymers in drug delivery., *Adv. Drug Deliv. Rev.*, **58**, 1655–1670, (2006)
- [145] Ward, M. A., Georgiou, T. K., Thermoresponsive polymers for biomedical applications., *Polymers (Basel)*, **3**, 1215–1242, (2011)
- [146] Men, K., Liu, W., Li, L., Duan, X., Wang, P., Gou, M., Wei, X., Gao, X., Wang, B., Du, Y., *et al.*, Delivering

- instilled hydrophobic drug to the bladder by a cationic nanoparticle and thermo-sensitive hydrogel composite system., *Nanoscale*, **4**, 6425–6433, (2012)
- [147] Shen, Z., Shi, B., Zhang, H., Bi, J., Dai, S., Exploring low-positively charged thermosensitive copolymers as gene delivery vectors., *Soft Matter*, **8**, 1385–1394, (2012)
- [148] Kono, K., Nakashima, S., Kokuryo, D., Aoki, I., Shimomoto, H., Aoshima, S., Maruyama, K., Yuba, E., Kojima, C., Harada, A., *et al.*, Multi-functional liposomes having temperature-triggered release and magnetic resonance imaging for tumor-specific chemotherapy., *Biomaterials*, **32**, 1387–1395, (2011)
- [149] Yu, F., Wu, H., Tang, Y., Xu, Y., Qian, X., Zhu, W., Temperature-sensitive copolymer-coated fluorescent mesoporous silica nanoparticles as a reactive oxygen species activated drug delivery system., *Int. J. Pharm.*, **536**, 11–20, (2018)
- [150] Moyer, H. R., Delman, K. A., The role of hyperthermia in optimizing tumor response to regional therapy., *Int. J. Hyperth.*, **24**, 251–261, (2008)
- [151] Li, C. Y., Dewhirst, M. W., Hyperthermia-regulated immunogene therapy., *Int. J. Hyperth.*, **18**, 586–596, (2002)
- [152] Kojima, C., Umeda, Y., Harada, A., Kono, K., Preparation of near-infrared light absorbing gold nanoparticles using polyethylene glycol-attached dendrimers., *Colloids Surfaces B Biointerfaces*, **81**, 648–651, (2010)
- [153] Nagasaki, T., Taniguchi, A., Tamagaki, S., Photoenhancement of transfection efficiency using novel cationic lipids having a photocleavable spacer., *Bioconjug. Chem.*, **14**, 513–516, (2003)
- [154] Nagasaki, T., Wada, K., Tamagaki, S., Photo-enhancement of transfection efficiency with a novel azobenzene-based cationic lipid., *Chem. Lett.*, **32**, 88–89, (2003)
- [155] Angelos, S., Yang, Y. W., Khashab, N. M., Stoddart, J. F., Zink, J. I., Dual-controlled nanoparticles exhibiting and logic., *J. Am. Chem. Soc.*, **131**, 11344–11346, (2009)
- [156] Linsley, C. S., Wu, B. M., Recent advances in light-responsive on-demand drug-delivery systems., *Ther. Deliv.*, **8**, 89–107, (2017)
- [157] Wang, X., Xuan, Z., Zhu, X., Sun, H., Li, J., Xie, Z., Near-infrared photoresponsive drug delivery nanosystems for cancer photo-chemotherapy., *J. Nanobiotechnology*, **18**, 1–19, (2020)
- [158] Zhang, C., Li, D., Pei, P., Wang, W., Chen, B., Chu, Z., Zha, Z., Yang, X., Wang, J., Qian, H., Rod-based urchin-like hollow microspheres of Bi₂S₃: Facile synthesis, photo-controlled drug release for photoacoustic imaging and chemo-photothermal therapy of tumor ablation., *Biomaterials*, **237**, 119835, (2020)
- [159] Lu, J., Choi, E., Tamanoi, F., Zink, J. I., Light-Activated Nanoimpeller-Controlled Drug Release in Cancer Cells., *Small*, **4**, 421–426, (2008)
- [160] Rwei, A. Y., Lee, J. J., Zhan, C., Liu, Q., Ok, M. T., Shankarappa, S. A., Langer, R., Kohane, D. S., Repeatable and adjustable on-demand sciatic nerve block with phototriggerable liposomes., *Proc. Natl. Acad. Sci. U. S. A.*, **112**, 15719–15724, (2015)
- [161] Goyal, A. K., Rath, G., Faujdar, C., Malik, B., *Application and Perspective of pH-Responsive Nano Drug Delivery Systems.*, *Applications of Targeted Nano Drugs and Delivery Systems*, (Elsevier Inc., 2019)., doi:10.1016/b978-0-12-814029-1.00002-8
- [162] Cui, J., Yan, Y., Wang, Y., Caruso, F., Templated assembly of pH-labile polymer-drug particles for intracellular drug delivery., *Adv. Funct. Mater.*, **22**, 4718–4723, (2012)

- [163] Paquin, F., Rivnay, J., Salleo, A., Stingelin, N., Silva, C., Multi-phase semicrystalline microstructures drive exciton dissociation in neat plastic semiconductors., *J. Mater. Chem. C*, **3**, 10715–10722, (2015)
- [164] Johnson, R. P., Uthaman, S., Augustine, R., Zhang, Y., Jin, H., Choi, C. I., Park, I. K., Kim, I., Glutathione and endosomal pH-responsive hybrid vesicles fabricated by zwitterionic polymer block poly(L-aspartic acid) as a smart anticancer delivery platform., *React. Funct. Polym.*, **119**, 47–56, (2017)
- [165] Deirram, N., Zhang, C., Kermaniyan, S. S., Johnston, A. P. R., Such, G. K., pH-Responsive Polymer Nanoparticles for Drug Delivery., *Macromol. Rapid Commun.*, **40**, 1–23, (2019)
- [166] Feng, W., Zhou, X., He, C., Qiu, K., Nie, W., Chen, L., Wang, H., Mo, X., Zhang, Y., Polyelectrolyte multilayer functionalized mesoporous silica nanoparticles for pH-responsive drug delivery: Layer thickness-dependent release profiles and biocompatibility., *J. Mater. Chem. B*, **1**, 5886–5898, (2013)

Chapter 2

Temperature-Responsive Polysaccharide Particles for Pulmonary Drug Delivery: Preparation of the Particles and Evaluation of Temperature-responsiveness and Aerosol-dispersion Performance

1. Introduction

As shown in chapter 1, in recent years, much attention has been paid to pulmonary administration^[1-7], i.e., the administration method by which drugs are delivered to the lungs. The method has many advantages, three of which are highly prominent: (1) a simple administration (inhalation), (2) highly efficient absorption^[8-10] due to both an enormous surface area (100 m²) and a highly permeable membrane (0.1–1 μm in thickness) in alveoli, and (3) no denaturation owing to the absence of digestive enzymes in the alveoli^[10]. The drug carriers used in the pulmonary administration need to satisfy the following four conditions for the delivery of drugs to alveoli: (1) an aerodynamic ability to reach alveoli, (2) biocompatibility and ability to avoid the immune system^[11], (3) proper control of the size of the carriers (1–5 μm in an aerodynamic diameter)^[12], and (4) rapid release of drugs^[12]. To date, there are various techniques for preparing particles suitable for use in pulmonary administration (e.g., spray drying, spray freeze drying, and emulsion formation)^[13-17]. However, research has yet to identify particles satisfying all of the above conditions.

Carrageenan (CRG), a linear sulfated polysaccharide that is extracted from red algae seaweed, is an anionic natural polymer in which 3,6-anhydro-D-galactose alternately repeats α -1,3 and β -1,4 glycosidic linkages. Depending on the number of sulfone groups and the presence or absence of an anhydro bond, CRG falls into one of three classes: κ , ι , and λ . Co-existing metal salts and proteins greatly affect the physical properties of CRG. Furthermore, novel physical properties of CRG become manifest when the polymer is mixed with other polysaccharides. These properties have made CRG a widely popular component of gelling, thickening, and stabilizing agents in the food and medical industries^[18,19]. In addition, aqueous solutions of polysaccharides form a gel at appropriate temperatures (sol-gel transition), where a coil-helix transition occurs and a subsequent aggregation of helices forms physically crosslinked domains^[18,19].

In chapter 2, I prepare drug carriers for pulmonary administration: temperature-responsive polysaccharide

particles prepared through an emulsion formation and a subsequent sol-gel transition of polysaccharides (Fig. 2-1). The particles are obtained by the cooling of w/o (water-in-oil) emulsions prepared from an aqueous polysaccharide solution and a surfactant-dissolving organic solvent. Although it has been reported that κ -CRG particles can be prepared through an emulsion formation and a subsequent sol-gel transition of polysaccharides^[20], the control of the diameter of the particles is difficult, so that there has been no application of such particles to pulmonary administration. Furthermore, although the resulting particles was expected to show a temperature-responsiveness, there have been no report to clarify the temperature-responsive collapse of the particles. Therefore, in chapter 2, I tried to prepare CRG particles having a proper diameter, show their temperature-responsive behavior, and aerodynamic properties in order to achieve a highly efficient delivery of the particles to the lungs. I evaluated both of the factors affecting the preparation of the CRG particles and their *in vitro* aerosol-dispersion performance.

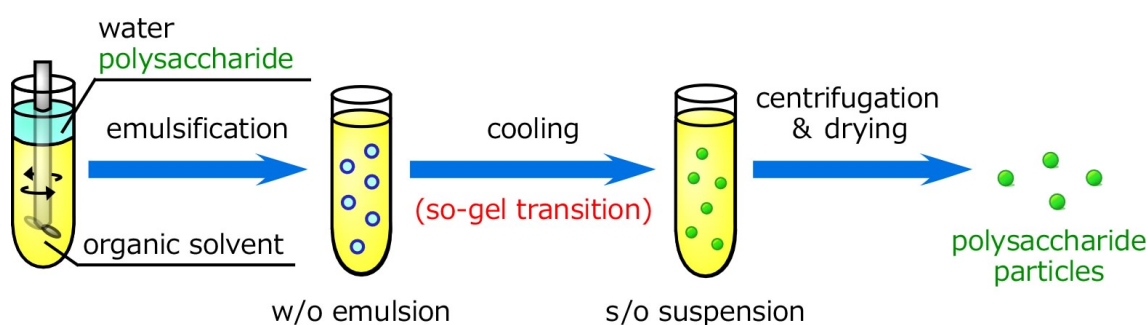


Fig. 2-1 Preparation of thermosensitive polysaccharide particles via sol-gel transition.

2. Materials and Methods

2.1. Materials

κ -Carrageenan (κ -CRG), potassium chloride, calcium lactate, and toluene were purchased from Wako Pure Chemical Industries (Osaka, Japan). Span40 (sorbitan monopalmitate), Span20 (sorbitan monolaurate), and Tween85 (polyoxyethylene sorbitan trioleate) were purchased from Tokyo Chemical Industry (Tokyo, Japan). SunSoft No.25CD (propylene glycol monostearate), and SunSoft No. 623 M (glyceryl monooleate citrate) were purchased from Taiyo Kagaku (Mie, Japan). RYOTO sugar ester S-1570 (sucrose monostearate) was purchased from Mitsubishi Chemical Foods (Tokyo, Japan). Block copolymers, poly(ethylene glycol)-b-poly(ϵ -caprolactone) (PEG-PCL)^[21,22] and poly(ethylene glycol)-b-poly(lactic acid) (PEG-PLA)^[23-25] were synthesized according to a previously reported method with a slight modification. All the other reagents were of analytical grade and were used without further purification.

2.2. Effect of surfactants on the formation and stability of s/o (solid-in-oil) suspension

κ -CRG (concentration: 1.2 w/v%) and cation (calcium lactate or potassium chloride, concentration: 32

mM) were dissolved in Milli-Q water (95°C, 40 mL). The mixture was stirred at 18,000 rpm for 30 minutes and placed in a water bath (80°C). I prepared the organic solvent by mixing toluene (10 mL) and the surfactant in a test tube. Then, I obtained a w/o emulsion by emulsifying an organic solvent containing surfactants and water containing both κ -CRG and cations with a high-speed homogenizer (NS-51K and NS-10, Microtec Co., Ltd., Japan). An s/o (solid-in-oil) suspension was obtained by gradually cooling the w/o emulsion in a water bath at room temperature. I observed the morphology of the s/o suspension with an optical microscope (BX41N-32, OLYMPUS, Japan). Span40, Span20, Tween85, SunSoft No.25CD, SunSoft No. 623M, and RYOTO sugar ester S-1570 were used as low-molecular weight surfactants, whereas PEG-*b*-PCL (PEG M_n : 3200, PCL M_n : 8300; PEG M_n : 3500, PCL M_n : 6000; PEG M_n : 3400, PCL M_n : 4700; PEG M_n : 4500, PCL M_n : 3500) and PEG-*b*-PLA (PEG M_n : 2100, PLA M_n : 5200; PEG M_n : 2700, PLA M_n : 4500; PEG M_n : 3400, PLA M_n : 4800; PEG M_n : 4100, PLA M_n : 3400) were used as high-molecular weight surfactants (Fig. 2-2). The HLB (hydrophile-lipophile balance) values of the surfactants were determined to be $20 \times (M_h/M_w)$, where M_h and M_w were respective molecular weights of hydrophilic groups and (hydrophilic + hydrophobic) groups of the molecules (Griffin's method)^[26].

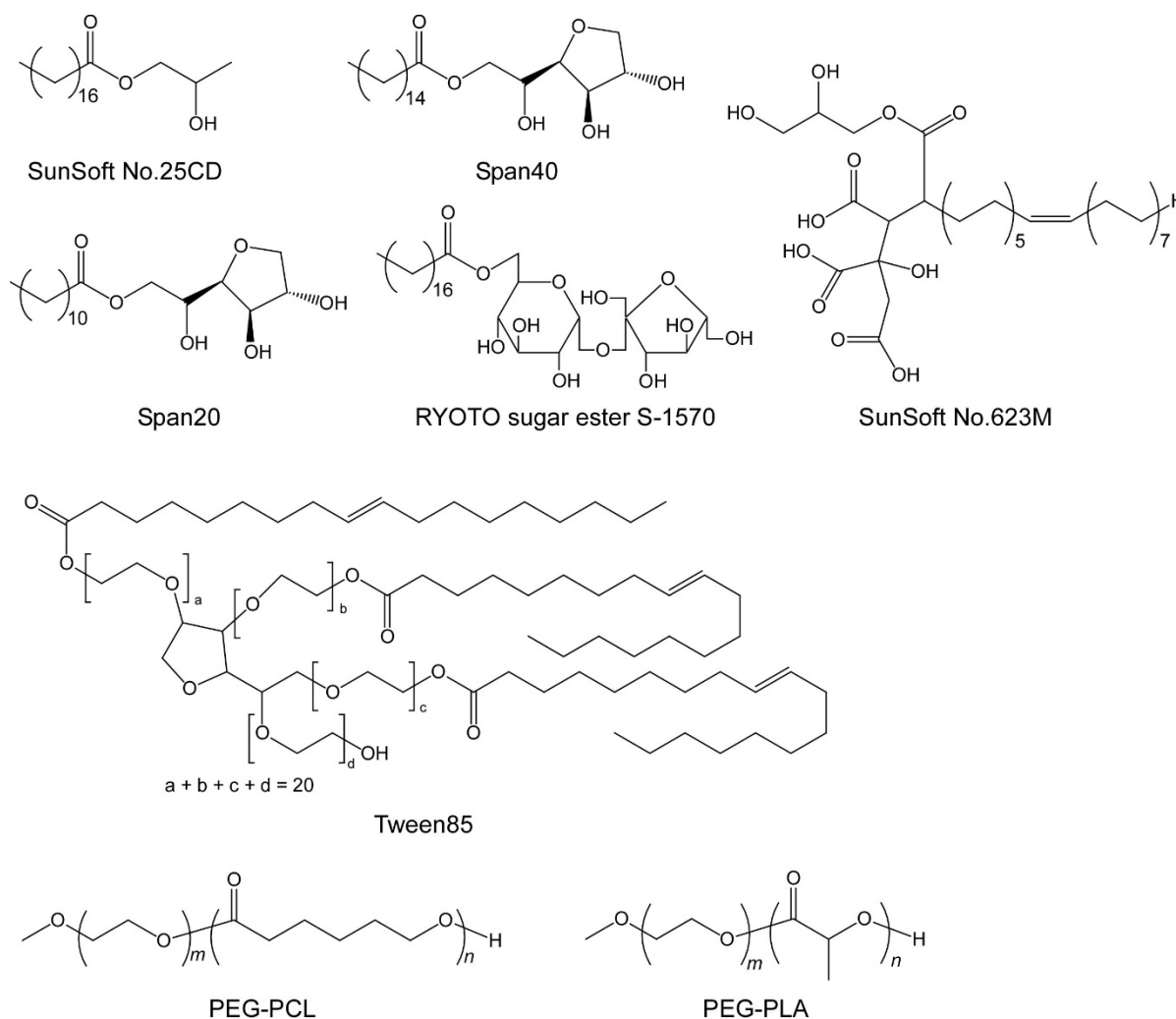


Fig. 2-2 Chemical structures of SunSoft No.25CD, Span40, SunSoft No.623M, Span20, RYOTO sugar ester S-1570, Tween85, PEG-PCL, and PEG-PLA

2.3. Preparation of κ -CRG particles and observation of their surface morphology

In order to remove the excessive surfactants present in s/o suspension obtained in section 2.2., I repeated a toluene addition and subsequent centrifugation (2000 rpm, 20 min) three times. κ -CRG particles were obtained after natural drying in a perfluoro alkoxyalkane (PFA) beaker. I prepared the specimens for SEM observation by placing the sample particles on an aluminum plate coating a thin platinum film (approximately 10.0 nm in thickness) on the sample under a reduced pressure with an MSP-1S ioncoater (Vacuum Device, Ibaraki, Japan). The surface morphology of the κ -CRG particles was observed with a scanning electron microscope (SEM, VE-9800, KEYENCE, Japan, accelerating voltage: 1.3 kV). The geometric diameter was determined from SEM images (n=100). In addition, I evaluated the effects of the concentration of the κ -CRG (1.2, 2.5, and 5.0 w/v%) on the surface morphology of the particles.

2.4. Evaluation of the temperature-responsiveness of the κ -CRG particles

The temperature-responsiveness of the κ -CRG particles was evaluated by a dynamic light scattering (DLS) measurement, a laser diffraction measurement, and optical microscope observation. First, the w/o emulsion was obtained by the emulsification (12,000 rpm, 5 min) of toluene containing PEG-PCL (PEG M_n : 3500, PCL M_n : 6000; 0.5 mM) and water containing κ -CRG (concentration was different for each measurement) and potassium chloride (32 mM) with a high-speed homogenizer. Then, s/o suspension was obtained after cooling of the w/o emulsion solutions at room temperature in a water bath. The κ -CRG particles were prepared by the removal of an excess amount of surfactants and a subsequent natural drying.

The particles prepared from s/o suspension containing κ -CRG (1.2, and 5.0 w/v% in a water phase) were dispersed in Milli-Q water (0.1 w/v%) for the determination of the particles' diameter with a DLS measurement (Zetasizer Nano-ZS, Malvern Instruments, UK) from 30 to 92°C (2°C/min). The particles prepared from s/o suspension containing κ -CRG (5.0 w/v% in a water phase) were dispersed in Milli-Q water (0.1 w/v%) for the determination of the particles' diameter with a laser diffraction measurement (LA-300, HORIBA, Japan) from 30 to 70°C, 5°C/min. The particles prepared from s/o suspension containing κ -CRG (5.0 w/v% in a water phase) were dispersed in Milli-Q water (0.1, 1.0, 2.5, and 5.0 w/v%) for observation with an optical microscope (BX 53, OLYMPUS, Japan) and a temperature raising device (HS 82 Hot Stage Controller, Mettler Toledo International, Japan).

2.5. In vitro aerosol-dispersion performance of κ -CRG particles

I prepare the w/o emulsion by undertaking the emulsification (12,000 rpm, 5 min or 16,000 rpm, 10 min) of toluene containing PEG-PCL (PEG M_n : 3500, PCL M_n : 6000; 0.5 mM) and water containing κ -CRG (concentration was different for each measurement) and potassium chloride (32 mM) with a high-speed homogenizer. Then, s/o suspension was obtained after cooling of the w/o emulsion solutions at room temperature in a water bath. The κ -CRG particles were prepared by the removal of an excess amount of surfactants and a subsequent natural drying. Aerosol-

dispersion performance of the particles was evaluated *in vitro* according to previous reports^[15,27]. Each particle (*ca.* 20 mg) was placed in a capsule made of hydroxypropylcellulose. The capsule was set into an inhalation device, a Jethaler dual chamber type (Hitachi Automotive Systems Measurement, Kanagawa, Japan, Fig. 2-3)^[28]. The particles were released into an Andersen cascade impactor (AN-200, Tokyo Dylec, Tokyo, Japan, Fig. 2-3) for 10 sec at the airflow rate of 28.3 L/min. At this airflow rate, the effective cutoff diameters and deposition sites at each stage in the cascade impactor were, in line with the manufacturer's pamphlet, as follows (Fig. 2-4): stage 1 (11 μm , nasal cavity); stage 2 (7.0 μm , pharynx); stage 3 (4.7 μm , trachea); stage 4 (3.3 μm , bronchi); stage 5 (2.1 μm , bronchi); stage 6 (1.1 μm , alveoli); stage 7 (0.65 μm , alveoli); and stage 8 (0.43 μm , alveoli). I determined the deposition ratio of each stage by measuring the weights of particles before and after inhalation. On the basis of the deposition ratio values, I determined the mass median aerodynamic diameter (MMAD), emitted dose (ED), and fine particle fraction (FPF) as follows. MMAD, the diameter that corresponds to 50% cumulative volume (i.e., a situation where 50% of the particles by weight are smaller than the MMAD), was determined from the approximation curve, which itself stemmed from diameter-cumulative volume plots. ED and FPF were obtained by the following equations^[29]:

$$\text{ED} = \frac{\text{Initial mass in capsules} - \text{Final mass in capsules}}{\text{Initial mass in capsules}} \times 100 [\%] \quad (1)$$

$$\text{FPF} = \frac{\text{Mass of particles of which } d_a \text{ is smaller than } 5 \mu\text{m}}{\text{Total mass of particles at all stages}} \times 100 [\%] \quad (2)$$

where d_a is an aerodynamic diameter. The particles after inhalation were observed by SEM. To collect the particles deposited at each stage, I adhered them to a fragment of carbon tape. I prepared the specimens for SEM observation (accelerating voltage: 1.3 kV) by placing the fragment on an aluminum plate and coating a thin platinum film (approximately 10.0 nm in thickness) on the sample under a reduced pressure with an MSP-1S ioncoater.

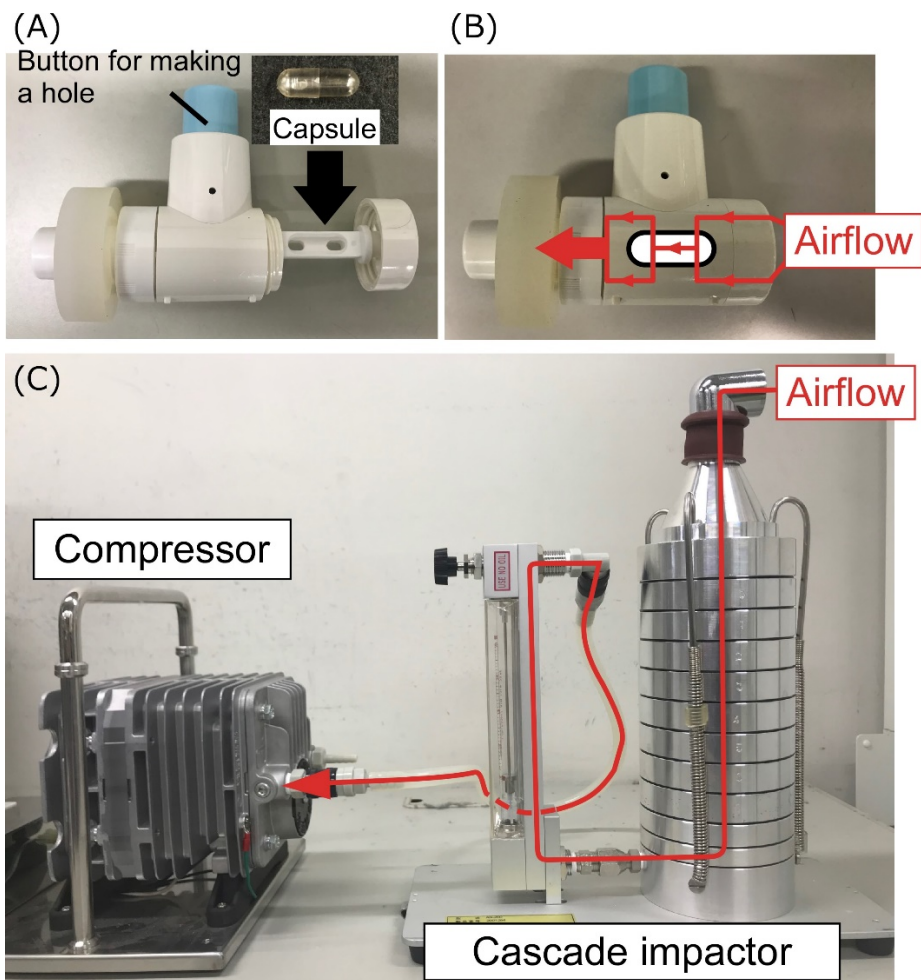


Fig. 2-3 Apparatus for evaluation of aerosol-dispersion performance: (A) (B) structure of DPI device (Jethaler) ; (C) appearance of a cascade impactor.

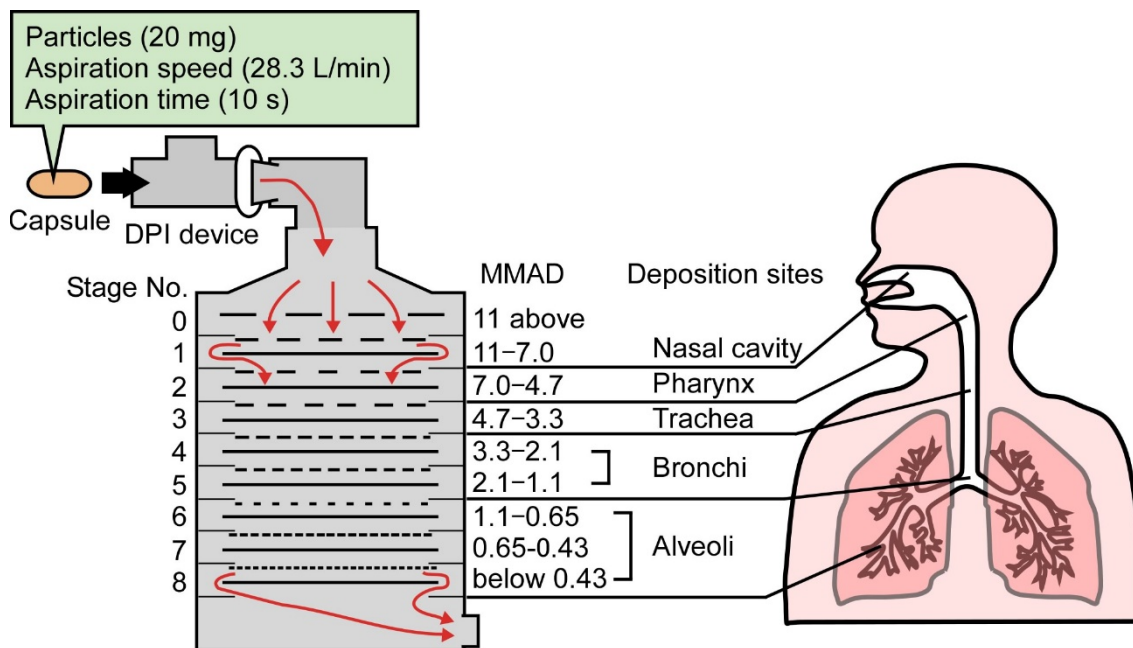


Fig. 2-4 Structure of a cascade impactor and deposition sites corresponding to each stage.

3. Results and Discussion

3.1. Effect of surfactants on the formation and stability of s/o suspension

Emulsions are systems where stable small droplets (the dispersed phase) suspend in another immiscible solution (the continuous phase)^[30-33]. The formation and stability of emulsion droplets are greatly affected by the surfactant present at the two-phase interface. In chapter 2, I evaluated the effect of surfactants on the formation and stability characterizing s/o suspensions that had been prepared from κ -CRG and surfactants with various HLB values. HLB value is an index showing the emulsion-forming ability of surfactants. Low and high HLB values were ascribed to lipophilic and hydrophilic surfactants, respectively. In general, w/o emulsions were obtained using surfactants with HLB values ranging between 3 and 8, whereas o/w emulsions were obtained using surfactants with HLB values between 9 and 18 (Fig. 2-5).

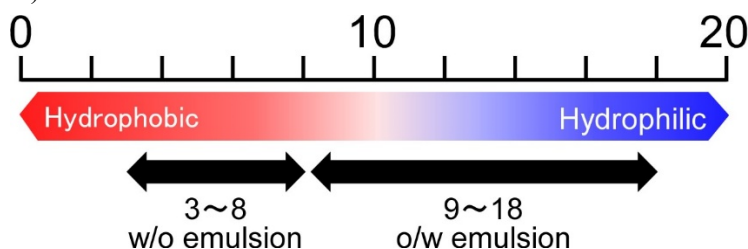


Fig. 2-5 Effect of HLB value on the formation of emulsions

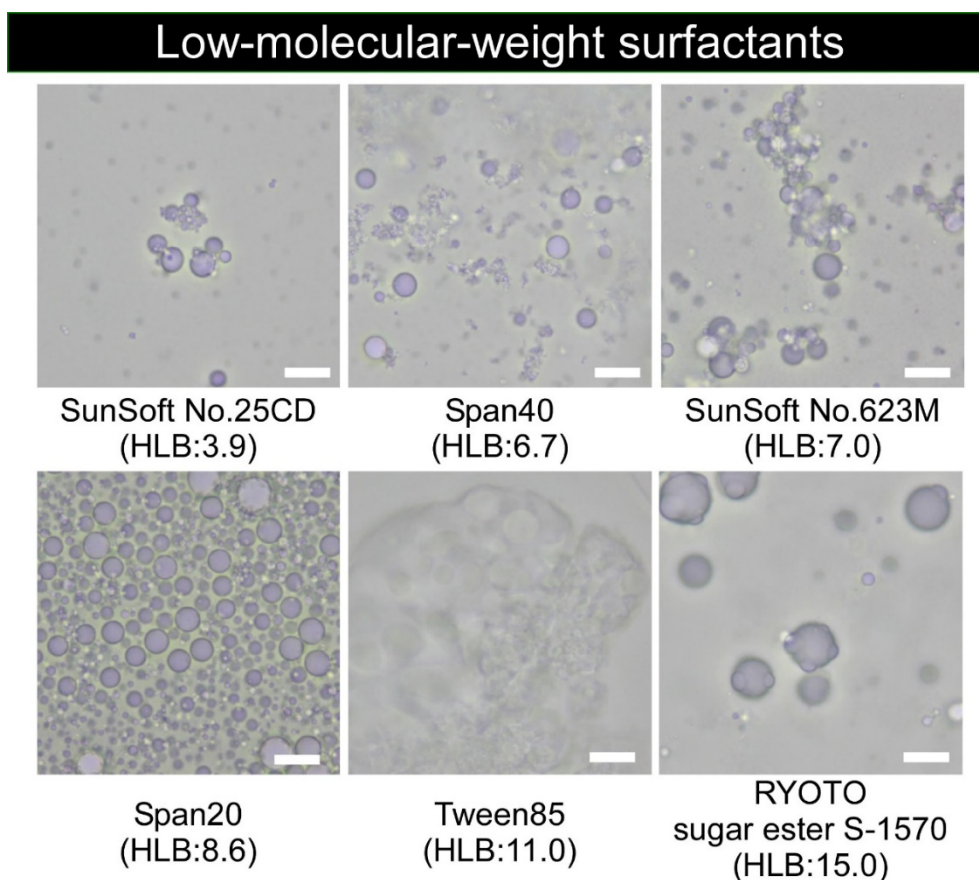


Fig. 2-6 Optical microscope images of s/o suspensions prepared in the presence of surfactants (bar: 10 μ m)

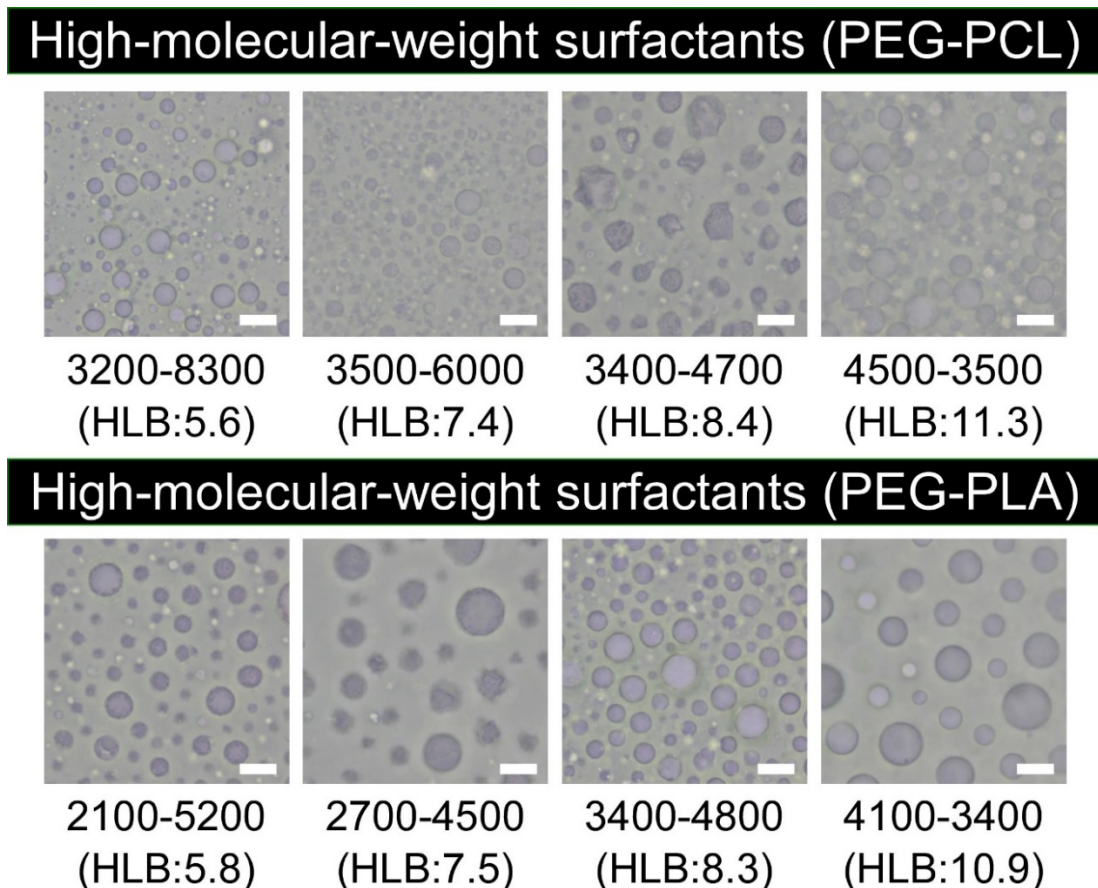


Fig. 2-7 Optical microscope images of s/o suspensions prepared in the presence of surfactants (bar: 10 μm ; A–B represents a block copolymer with a composition of PEG M_n (A) and PCL or PLA M_n (B)).

Figs. 2-6 and 2-7 show the optical microscope images of the s/o suspensions prepared in the presence of either low-molecular-weight or high-molecular-weight surfactants. As shown in Figs. 2-6 and 2-7, the stability of s/o suspensions were low in most of the cases where low-molecular-weight surfactants with an HLB less than 8 were suitable for forming w/o emulsions and where low-molecular-weight surfactants with an HLB higher than 9 were unsuitable for forming w/o emulsions. In addition, aggregates formed when surfactants having branched hydrophilic parts in the molecules (SunSoft No. 623M and Tween85) were used. I assume that the following phenomena occur when s/o suspensions coexist with polysaccharides: (1) polysaccharides in water droplets (as a main component of particles) inhibit an alignment of surfactants at solid-liquid interfaces, and (2) the contact of polysaccharides with organic solvents at unstable oil-water interfaces and the subsequent formation of aggregates occur when surfactants having branched hydrophilic parts in the molecules are used.

A highly stable and uniform s/o suspension was formed only in the presence of Span20 (HLB value: 8.6), which is considered to have a low ability to form w/o emulsions. Although, in general, a stable w/o emulsion was obtained when surfactants having an HLB value ranging from 3 to 8 was used, the changes in the density and ionization state of the aqueous phase affected the ability of surfactants to form w/o emulsions. For example, stable w/o emulsions were obtained even with surfactants having HLB values greater than 6 when the density of the aqueous phase increased and the ionization state changed regarding the coexistence of $\text{ZrO}(\text{Ac})_2$ ^[34]. In addition, the ionization

state of the aqueous phase affected the stability of the w/o emulsion, and consequently, it was necessary to select suitable surfactants in consideration of the ionization state of water^[35]. Therefore, in my experiments, only Span20 formed stable w/o emulsions even though it generally had a low ability to form w/o emulsion for two reasons: (1) the density of the aqueous phase in w/o droplets was higher than water owing to the presence of dissolving κ -CRG, and (2) the charge of the aqueous phase in w/o droplets was negative because κ -CRG has sulfone groups in the molecule. These results suggest that the stability of w/o emulsions (and s/o suspensions formed by cooling w/o emulsions) increases only when suitable surfactants with both an appropriate HLB value and an appropriate structure are used and when the surfactants have a low molecular weight.

By contrast, as shown in Figs. 2-6 and 2-7, highly stable s/o suspensions were formed regardless of the HLB value, structure, and composition of the surfactants when the surfactants had a high molecular weight. In addition, the molecular weight of the surfactants affected the stability of the s/o suspensions, and stable s/o suspension with a spherical shape was formed when high-molecular-weight surfactants were used (data not shown). These results suggest that stable w/o emulsions form as a result of the entanglement between the polymer chains of the surfactants (aligned at the oil-water interfaces) and κ -CRG molecules.

3.2. Preparation of κ -CRG particles and observation of their surface morphology

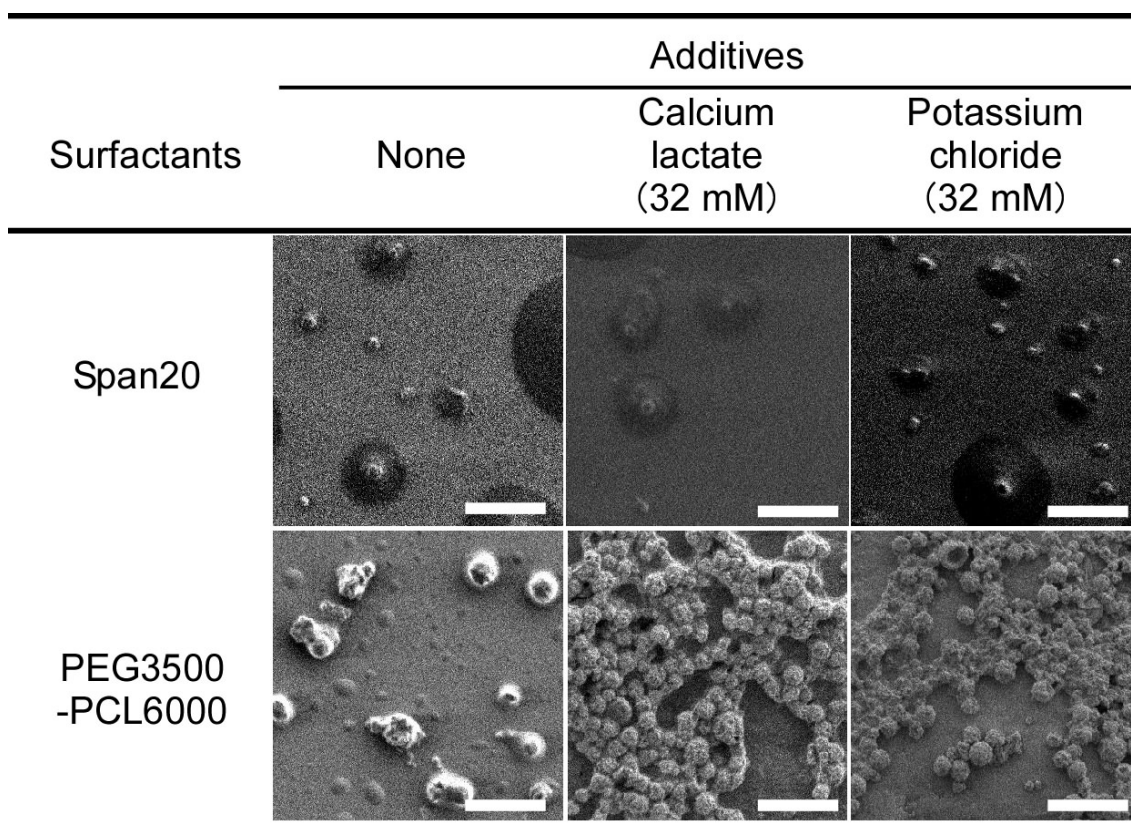


Fig. 2-8 Effect of surfactants and additives on the surface morphology of the κ -CRG particles (bar: 10 μ m; PEG3500-PCL6000 represents a block copolymer with a composition of PEG M_n (A) and PCL M_n (B)).

Fig. 2-8 shows the effect of additives (cations) and surfactants on the surface morphology of κ -CRG

particles. I used a natural drying to dry the particles to simplify the preparation process. A large number of particles having a dimpled surface were observed when a high-molecular-weight surfactant was used, whereas a small number of particles were observed when a low-molecular-weight surfactant was used. The zeta potential of the particles obtained in chapter 2 was -44.1 ± 0.78 mV for the particles prepared in the following condition: κ -CRG concentration was 5.0 w/v%, surfactant used was PEG-PCL (PEG M_n : 3500, PCL M_n : 6000), emulsification condition was 12,000 rpm \times 5 min). The value is comparable to that of κ -CRG particles in another report^[36]. Because the zeta potential is important factors affecting the particles' delivery and retention during a pulmonary administration, further detailed study evaluating zeta potential of the particles is necessary in the future.

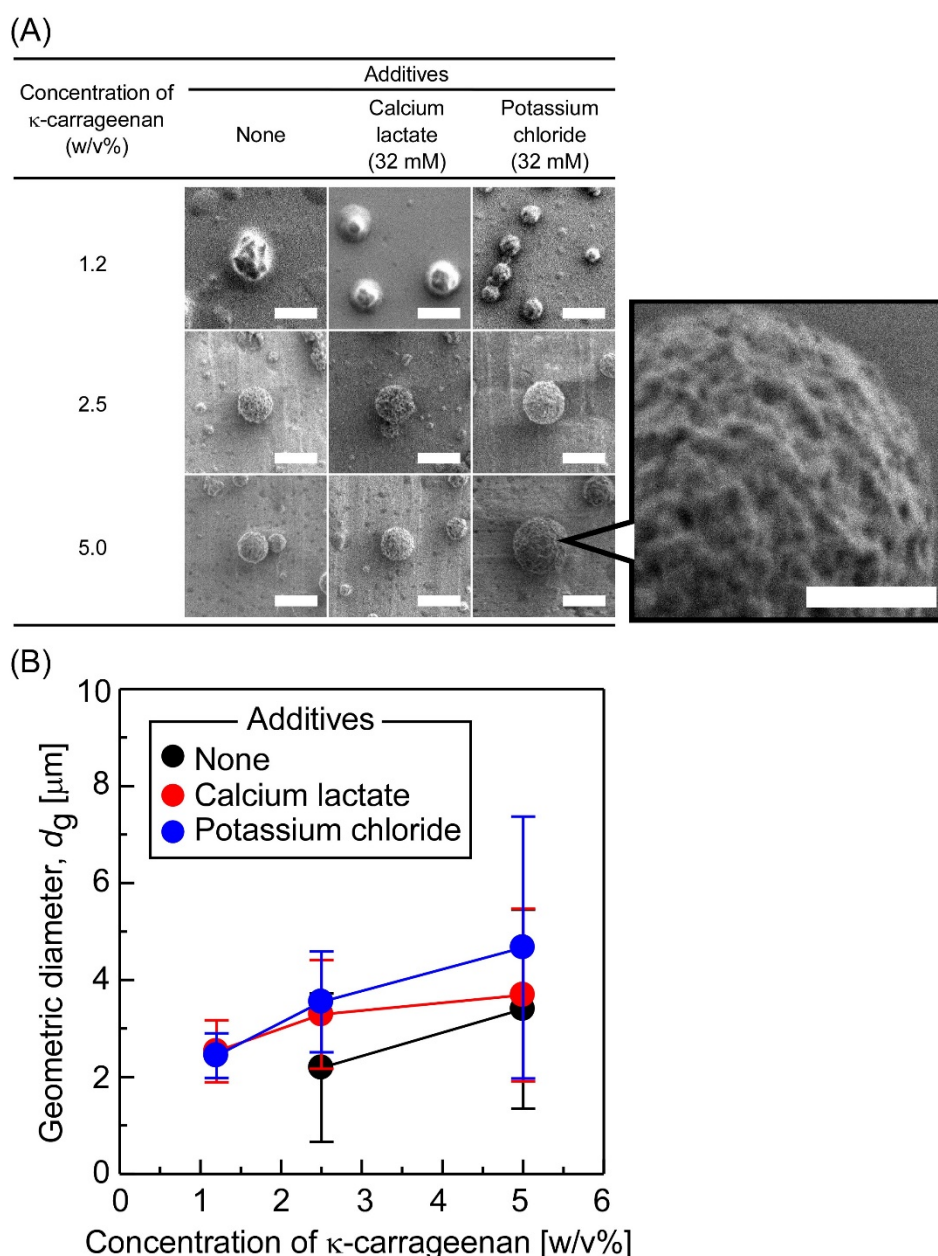


Fig. 2-9 Effect of additives and the concentration of κ -CRG on the (A) surface morphology of κ -CRG particles (bar: 5 μm or 2 μm in the enlarged image) and (B) the geometric diameter of the κ -CRG particles (error bar shows standard deviation ($n = 100$)).

Fig. 2-9 shows the effect of additives (cations) and the concentration of κ -CRG on the surface morphology and the geometric diameter of κ -CRG particles. As shown in Fig. 2-9, the number of spherical particles increased and the geometric diameter became slightly larger, as the concentration of κ -CRG increased and cations were added. The results obtained in Figs. 2-6, 2-7, 2-8, and 2-9 suggest that there are two possible important factors affecting the formation of spherical κ -CRG particles: (1) the formation of physically crosslinked domains inside the particle by the increase of concentrations of polysaccharides and cations and (2) the formation of a stable solid-liquid interfaces by using high-molecular-weight surfactants.

For the first factor, cations and polysaccharides play important roles in forming stable polysaccharide particles (Fig. 2-10). In general, cations^[37-39] and polysaccharides increase the rigidity of the polysaccharide gels because they act as cross-linkers and main chains to form gels. In my study, the concentration of κ -CRG greatly affected the surface morphology of the particles; that is, dimpled particles having a distorted shape were formed when the concentration of κ -CRG was low. The dimpled surface morphology presumably derived from a decrease of the particles' interior crosslinking density due to a decrease of the κ -CRG concentration. Therefore, at a low κ -CRG concentration, dimpled particles having a distorted shape were obtained because the amounts of water evaporated from the particles increase during a natural drying process. Takami *et al.*, have reported that "dimpled" poly(lactide-co-glycolide) (PLGA) microparticles was obtained by mixing an water and an organic solvent containing PLGA^[40]. Furthermore, Mohamed *et al.* reported the dimpled DNA-loaded PLGA microcapsules was obtained by using two surfactant series based on hydrophilic-hydrophobic balance and the molecular weight of surfactants^[41]. However, the mechanism of the dimple formation was still unclear in these cases (PLGA, a hydrophobic polymer) and the present study (κ -CRG, a hydrophilic polysaccharide).

For the second factor, high-molecular-weight surfactants play important roles in forming stable and spherical polysaccharide particles with controlled diameters. In my results, as shown in Fig. 2-6, it was difficult to obtain stable s/o suspensions when low-molecular-weight surfactants were used, whereas it was easy to obtain highly stable s/o suspensions regardless of the HLB value, structure, and composition of the surfactants when high-molecular-weight surfactants were used. These results seem to derive from the difference between the hydrogen bonding forces of the polysaccharide chain and those of surfactants. Previous research had already reported that the viscosity of polysaccharide solutions increases when PEG coexists with the polysaccharide and that this increase is due to the formation of hydrogen bonding between polysaccharide and PEG^[42,43]. In hydrophilic parts of surfactants, PEG with a molecular weight of 3500 has 79 oxygen atoms, whereas Span20 has 5 oxygen atoms. Furthermore, the number of surfactants aligned at the particle surfaces was limited, as was clear from the finding that branched low-molecular-weight surfactants reduced the stability of s/o suspension (Fig. 2-6). Therefore, strong hydrogen bonding seems to have formed between κ -CRG and PEG molecules in the aqueous phase, when there was PEG-PCL having a molecular weight and oxygen content that were suitable for alignment at the particle surfaces. In addition, a concentration gradient of surfactants formed between the solid-liquid interface and the organic phase after the removal of excessive surfactants dissolving in the organic phase. In such a gradient, the desorption of high-molecular-weight surfactants would likely be harder from particle surfaces than the of low-molecular-weight surfactants, because of strong hydrogen bonding between polysaccharides and surfactants on the solid-liquid interfaces (Fig. 2-10).

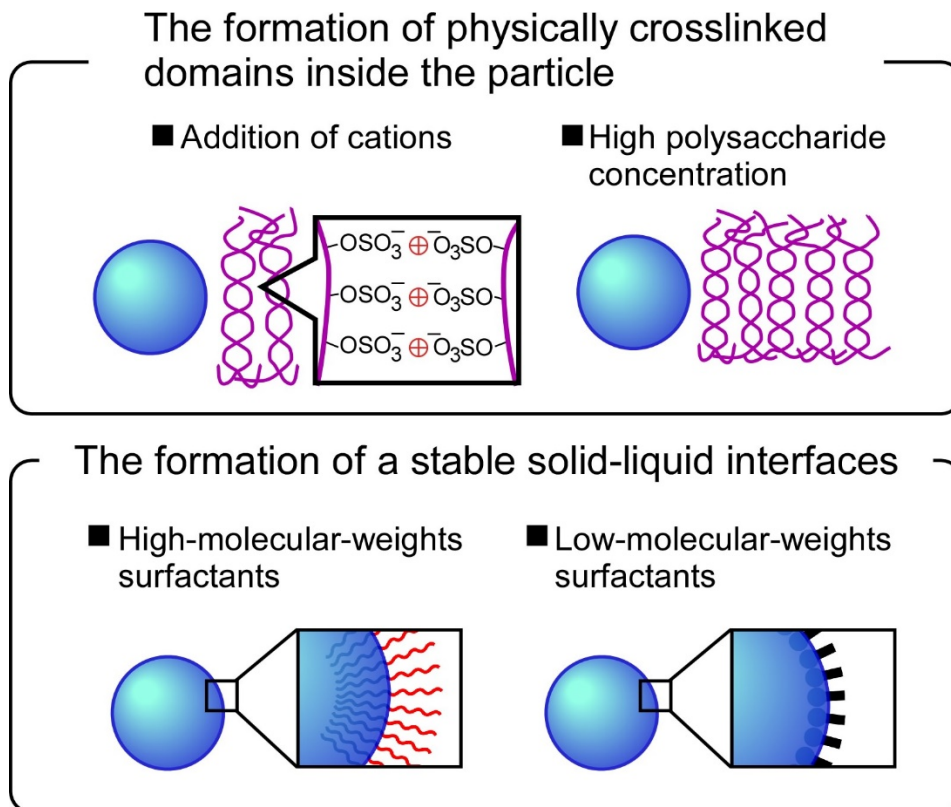


Fig. 2-10 The important factors affecting the formation of spherical κ -CRG particles.

3.3. Evaluation of the temperature-responsiveness of the κ -CRG particles

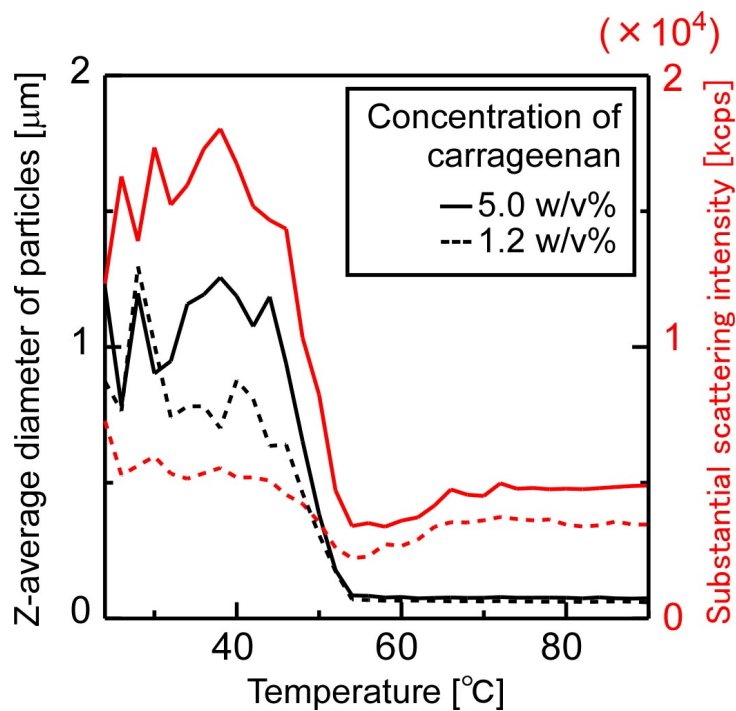


Fig. 2-11 Effect of temperature on the diameter of κ -CRG particles using DLS.

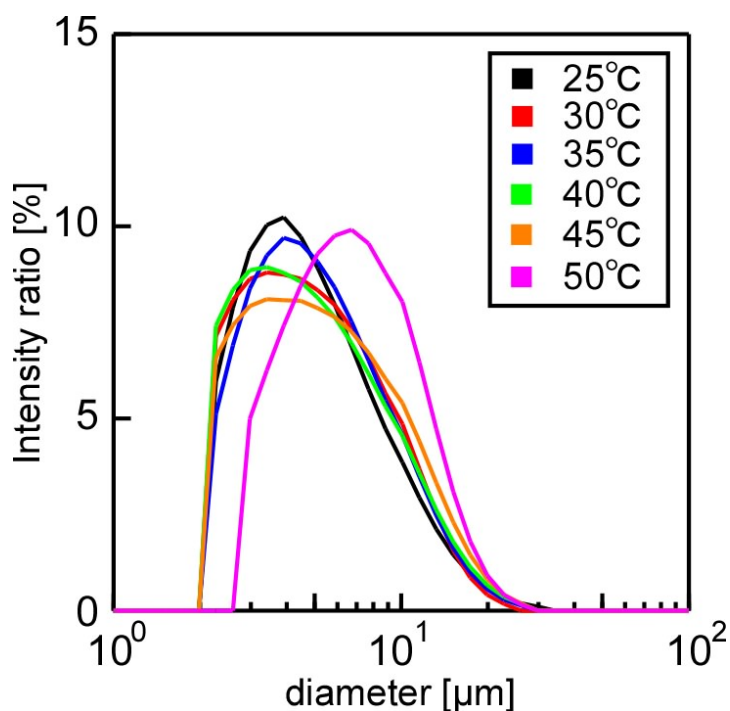


Fig. 2-12 Effect of temperature on the diameter of the κ CRG particles by laser diffraction measurements.

Temperature responsiveness of particles is important for their use with effective drug-release properties in pulmonary administration. Temperature responsiveness of κ -CRG particles was evaluated by three methods: DLS measurement, laser diffraction measurement, and optical microscope observation.

Fig. 2-11 shows the effect of temperature on the Z-average diameter and the substantial scattering intensity of the κ -CRG particles by DLS. By the comparison with a weight-average particle diameter, Z-average particle diameter (hydrodynamic particle size)^[44], which is easy to calculate from the laser intensity by DLS, was affected by high-molecular-weight compounds. Substantial scattering intensity, obtained by irradiating particles with light through a Brownian-moving, indicates the number of particles in a dispersion medium. As shown in Fig. 2-11, the Z-average particle diameters obtained by DLS were smaller than the geometric diameters observed by SEM (Fig. 2-9). This result was presumably attributable to the general phenomenon wherein light—when scattered by the dimpled structures of the surfaces of κ -CRG particles—affected the DLS-based diameters because laser irradiation determines the particle diameters in DLS measurements. In addition, regardless of the κ -CRG concentration in the particle-formation stage, both the Z-average particle diameters and substantial scattering intensity decreased at about 55°C. I presume that the particles collapsed at over 55°C because there was no significant change in either the Z-average particle diameters or substantial scattering intensity.

Fig. 2-12 shows the effect of temperature on the diameter of the κ -CRG particles by laser diffraction measurements. The particle diameter shown in Fig. 2-12 was almost the same as the geometric diameter determined by SEM (Fig. 2-9) at temperatures ranging from 25 to 50°C. The particles collapsed at temperature between 50 and 55°C because no particles were detected at over 55°C. This result was consistent with the results shown in Fig. 2-11. In addition, κ -CRG particles collapsed after seeming to have slightly swelled because the particle diameters increased just before the collapse. It was generally reported that, in alveoli, the deposited particles with an aerodynamic

diameter of 1-3 μm are phagocytosed if they are recognized by alveolar macrophages^[45,46]. Thus, κ -CRG particles having a diameter of over 3 μm can be used as drug carriers capable of releasing drugs stably in the alveoli.

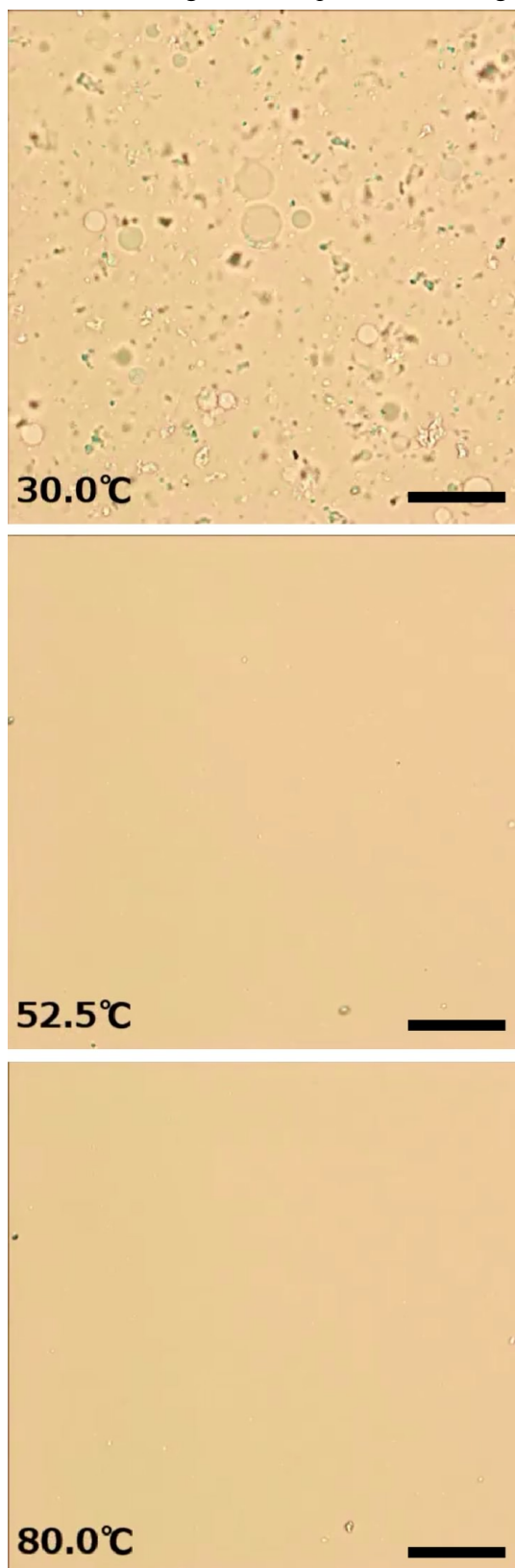


Fig. 2-13 Effect of temperature on the shape change in the κ -CRG particles evaluated by an optical microscope (bar: 50 μm).

Fig. 2-13 shows the effect of temperature on the diameters of κ -CRG particles by direct observation with an optical microscope. As shown in Fig. 2-13, although a large number of the κ -CRG particles were observed at 30°C, almost no κ -CRG particles were observed at over 52°C. Moreover, there were no changes in the appearance of the solution after 52°C; that is, no aggregation was observed. From the results uncovered by DLS measurement, laser diffraction measurements, and optical microscope observation (Figs. 2-11, 2-12 and 2-13), I can see that κ -CRG particles obviously collapsed at 52°C. In my preliminary experiments based on differential scanning calorimetry (DSC), I observed that the sol-gel transition of κ -CRG had temperature of 59°C (1.2 w/v %) and 73°C (5.0w/v%) in the presence of potassium chloride (32 mM) (detailed data not shown). It seems, therefore, that the collapse phenomenon of κ -CRG particles shown in Figs. 2-11, 2-12 and 2-13 did not occur via sol-gel transition because the κ -CRG particles collapsed at 52°C in all cases independent of κ -CRG concentrations, of solution concentrations where the κ -CRG particles were dispersed, and of particle diameters. One possibility is that the melting point of the surfactants may have affected the dissolution temperature of the κ -CRG particles. As will be discussed in chapter 3, the polymeric surfactant oriented on the surface of the κ -CRG particles may have dissolved due to the driving force of the melting point of the surfactant, and the κ -CRG particles may have finally dissolved.

3.4. *In vitro* aerosol-dispersion performance of κ -CRG particles

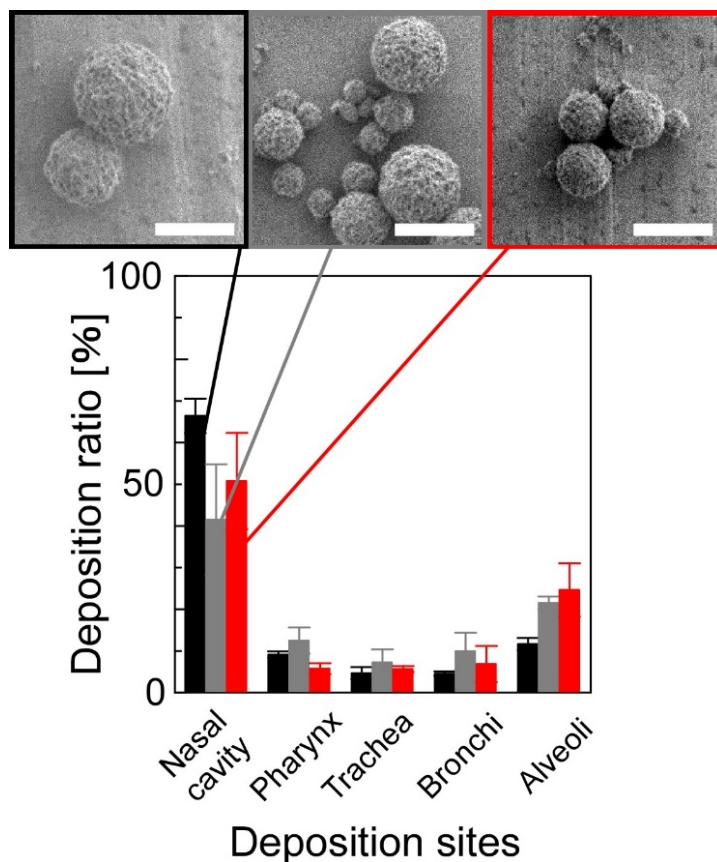


Fig. 2-14 The surface morphology (bar: 5 μm) and the deposition ratio of the κ -CRG particles on the respiratory organs (error bar shows standard deviation, $n = 3$). The particles were prepared from κ -CRG and PEG-PCL (PEG M_n : 3500, PCL M_n : 6000). The κ -CRG concentration and rate and time of emulsification were 5.0 w/v%, 12,000 rpm, and 5 min (black bar), and 5.0 w/v%, 16,000 rpm, and 10 min (gray bar), 2.5 w/v%, 16,000 rpm, and 10 min (red bar), respectively.

Fig. 2-14 shows the cascade impactor-based evaluation of the deposition ratio related to the κ -CRG particles on the respiratory organ (nasal cavity, pharynx, trachea, bronchi, and alveoli). I evaluated the deposition ratio by using three kinds of particles: particles having a geometric diameter of $5.14 \pm 2.82 \mu\text{m}$ (κ -CRG concentration: 5.0 w/v%, emulsification: 12,000 rpm, 5 min), particles having a geometric diameter of $3.76 \pm 1.66 \mu\text{m}$ (κ -CRG concentration: 5.0 w/v%, emulsification: 16,000 rpm, 10 min), and particles having a geometric diameter of $1.84 \pm 0.62 \mu\text{m}$ (κ -CRG concentration: 2.5 w/v%, emulsification: 16,000 rpm, 10 min). By changing the emulsification conditions, I obtained the particles having different geometric diameters. The emulsion solution was mechanically emulsified by a homogenizer during the preparation of the particles. Consequently, a shear stress both greatly affected the emulsion droplets dispersing in toluene and decreased the diameters of the particles. For the first particles, ED, FPF, and MMAD were $91.8 \pm 5.1\%$, $33.0 \pm 3.3\%$, and $8.52 \pm 1.20 \mu\text{m}$, for the second particles, ED, FPF, and MMAD were $29.6 \pm 11.1\%$, $52.1 \pm 7.8\%$, and $4.93 \pm 0.86 \mu\text{m}$, and for the third particles, ED, FPF, and MMAD were $31.9 \pm 11.6\%$, $50.1 \pm 9.0\%$, and $5.2 \pm 1.6 \mu\text{m}$. These results shown that the κ -CRG concentration and emulsification

conditions (corresponding to particles' geometric diameters) affected the ED and FPF, suggesting that the particles having a geometric diameter suitable for pulmonary administration were delivered to the deeper sites in lung. As shown in Fig. 2-14, the κ -CRG particles exhibited characteristic delivery behavior: although the κ -CRG particles deposited in the nasal cavity, they were delivered more to the alveoli than to the pharynx and bronchi. The dimpled surfaces of κ -CRG particles are thought to induce the particles' characteristic delivery behavior. During an inhalation, the Magnus effect occurs, i.e. an aerodynamic lift force affects a spinning sphere in a uniform flow. In general, aerodynamic lift force induced by the Magnus effect is expressed by the following equations^[47,48].

$$C_L \equiv 2L/(\rho U^2 d) = f(\alpha, Re) \quad (4)$$

where C_L is a lift coefficient, α is a rotational speed ratio defined by Nd/U , Re is a Reynolds number defined as $\rho Ud/\mu$, U is a fluid velocity, ρ is a fluid density, L is a lift force, d is a particle diameter, N is rotational speed, and μ is a viscosity coefficient. The equation shows that particles having dimpled surfaces induce a turbulent flow at a lower speed than particles having smooth surfaces because of a low Reynolds number. A turbulent flow both prevents separation of airflows from particle surfaces and maintains the Magnus effect. Furthermore, it has been known that particles having dimpled surfaces fly into airflows easily because of both dimple-induced disturbances of boundary layers on surfaces and the consequent decrease in the air resistance pulling the particles backward^[47,49-51]. On the other hand, it is difficult to execute the highly efficient delivery of particles to alveoli even though the particles exhibit high FPF values^[52-54]. In some other reports, even when the particles had high FPF values (ranging from 50 to 70%), the amount of deposition on the stage corresponding to alveoli was low, whereas the amount of deposition on the stage corresponding to bronchi was high. In contrast, in the present study, the particles exhibiting high FPF values delivered predominantly to the alveoli. My results clearly demonstrate that κ -CRG particles with dimpled surfaces obtained in the present study can likely serve as drug carriers targeting alveoli.

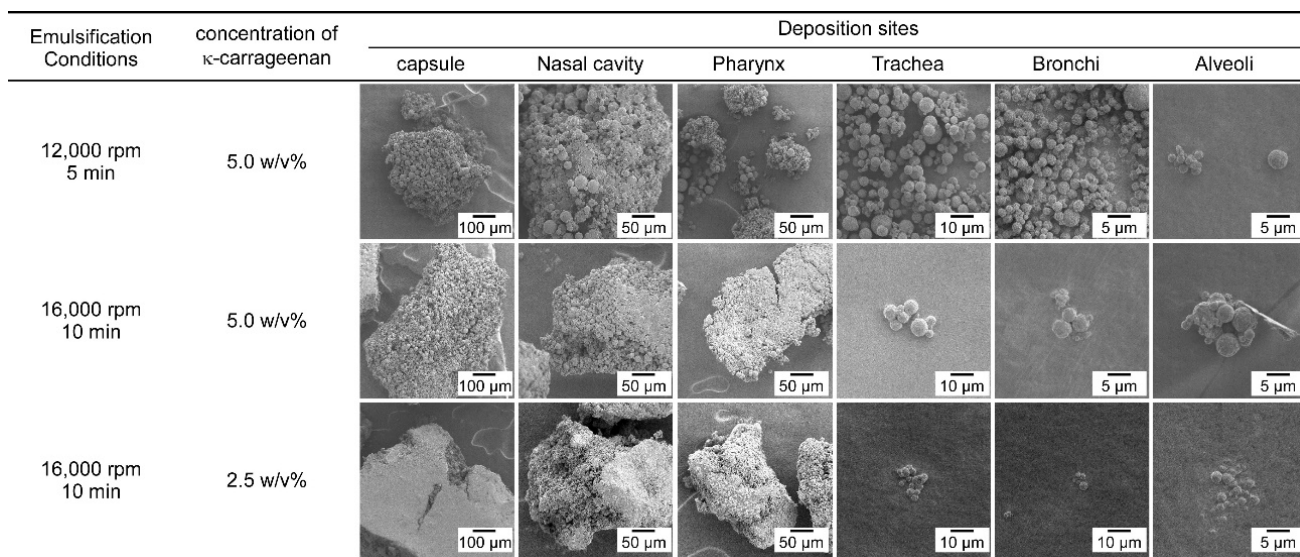


Fig. 2-15 SEM images of the polymeric particles on the site of deposition. The particles were prepared from κ -CRG and PEG-PCL (PEG M_n : 3500, PCL M_n : 6000). The κ -CRG concentration and rate and time of emulsification were 5.0 w/v%, 12,000 rpm, and 5 min, and 5.0 w/v%, 16,000 rpm, and 10 min, 2.5 w/v%, 16,000 rpm, and 10 min (red bar), respectively.

Fig. 2-15 shows SEM images of the κ -CRG particles on the site of deposition after inhalation through the cascade impactor. As shown in Fig. 2-15, the aggregates of the particles were deposited in the capsule, nasal cavity, and pharynx. Particles prepared under the emulsification condition of 16,000 rpm \times 10 min tended to form aggregates, whereas unaggregated small particles were delivered to alveoli. An aggregation of materials is generally caused by some forces including Van der Waals force^[55] and electrostatic force^[56]. In particular, Van der Waals force, which is dominant in the aggregation phenomenon of fine particles, is theoretically expressed as^[55]:

$$F = \frac{AR}{12H^2} + \frac{A}{6\pi H^3} \pi r^3 \quad (5)$$

where F is Van der Waals force, A is the Hamaker constant, H is the separation distance between two particle surfaces, and r is the radius of the contact area. Apparently from this equation, the aggregation of particles was reduced when their surfaces were dimpled because F decreases as H increases. On the other hand, it is generally understood that polysaccharide particles are easy to aggregate (for example, polysaccharide particles prepared by spray drying exhibit both low fluidity and high aggregability^[14-16]). The high aggregability of the polysaccharide particles obtained in this study suggests that the intermolecular interaction of polysaccharide is most dominant and that the particles are not completely covered with the surfactants. As shown in Figs. 2-14 and 2-15, although the particles prepared under the emulsification condition of 12,000 rpm \times 5 min were released from the capsules (i.e., ED was very high, *ca.* 92%), the large mass of the particles deposited in the nasal cavity and pharynx because the particles formed aggregates, and consequently, the FPF value was considered to be low (*ca.* 33%). By contrast, regarding the

particles prepared under the emulsification condition of 16,000 rpm×10 min, their release from the capsules was difficult (i.e., ED was only *ca.* 30%) because of the unexpected formation of large aggregates. Furthermore, in both cases, the MMAD of the particles exhibited a larger value than their geometric diameter. This result suggests that the density of the particles is considered to be high according to the following equation^[57]:

$$MMAD \cong d_g \sqrt{\frac{\rho_p}{\rho_1}} \quad (6)$$

where d_g is geometric diameter, ρ_p is particle density, and ρ_1 is 1 g/cm³. There have been many reports^[52,58–60] showing that “porous” particles having a low density (less than 0.4 g/cm³) easily fly into the airflow, so that the particles are delivered to alveoli. However, interestingly, my results show that the κ -CRG particles tend to be delivered to alveoli despite the particles’ high density. One possible explanation of this result hinges on the “dimpled” surface of the κ -CRG particles. There have been a few report concerning dimpled hydrophobic (such as PLGA) microparticles^[40,41] having a hydrophobic core where hydrophobic drugs can be loaded. However, since the polysaccharide microparticles can contain hydrophilic drugs^[36], the dimpled κ -CRG microparticles can be used as drug carriers that can deliver hydrophilic drugs to the lungs. Furthermore, there is a possibility that the optimization of emulsification conditions further reduces the particles’ MMAD because the conditions affect the particles’ geometric diameters.

4. Conclusion

In chapter 2, I have prepared drug carriers for pulmonary administration: temperature-responsive polysaccharide particles prepared through an emulsion formation and a subsequent sol-gel transition of polysaccharides. The particles are obtained by the cooling of w/o emulsions prepared from an aqueous polysaccharide solution and a surfactant-dissolving organic solvent. I found that highly stable s/o suspensions were formed regardless of the HLB value, structure, and composition of the surfactants when high-molecular-weight surfactants were used. There are two possible important factors affecting the formation of spherical κ -CRG particles: (1) the formation of physically crosslinked domains inside the particle by the increase of concentrations of polysaccharides and cations and (2) the formation of a stable solid-liquid interfaces by using high-molecular-weight surfactants. I obtained stable polysaccharide particles with dimpled surfaces. From the results of my DLS measurement, laser diffraction measurements, and optical microscope observations, the κ -CRG particles in chapter 2 exhibited temperature responsiveness to collapse at 52°C. Furthermore, as a result of the *in vitro* aerosol dispersion performance of the κ -CRG particles with the cascade impactor, I identified the characteristic delivery behavior of κ -CRG particles: the particles delivered more to the alveoli than to the pharynx and bronchi, despite their high density. From the perspective of material design, the present study shows that the “dimpled” κ -CRG particles can likely stay in the alveoli so that high therapeutic effects will likely occur in pulmonary administration.

5. Reference

- [1] Patton, J. S., Byron, P. R., Inhaling medicines: Delivering drugs to the body through the lungs., *Nat. Rev. Drug Discov.*, **6**, 67–74, (2007)
- [2] Loira-Pastoriza, C., Todoroff, J., Vanbever, R., Delivery strategies for sustained drug release in the lungs., *Adv. Drug Deliv. Rev.*, **75**, 81–91, (2014)
- [3] Bangyozova, M., Jordanova, A., Tsanova, A., Stoyanova, V., Tasheva, E., Ivanova, K., Todorov, R., Hristova, E., Lalchev, Z., Application of axisymmetric drop shape analysis and brewster angle microscopy for assessment of clinical samples from prematurely born infants with NRDS., *Colloids Surfaces A Physicochem. Eng. Asp.*, **519**, 187–191, (2017)
- [4] Takeuchi, I., Taniguchi, Y., Tamura, Y., Ochiai, K., Makino, K., Effects of L-leucine on PLGA microparticles for pulmonary administration prepared using spray drying: Fine particle fraction and phagocytotic ratio of alveolar macrophages., *Colloids Surfaces A Physicochem. Eng. Asp.*, **537**, 411–417, (2018)
- [5] Takeuchi, I., Tetsuka, Y., Nii, T., Shinogase, M., Makino, K., Inhalable nanocomposite particles using amino acids with improved drug content and humidity resistance., *Colloids Surfaces A Physicochem. Eng. Asp.*, **529**, 387–393, (2017)
- [6] Gonçalves, A., Nikmaram, N., Roohinejad, S., Estevinho, B. N., Rocha, F., Greiner, R., McClements, D. J., Production, properties, and applications of solid self-emulsifying delivery systems (S-SEDS) in the food and pharmaceutical industries., *Colloids Surfaces A Physicochem. Eng. Asp.*, **538**, 108–126, (2018)
- [7] d'Angelo, I., Conte, C., La Rotonda, M. I., Miro, A., Quaglia, F., Ungaro, F., Improving the efficacy of inhaled drugs in cystic fibrosis: Challenges and emerging drug delivery strategies., *Adv. Drug Deliv. Rev.*, **75**, 92–111, (2014)
- [8] Bosquillon, C., Lombry, C., Pr eat, V., Vanbever, R., Influence of formulation excipients and physical characteristics of inhalation dry powders on their aerosolization performance., *J. Control. Release*, **70**, 329–339, (2001)
- [9] Wall, D. A., Pulmonary absorption of peptides and proteins., *Drug Deliv.*, **2**, 1–20, (1995)
- [10] Agu, R. U., Ugwoke, M. I., Armand, M., Kinget, R., Verbeke, N., Agu - 2001 - Lung as a route for peptide administration., (2001)
- [11] Nair, L. S., Laurencin, C. T., Biodegradable polymers as biomaterials., *Prog. Polym. Sci.*, **32**, 762–798, (2007)
- [12] Park, S. S., Wexler, A. S., Size-dependent deposition of particles in the human lung at steady-state breathing., *J. Aerosol Sci.*, **39**, 266–276, (2008)
- [13] Li, H. Y., Xu, E. Y., Innovative pMDI formulations of spray-dried nanoparticles for efficient pulmonary drug delivery., *Int. J. Pharm.*, **530**, 12–20, (2017)
- [14] Kadota, K., Senda, A., Tagishi, H., Ayorinde, J. O., Tozuka, Y., Evaluation of highly branched cyclic dextrin in inhalable particles of combined antibiotics for the pulmonary delivery of anti-tuberculosis drugs., *Int. J. Pharm.*, **517**, 8–18, (2017)
- [15] Gallo, L., Bucal a, V., Ram irez-Rigo, M. V., Formulation and Characterization of Polysaccharide Microparticles for Pulmonary Delivery of Sodium Cromoglycate., *AAPS PharmSciTech*, **18**, 1634–1645, (2017)

- [16] Zhou, M., Wang, T., Hu, Q., Luo, Y., Low density lipoprotein/pectin complex nanogels as potential oral delivery vehicles for curcumin., *Food Hydrocoll.*, **57**, 20–29, (2016)
- [17] Patil, J. S., Sarasija, S., Pulmonary drug delivery strategies: A concise, systematic review., *Lung India*, **29**, 44–49, (2012)
- [18] Yegappan, R., Selvaprithviraj, V., Amirthalingam, S., Jayakumar, R., Carrageenan based hydrogels for drug delivery, tissue engineering and wound healing., *Carbohydr. Polym.*, **198**, 385–400, (2018)
- [19] Li, L., Zhang, Z., Xu, J., A generalized nonlinear H^∞ filter design for discrete-time Lipschitz descriptor systems., *Nonlinear Anal. Real World Appl.*, **15**, 1–11, (2014)
- [20] Alnaief, M., Obaidat, R., Mashaqbeh, H., Effect of processing parameters on preparation of carrageenan aerogel microparticles., *Carbohydr. Polym.*, **180**, 264–275, (2018)
- [21] Anzai, R., Murakami, Y., Poly(ϵ -caprolactone) (PCL)-polymeric micelle hybrid sheets for the incorporation and release of hydrophilic proteins., *Colloids Surfaces B Biointerfaces*, **127**, 292–299, (2015)
- [22] Anzai, R., Takami, T., Uchida, Y., Murakami, Y., Poly(ϵ -caprolactone) (PCL) hybrid sheets containing polymeric micelles: Effects of inner structures on the material properties of the sheets., *Mater. Sci. Eng. C*, **72**, 325–331, (2017)
- [23] Uchida, Y., Murakami, Y., Colloids and Surfaces B : Biointerfaces Trilayered polymeric micelle : A newly developed macromolecular assembly that can incorporate hydrophilic compounds., *Colloids Surfaces B Biointerfaces*, **79**, 198–204, (2010)
- [24] Kanakubo, Y., Ito, F., Murakami, Y., Novel one-pot facile technique for preparing nanoparticles modified with hydrophilic polymers on the surface via block polymer-assisted emulsification/evaporation process., *Colloids Surfaces B Biointerfaces*, **78**, 85–91, (2010)
- [25] Moroishi, H., Yoshida, C., Murakami, Y., A free-standing, sheet-shaped, ‘hydrophobic’ biomaterial containing polymeric micelles formed from poly(ethylene glycol)-poly(lactic acid) block copolymer for possible incorporation/release of ‘hydrophilic’ compounds., *Colloids Surfaces B Biointerfaces*, **102**, 597–603, (2013)
- [26] Ohba, N., Hydrophile-Lipophile Balance Values for O/W Emulsions Stabilized by Nonionic Surfactants. II. “Required Hydrophile-Lipophile Balance Values” of the Oil Mixture., *Bull. Chem. Soc. Jpn.*, **35**, 1021–1025, (1962)
- [27] Todo, H., Okamoto, H., Iida, K., Danjo, K., Improvement of stability and absorbability of dry insulin powder for inhalation by powder-combination technique., *Int. J. Pharm.*, **271**, 41–52, (2004)
- [28] Murakoshi, H., Saotome, T., Fujii, Y., Ozeki, T., Takashima, Y., Yuasa, H., Okada, H., Effect of physical properties of carrier particles on drug emission from a dry powder inhaler device., *J. Drug Deliv. Sci. Technol.*, **15**, 223–226, (2005)
- [29] Psimadas, D., Georgoulas, P., Valotassiou, V., Loudos, G., Molecular Nanomedicine Towards Cancer :, *J. Pharm. Sci.*, **101**, 2271–2280, (2012)
- [30] Harman, C. L. G., Patel, M. A., Guldin, S., Davies, G. L., Recent developments in Pickering emulsions for biomedical applications., *Curr. Opin. Colloid Interface Sci.*, **39**, 173–189, (2019)
- [31] Hirata, M., Ishimine, T., Hirata, A., Development of Novel Method for Enzymatic Peptide Synthesis Utilizing Extractive Reaction., *J. Chem. Eng. JAPAN*, **30**, 467–477, (1997)

- [32] Murakami, Y., Hirata, A., Continuous enzymatic synthesis of aspartame precursor at low pH using an extractive reaction., *J. Ferment. Bioeng.*, **84**, 264–267, (1997)
- [33] Silva, B. F. B., Rodríguez-Abreu, C., Vilanova, N., Recent advances in multiple emulsions and their application as templates., *Curr. Opin. Colloid Interface Sci.*, **25**, 98–108, (2016)
- [34] Lee, M. H., Tai, C. Y., Lu, C. H., Synthesis of Spherical Zirconia by Reverse Emulsion Precipitation - Effects of Surfactant Type -, *Korean J. Chem. Eng.*, **16**, 818–822, (1999)
- [35] Gacek, M. M., Berg, J. C., Effect of surfactant hydrophile-lipophile balance (HLB) value on mineral oxide charging in apolar media., *J. Colloid Interface Sci.*, **449**, 192–197, (2015)
- [36] Obaidat, R. M., Alnaief, M., Mashaqbeh, H., Investigation of Carrageenan Aerogel Microparticles as a Potential Drug Carrier., *AAPS PharmSciTech*, **19**, 2226–2236, (2018)
- [37] Robal, M., Brenner, T., Matsukawa, S., Ogawa, H., Truus, K., Rudolph, B., Tuvikene, R., Monocationic salts of carrageenans: Preparation and physico-chemical properties., *Food Hydrocoll.*, **63**, 656–667, (2017)
- [38] Norton, I. T., Goodall, D. M., Morris, E. R., Rees, D. A., Role of cations in the conformation of iota and kappa carrageenan., *J. Chem. Soc. Faraday Trans. 1 Phys. Chem. Condens. Phases*, **79**, 2475–2488, (1983)
- [39] Michel, A. S., Mestdagh, M. M., Axelos, M. A. V., Physico-chemical properties of carrageenan gels in presence of various cations., *International Journal of Biological Macromolecules*, vol. 21, 195–200, (1997)
- [40] Takami, T., Murakami, Y., Development of PEG-PLA/PLGA microparticles for pulmonary drug delivery prepared by a novel emulsification technique assisted with amphiphilic block copolymers., *Colloids Surfaces B Biointerfaces*, **87**, 433–438, (2011)
- [41] Mohamed, F., Van Der Walle, C. F., PLGA microcapsules with novel dimpled surfaces for pulmonary delivery of DNA., *Int. J. Pharm.*, **311**, 97–107, (2006)
- [42] Geetha, D., Prakash, M., Ramesh, P. S., Rakkappan, C., Compatibility studies of polysaccharide-based natural and synthetic polymers in aqueous solution., *Compos. Interfaces*, **17**, 239–245, (2010)
- [43] Basavaraju, K. C., Demappa, T., Rai, S. K., Miscibility studies of polysaccharide Xanthan gum and PEO (polyethylene oxide) in dilute solution., *Carbohydr. Polym.*, **69**, 462–466, (2007)
- [44] Maguire, C. M., Rösslein, M., Wick, P., Prina-Mello, A., Characterisation of particles in solution—a perspective on light scattering and comparative technologies., *Sci. Technol. Adv. Mater.*, **19**, 732–745, (2018)
- [45] Liang, Z., Ni, R., Zhou, J., Mao, S., Recent advances in controlled pulmonary drug delivery., *Drug Discov. Today*, **20**, 380–389, (2015)
- [46] Oberdörster, G., Lung dosimetry: Pulmonary clearance of inhaled particles., *Aerosol Sci. Technol.*, **18**, 279–289, (1993)
- [47] Smits, A. J., A new aerodynamic model of a golf ball in flight., in *Science and Golf II*, 433–442, (Taylor & Francis, 2002)., doi:10.4324/9780203474709-58
- [48] Liu, R. J., Xiao, R., Ye, M., Liu, Z., Analysis of particle rotation in fluidized bed by use of discrete particle model., *Adv. Powder Technol.*, **29**, 1655–1663, (2018)
- [49] Zhou, B., Wang, X., Guo, W., Gho, W. M., Tan, S. K., Control of flow past a dimpled circular cylinder., *Exp. Therm. Fluid Sci.*, **69**, 19–26, (2015)
- [50] Aoki, K., Ohike, A., Yamaguchi, K., Nakayama, Y., Flying Characteristics and Flow Pattern of a Sphere with

- Dimples., *J. Vis.*, **6**, 67–76, (2003)
- [51] Aoki, K., Kinoshita, Y., Nagase, J., Nakayama, Y., Dependence of Aerodynamic Characteristics and Flow Pattern on Surface Structure of a Baseball., *J. Vis.*, **6**, 185–193, (2003)
- [52] Nishimura, S., Takami, T., Murakami, Y., Porous PLGA microparticles formed by “one-step” emulsification for pulmonary drug delivery: The surface morphology and the aerodynamic properties., *Colloids Surfaces B Biointerfaces*, **159**, 318–326, (2017)
- [53] Eedara, B. B., Rangnekar, B., Sinha, S., Doyle, C., Cavallaro, A., Das, S. C., Development and characterization of high payload combination dry powders of anti-tubercular drugs for treating pulmonary tuberculosis., *Eur. J. Pharm. Sci.*, **118**, 216–226, (2018)
- [54] Yildiz-Peköz, A., Akbal, O., Tekarslan, S. H., Sagirli, A. O., Mulazimoglu, L., Morina, D., Cevher, E., Preparation and characterization of doripenem-loaded microparticles for pulmonary delivery., *J. Aerosol Med. Pulm. Drug Deliv.*, **31**, 347–357, (2018)
- [55] Visser, J., Van der Waals and other cohesive forces affecting powder fluidization., *Powder Technol.*, **58**, 1–10, (1989)
- [56] Peart, J., Powder electrostatics: Theory, techniques and applications., *KONA Powder Part. J.*, **19**, 34–45, (2001)
- [57] Vanbever, R., Mintzes, J. D., Wang, J., Nice, J., Chen, D., Batycky, R., Langer, R., Edwards, D. A., Formulation and physical characterization of large porous particles for inhalation., *Pharmaceutical Research*, vol. 16, 1735–1742, (1999)
- [58] Edwards, D. A., Hanes, J., Caponetti, G., Hrkach, J., Ben-Jebria, A., Eskew, M. Lou, Mintzes, J., Deaver, D., Lotan, N., Langer, R., Large Porous Particles for Pulmonary Drug Delivery., *Science (80-.)*, **276**, 1868–1872, (1997)
- [59] Meenach, S. A., Kim, Y. J., Kauffman, K. J., Kanthamneni, N., Bachelder, E. M., Ainslie, K. M., Synthesis, optimization, and characterization of camptothecin-loaded acetalated dextran porous microparticles for pulmonary delivery., *Mol. Pharm.*, **9**, 290–298, (2012)
- [60] Lee, E. S., Kwon, M. J., Na, K., Bae, J. H., Protein release behavior from porous microparticle with lysozyme/hyaluronate ionic complex., *Colloids Surfaces B Biointerfaces*, **55**, 125–130, (2007)

Chapter 3

Temperature-Responsive Polysaccharide Particles for Pulmonary Drug Delivery: Control of Dissolution and Release Properties

1 Introduction

As shown in chapter 1, pulmonary administration is a method of inhaling drugs and absorbing them into the body via the lungs^[1-4]. The pulmonary administration is a very effective route of drug administration due to the various advantages of the pulmonary administration^[5,6]. Pulmonary administration would be superior not only for pulmonary diseases but also for urgent diseases due to rapid absorption of drugs^[7,8]. Drug carriers should release the drugs rapidly after reaching the alveoli to take advantage of the immediate effects of pulmonary administration. To date, drug carriers that respond to stimuli such as pH, light, and temperature have been developed^[9-15]. In pH-responsive drug carriers, the encapsulated drugs are released when the structures of the molecules forming the carriers or their intermolecular interactions change due to pH changes in the environment. In tumor tissues, it is known that the pH is changed by substances, such as lactic acid and glutathione, produced during the metabolic process, and the drugs can be released locally into the tumor in response to such pH changes^[9,10]. In photo-responsive drug carriers, the encapsulated drugs are released when the structure of the molecules forming the carriers is altered by light irradiation (e.g., light-induced structural change of molecules via cis-trans isomerization reactions^[11-13]). In addition, temperature-responsive drug carriers release the encapsulated drugs by changing the steric configuration and physical properties of the molecules forming the carrier in response to temperature^[14,15].

As shown in chapter 1, carrageenan (CRG) is a linear sulfated polysaccharide and an anionic natural polymer. Depending on the number of sulfone groups and the presence or absence of an anhydro bond, CRG is classified into three types: κ , ι , and λ ^[16-18]. Drug carriers formed from CRG are expected to improve the encapsulation efficiency of positively charged compounds and control their release characteristics by electrostatic interaction.

In chapter 2, I have developed temperature-responsive polysaccharide microparticles by an emulsion technique utilizing the sol-gel transition phenomenon of CRG. By adjusting the emulsification conditions, I successfully prepared κ -CRG microparticles with controlled particle diameters and high pulmonary delivery capacity. However, the response temperature of the obtained particles was relatively high (50°C), and further reduction of the response temperature of the particles could not be achieved by simply utilizing the sol-gel transition of CRG. In chapter 3, I report (1) the development of temperature-responsive CRG particles by changing the melting point of

the polymeric surfactants (amphiphilic block copolymers that stabilize emulsions) used in particle formation by varying the composition of the block copolymers and using the melting of the surfactants oriented on the particle surface as the driving force for particle dissolution, and (2) the investigation of the release properties of the particles.

2. Material and method

2.1. Materials

κ -Carrageenan (κ -CRG), potassium chloride, methylene blue trihydrate (Mb), and toluene were purchased from Wako Pure Chemical Industries (Osaka, Japan). ι -Carrageenan (ι -CRG) was purchased from Sigma-Aldrich (St. Louis MO, USA). Block copolymers, poly(ethylene glycol)-*b*-poly(ϵ -caprolactone) (PEG-PCL)^[19,20] and poly(ethylene glycol)-*b*-poly(lactic acid) (PEG-PLA)^[21–23], were synthesized according to a previously reported method with a slight modification. All the other reagents were of analytical grade and were used without further purification.

2.2. Evaluation of the effect of the composition of the block copolymers on their melting point using DSC (differential scanning calorimetry)

The synthesized polymeric surfactant (each 3 mg) was placed in a sealed aluminum pan. DSC (differential scanning calorimetry) measurements were performed at a heating rate of 10°C/min to obtain a series of DSC curves from 20 to 90°C using DSC (DSC-60A plus, SHIMADZU, Japan) to determine the melting point of the block copolymers (Table 3-1, 3-2).

Table 3-1 Characterization of the PEG-PCL

Code ¹⁾	PEG (including methoxy terminus)		PCL	PEG-PCL (including methoxy terminus)	
	$M_n^{2)}$	$M_w/M_n^{2)}$	$M_n^{3)}$	$M_n^{2,3)}$	$M_w/M_n^{2)}$
PEG2100-PCL9700	2100	1.08	9700	11800	1.40
PEG3000-PCL7000	3000	1.09	7000	10000	1.38
PEG3100-PCL1000	3100	1.07	1000	4100	1.18
PEG3200-PCL2800	3200	1.08	2800	6000	1.30
PEG3200-PCL8300	3200	1.07	8300	11500	1.43
PEG3400-PCL4800	3400	1.05	4800	8200	1.36

PEG3500-PCL4300	3500	1.09	4300	7800	1.35
PEG3500-PCL4300	3500	1.06	4300	9500	1.33
PEG4500-PCL3500	4500	1.03	3500	8000	1.18
PEG4500-PCL5300	4500	1.03	5300	9800	1.24
PEG4500-PCL8800	4500	1.03	8800	13300	1.27

- 1) In the notation of PEG p -PCL q , p and q represent the M_n of the PEG and PCL blocks, respectively;
 2) gel permeation chromatography (GPC); 3) $^1\text{H-NMR}$

Table 3-2 Characterization of PEG-PCL

Code ¹⁾	PEG (including methoxy terminus)		PLA	PEG-PLA(including methoxy terminus)	
	$M_n^{2)}$	$M_w/M_n^{2)}$	$M_n^{3)}$	$M_n^{2,3)}$	$M_w/M_n^{2)}$
PEG1400-PLA2800	1400	1.10	2800	4200	1.31
PEG2000-PLA7300	2000	1.08	7300	9300	1.28
PEG2100-PLA5200	2100	1.06	5200	7300	1.28
PEG2400-PLA7300	2400	1.07	7300	9700	1.22
PEG2500-PLA2200	2500	1.07	2200	4700	1.17
PEG3400-PLA4800	3400	1.05	4800	8200	1.25
PEG4600-PLA4400	4600	1.07	4400	9000	1.13
PEG4800-PLA2500	4800	1.06	2500	7300	1.09
PEG5100-PLA8500	5100	1.07	8500	13600	1.08

- 1) In the notation of PEG p -PLA q , p and q represent the M_n of the PEG and PLA blocks, respectively;
 2) gel permeation chromatography (GPC); 3) $^1\text{H-NMR}$

2.3. Preparation of κ -CRG, ι -CRG and mixed κ,ι -CRG particles with or without methylene blue (Mb) and observation of their surface morphology

CRG particles were prepared according to the method in chapter 2. A polysaccharide solution was prepared by dissolving κ -CRG (2.5 w/v%), ι -CRG (2.5 w/v%), and potassium chloride (32 mM) in Milli-Q water (70°C, 40 mL). Mb (7.3 mM) was dissolved in the polysaccharide solution only when the compound release behavior of the particles was evaluated. I prepared the organic solvent by mixing toluene (10 mL) and the synthesized polymeric surfactant (PEG-PCL (0.5 mM) or PEG-PLA (0.5 or 2.0 mM)). Then, I obtained w/o (water-in-oil) emulsions by emulsifying (70°C, 16000 rpm, 10 min) the organic solvent and the polysaccharide solution (0.35 g) using a high-speed homogenizer (NS-51 K and NS-10, Microtec Co., Ltd., Japan). The resulting emulsion solutions were gradually cooled at 25°C in a water bath and washed three times by centrifugation (1500 rpm, 20 min), and toluene was added to remove excess polymeric surfactants. The κ -CRG, ι -CRG and κ,ι -CRG microparticles were obtained after natural drying in a perfluoro alkoxyalkane (PFA) beaker. I prepared the specimens for scanning electron microscope (SEM) observation by placing the sample microparticles on an aluminum plate coating a thin platinum film (approximately 10.0 nm in thickness) on the sample under a reduced pressure with an MSP-1S ioncoater (Vacuum Device, Ibaraki, Japan). The surface morphology of the sample microparticles were observed using SEM (VE-9800, KEYENCE, Japan, acceleration voltage of 1.3 kV).

2.4. Evaluation of the temperature-responsiveness of the CRG particles

The temperature-responsiveness of the κ -CRG particles was evaluated by DSC measurements and optical microscopy. The κ -CRG particles (5 mg) were placed in a sealed aluminum pan. The DSC measurements were performed at a heating rate of 10°C to obtain a series of DSC curves from 20 to 90°C using DSC. The κ -CRG particles were dispersed in Milli-Q water (1 w/v%) for observation using both an optical microscope (BX 53, OLYMPUS, Japan) and a temperature raising device (HS 82 Hot Stage Controller, Mettler Toledo International, Japan).

2.5. Evaluation of profiles depicting the release of Mb from the CRG particles

According to a previous report^[24], the profiles depicting the release of the Mb from the CRG microparticles were evaluated using a dialysis method ($n = 3$). The phosphate-buffered saline (PBS) solution (4 mL) in which the particles (4 mg) were dispersed was dialyzed against a PBS solution (36 mL) through a Spectra/Por6 dialysis membrane (molecular weight cut-off: 10000; Spectrum, Houston, TX, USA). The sustained releases of the Mb from the CRG microparticles were performed under gentle stirring. Each sample were collected periodically (1 mL/15 min), and the same amount of PBS (1 mL) was added to the solution. I evaluated the temperature response of the nanoparticle and microparticle release behavior under two different experimental conditions: (1) keeping the solvent temperature constant (10 or 70°C) for 3 h, and (2) shifting the solvent temperature from 10°C to 70°C 1 h after starting the measurement. The following (1) and (2) were determined using a spectrofluorometer (FP-6500, JASCO Co., Japan, $\lambda_{\text{ex}} = 640 \text{ nm}$, $\lambda_{\text{em}} = 680 \text{ nm}$ for Mb): (1) the release ratio of the Mb from the CRG microparticles and (2)

the encapsulation ratio and encapsulation efficiency of the Mb in the CRG microparticles. The encapsulation ratio and encapsulation efficiency of the Mb in the CRG microparticles were calculated using the following (1) and (2) equations.

$$\text{Encapsulation ratio: } \frac{\text{weight of the Mb in the CRG microparticles (mg)}}{\text{weight of the CRG microparticles (mg)}} \times 100 \text{ [\%]} \quad (1)$$

$$\text{Encapsulation efficiency: } \frac{\text{weight of the Mb in the CRG microparticles (mg)}}{\text{weight of the Mb (mg)}} \times 100 \text{ [\%]} \quad (2)$$

3. Results and Discussion

3.1. Determination of the effect of the compositions of polymeric surfactants on their melting point using DSC

Polymeric surfactants can be used to improve the stability of w/o emulsions and solid-in-oil (s/o) suspensions during the formation of polysaccharide particles. In chapter 2, I successfully prepared the κ -CRG particles with diameters of several micrometers by using polymeric surfactants (amphiphilic block copolymers) that significantly increased the interfacial stability of the w/o emulsions.

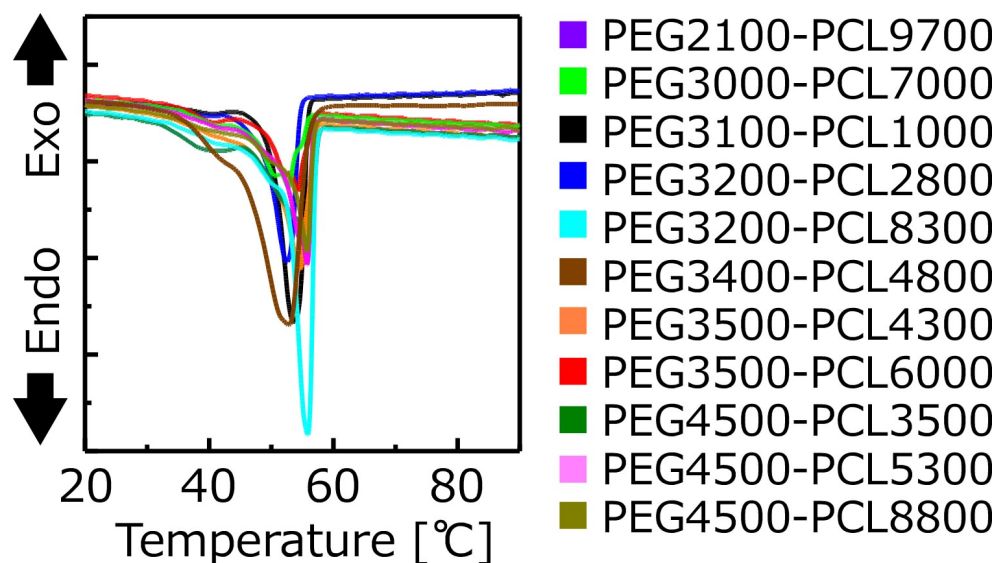


Fig. 3-1 Effect of the composition of PEG-PCL on the melting point using DSC.

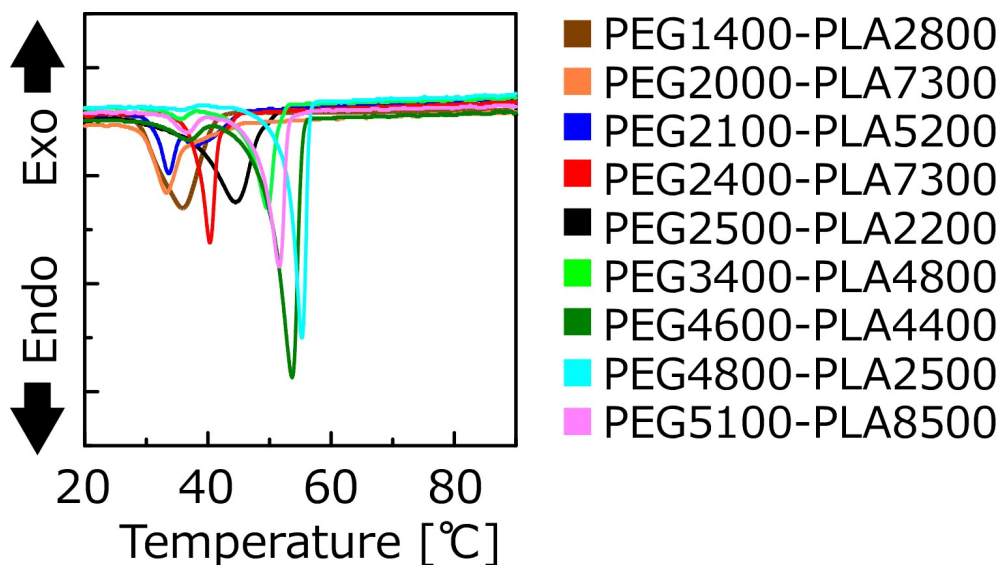


Fig. 3-2 Effect of the composition of PEG-PLA on the melting point using DSC.

Figs. 3-1 and 3-2 show the effect of the composition of PEG-PCL or PEG-PLA on the melting point. As shown in Fig. 3-1, the melting point (corresponding to endothermic peak) of PEG-PCLs is approximately 55°C, and is independent of their molecular weight. For some compositions, the melting point of PEG-PCL has been reported in other studies to be 50–60°C^[25–27], indicating that it is almost independent of the molecular weight. Because PEG-PCL is a synthetic polymer with a high crystallinity^[25,28–30], it can be considered that crystallinity has a dominant effect and intermolecular hydrogen bonding and molecular mobility have little effect on the melting point. In contrast, the melting point of PEG-PLAs vary significantly depending on their molecular weight. For instance, PEG2000-PLA7300 and PEG4800-PLA2500 have the lowest and highest melting point of 33.2°C and 55.2°C, respectively. The melting point of the PEG-PLA species tended to decrease as the molecular weight of the PEG block decreased. Although there are no systematic examples of the molecular weight dependence of the melting point of PEG-PLA, it has been reported that the melting point of PEG-PLA varies noticeably with the molecular weight^[31–35]. Compared to PEG-PCL, PEG-PLA is less crystalline and forms amorphous structures^[32,36]. Therefore, the change in the molecular weight may affect the intermolecular hydrogen bonding, resulting in a large variation in the melting point depending on the molecular weight. Compared with this doctoral thesis in chapter 2 concerning the temperature-responsive behavior of κ -CRG particles, the dissolution temperature of the particles and melting point of the polymeric surfactant were almost similar. This implies that the dissolution temperature of the particles may be arbitrarily controlled by using the melting of the surfactant as a driving force for particle dissolution.

3.2. Surface morphology of κ -CRG particles

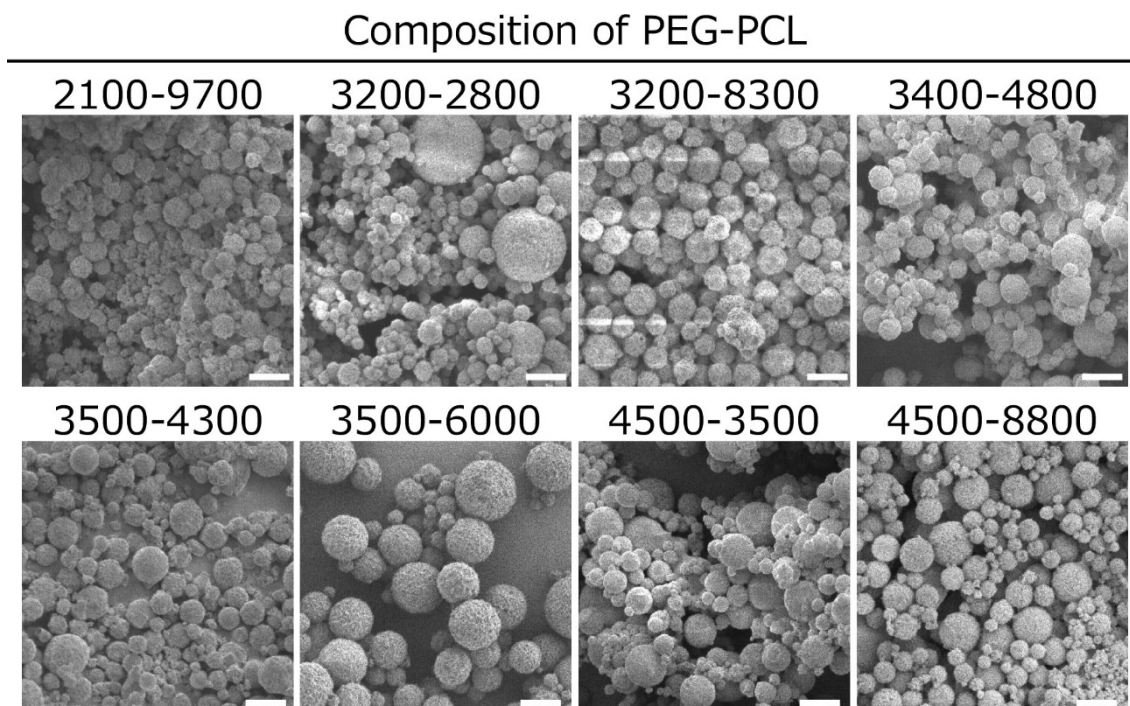


Fig. 3-3 Effect of composition of the PEG-PCL on the formation and surface morphology of the κ -CRG particles as observed using SEM (bar: 5 μ m). The concentration of the PEG-PCL is 0.5 mM.

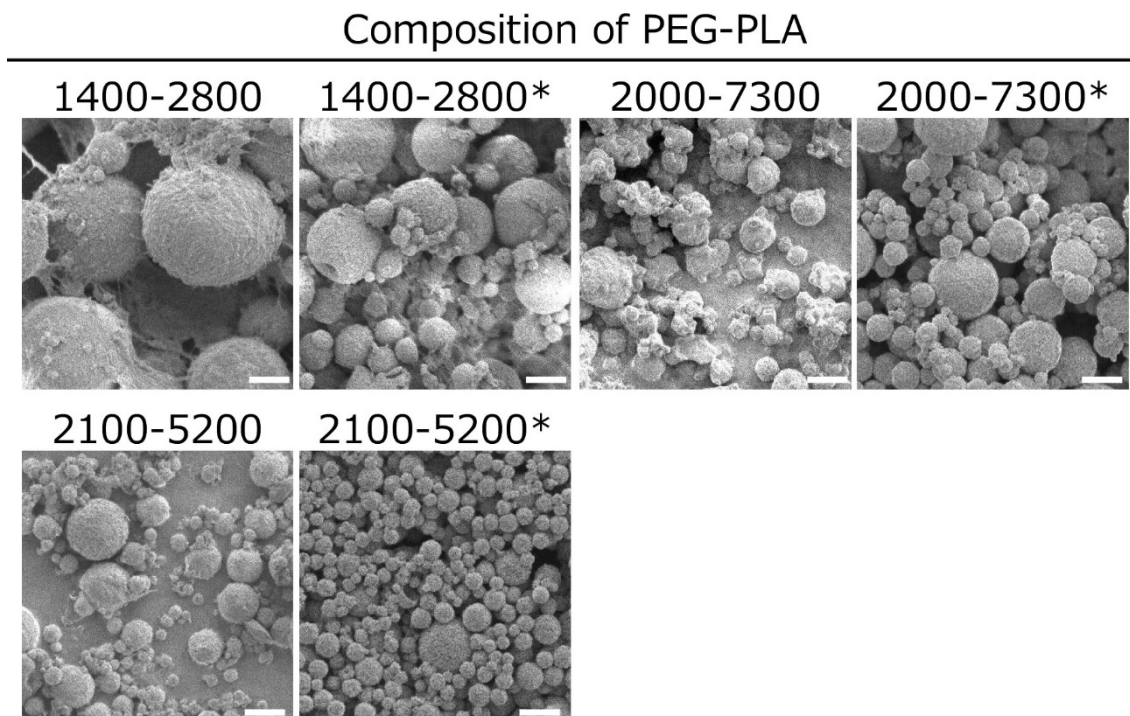


Fig. 3-4 Effect of composition of the PEG-PLA on the formation and surface morphology of the κ -CRG particles as observed using SEM (bar: 5 μ m). The concentration of the PEG-PLA is 0.5 mM (for compositions marked with *, the concentration is 2 mM).

Figs. 3-3 and 3-4 show the effect of composition of the polymeric surfactants on the formation and surface morphology of the κ -CRG particles, which was observed using SEM. As shown in Fig. 3-3, when PEG-PCL was used as a polymeric surfactant, spherical particles with a uniform surface morphology were obtained regardless of the molecular weight of PEG-PCL. As shown in Fig. 3-4, when PEG-PLA was used as a polymeric surfactant, particles with distorted shapes were obtained when its concentration was 0.5 mM during s/o suspension preparation. Upon increasing the concentration to 2 mM, particles with almost the same morphology as those formed in the presence of PEG-PCL were obtained. It is postulated that the crystallinity of PEG-PCL is responsible for the formation of spherical particles at a PEG-PCL concentration lower than that of PEG-PLA. As described in the previous section, because PEG-PCL is crystalline, the water-cooling operation during the formation of the s/o suspension may have crystallized the PEG-PCL oriented on the particle surface and increased the structural stability of the particles. In contrast, because PEG-PLA is amorphous, the amount of PEG-PLA oriented on the particle surface is less than that of PEG-PCL because of its steric repulsion, and the concentration of PEG-PLA required to increase the structural stability of the particles is probably higher than that of PEG-PCL.

3.3. Evaluation of the temperature-responsiveness of the κ -CRG particles

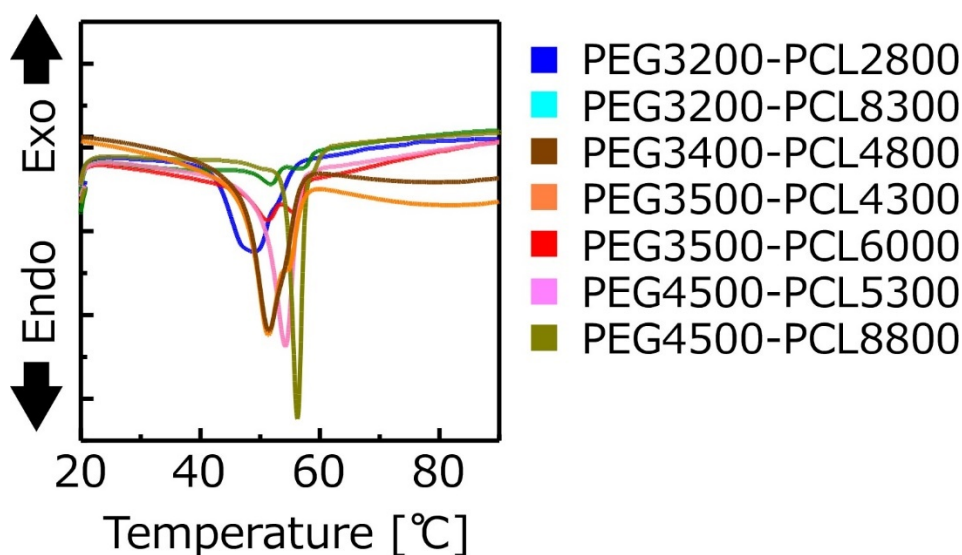


Fig. 3-5 Effect of the composition of the PEG-PCL on the dissolution temperature of the κ -CRG particles using DSC.

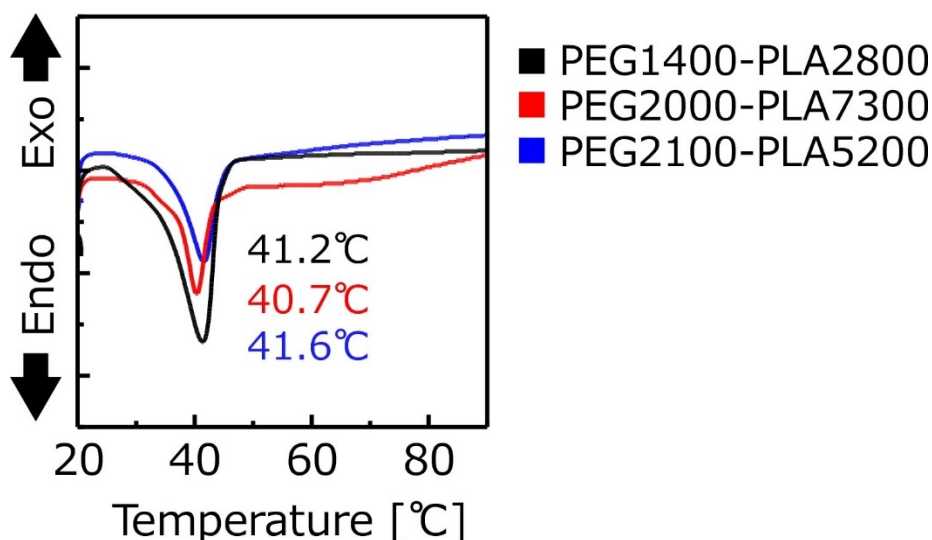


Fig. 3-6 Effect of the composition of the PEG-PLA on the dissolution temperature of the κ -CRG particles using DSC.

The temperature-responsiveness of the κ -CRG particles was evaluated using both DSC and optical microscopy. Figs. 3-5 and 3-6 show the effect of the composition of the PEG-PCL and PEG-PLA on the dissolution temperature of the κ -CRG particles evaluated using DSC in the range of 20–90°C. According to the results illustrated in Figs. 3-1, 3-2, 3-5, and 3-6, the dissolution temperature of the particles was similar to and higher than the melting points of PEG-PCL and PEG-PLA, respectively (PEG-PCL and PEG-PLA were oriented on the particle surface). As mentioned above, the melting point of PEG-PLA varies substantially depending on the molecular weight of the PEG block, and the effect of intermolecular forces (hydrogen bonding forces) on its physical properties is significant. Therefore, it is postulated that the formation of hydrogen bonds between the κ -CRG chains and PEG block of PEG-PLA oriented on the particle surface resulted in a higher dissolution temperature of PEG-PLA-oriented particles than that of PEG-PLA alone.

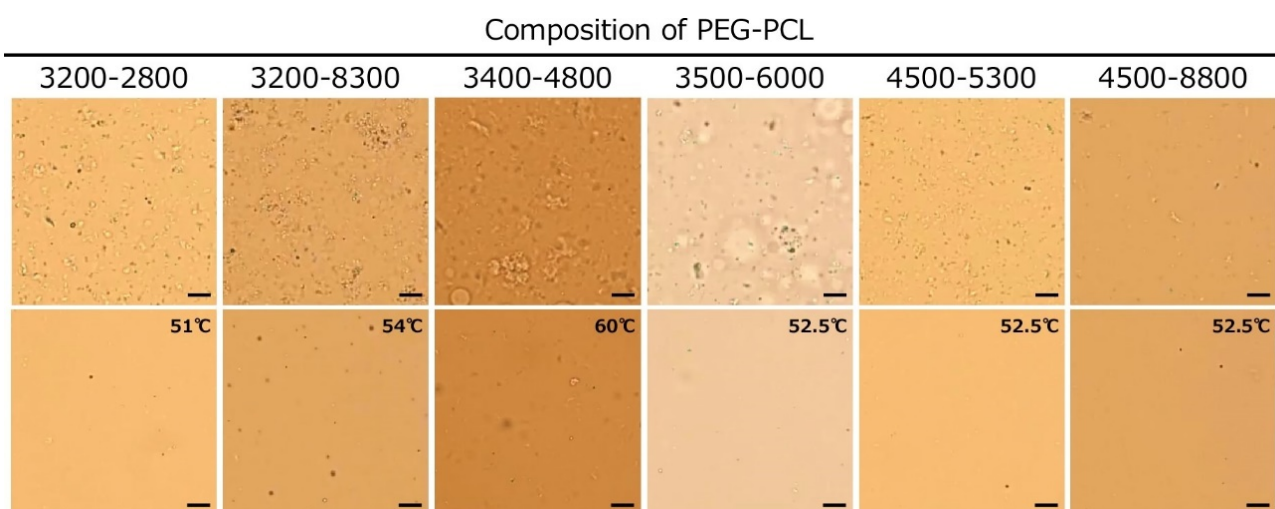


Fig. 3-7 Effect of the composition of the PEG-PCL on the dissolution temperature of the κ -CRG particles as observed directly through an optical microscope (bar: 20 μ m).

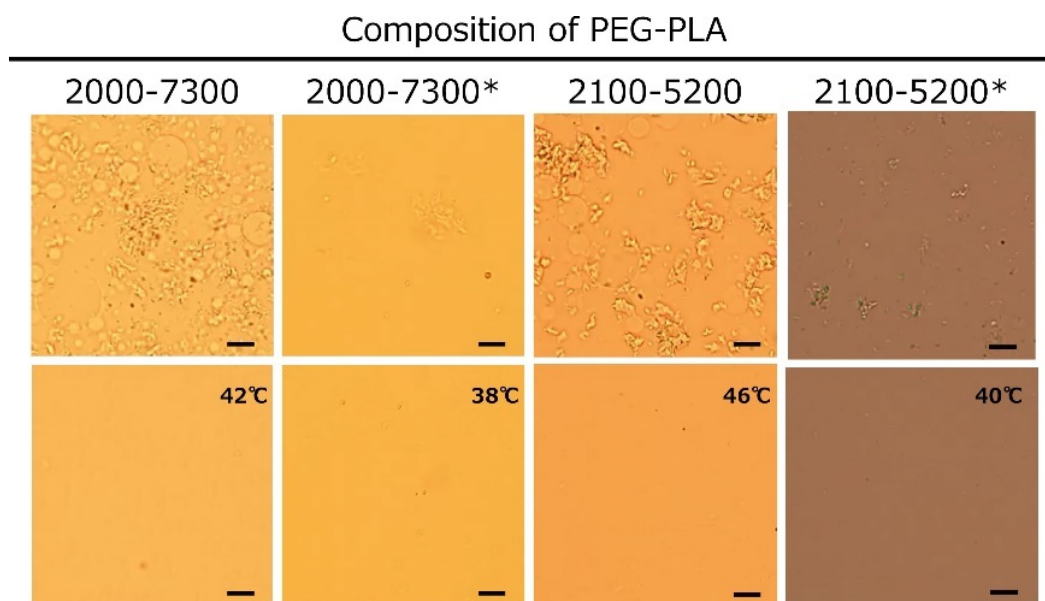


Fig. 3-8 Effect of the composition and concentration of the PEG-PLA on the dissolution temperature of the κ -CRG particles as observed directly through an optical microscope (bar: 20 μ m). The concentration of the PEG-PLA is 0.5 mM (for compositions marked with *, the concentration is 2 mM).

Figs. 3-7 and 3-8 show the effect of the composition and concentration of the polymeric surfactants on the dissolution temperature of the κ -CRG particles evaluated by direct observation using an optical microscope. As shown in Fig. 3-7, when PEG-PCL was used, CRG particles were not observed upon increasing the temperature from 30 to 50–60°C. A further increase in temperature did not cause any change in the microscopic images, suggesting that the PEG-PCL-oriented particles dissolved at 50–60°C. In contrast, as shown in Fig. 3-8, when PEG-PLA was used, the dissolution temperature of the particles varied depending on the concentration of PEG-PLA used during particle preparation. When the particles were prepared at a PEG-PLA concentration of 0.5 mM, the dissolution temperature of the particles was raised by 5–10°C above the melting point of PEG-PLA. Furthermore, when the particles were prepared at a PEG-PLA concentration of 2 mM, the dissolution temperature of the particles was lower than that obtained when the concentration of PEG-PLA used during particle preparation was 0.5 mM. This may be due to the preferential formation of hydrogen bonds between the PEG-CRG chains over the entanglement of the CRG chains with the increase in the amount of PEG-PLA oriented on the particle surface, which led to the lowering of the dissolution temperature of the particles.

3.4. Observation of the surface morphology of the κ -CRG particles containing Mb and evaluation of their release behavior

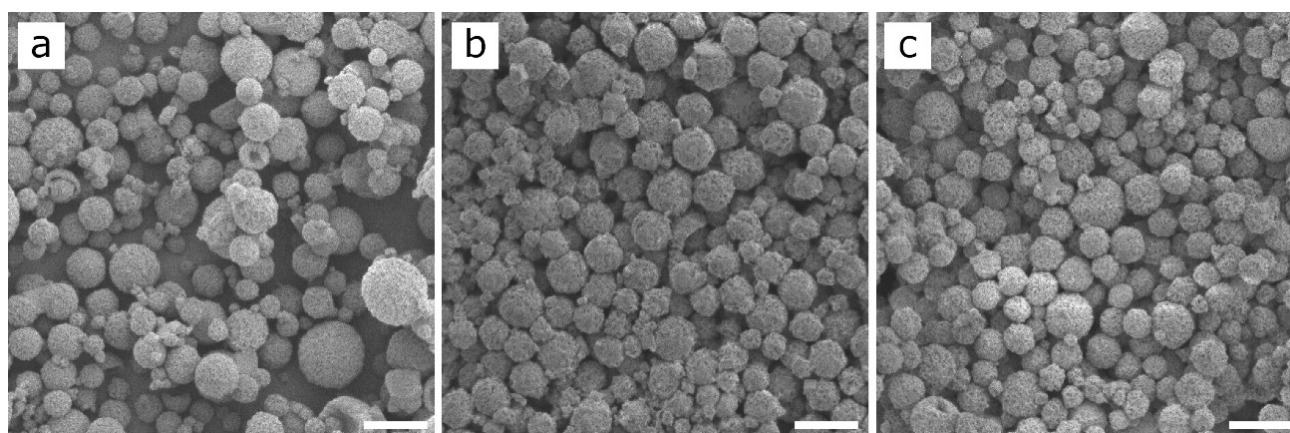


Fig. 3-9 Surface morphology of the particles prepared from various polymeric surfactants (bar: 5 μ m). The polymeric surfactants used were (a) PEG2100-PCL9700 (b) PEG3200-PCL8300, and (c) PEG3400-PCL4300.

Fig. 3-9 shows the surface morphology of the κ -CRG particles prepared from the PEG2100-PCL9700, PEG3200-PCL8300, and PEG3200-PCL4300. According to the SEM images in Fig. 3-9, the encapsulation of Mb had little effect on the formation and surface morphology of the CRG particles.

Table 3-3 Encapsulation ratio and encapsulation efficiency of the Mb for the κ -CRG particles.

Polymeric surfactants	Encapsulation ratio [%]	Encapsulation efficiency [%]
PEG2100-PCL9700	1.60 \pm 0.21	21.1 \pm 4.57
PEG3200-PCL8300	1.19 \pm 0.46	26.2 \pm 13.3
PEG3500-PCL4300	1.31 \pm 0.90	37.4 \pm 22.1

Table 3-3 shows the encapsulation ratio and the encapsulation efficiency of Mb in the κ -CRG particles. The encapsulation ratio and encapsulation efficiency of Mb in the particles were 1.60 \pm 0.21 and 21.1% \pm 4.57%, 1.19 \pm 0.46 and 26.2% \pm 13.3%, and 1.31 \pm 0.90 and 37.4% \pm 22.1% for the particles prepared from PEG2100-PCL9700, PEG3200-PCL8300, and PEG3500-PCL4300, respectively, indicating a high encapsulation efficiency of Mb in the particles. It is plausible that the electrostatic interaction between κ -CRG and Mb is responsible for the high encapsulation efficiency of Mb in the κ -CRG particles. κ -CRG has one sulfate group in its molecular chain and has a negative charge in water, whereas Mb contains sulfur in its molecules and has a positive charge in water. In addition, Mb has a high solubility in water (43.6 g/L, 25°C). It is plausible that the positively charged Mb was distributed in the dispersed phase (water) during particle formation and retained inside the negatively charged CRG particles by electrostatic interactions. Based on this argument, the particles can be expected to incorporate positively charged compounds with a high incorporation efficiency.

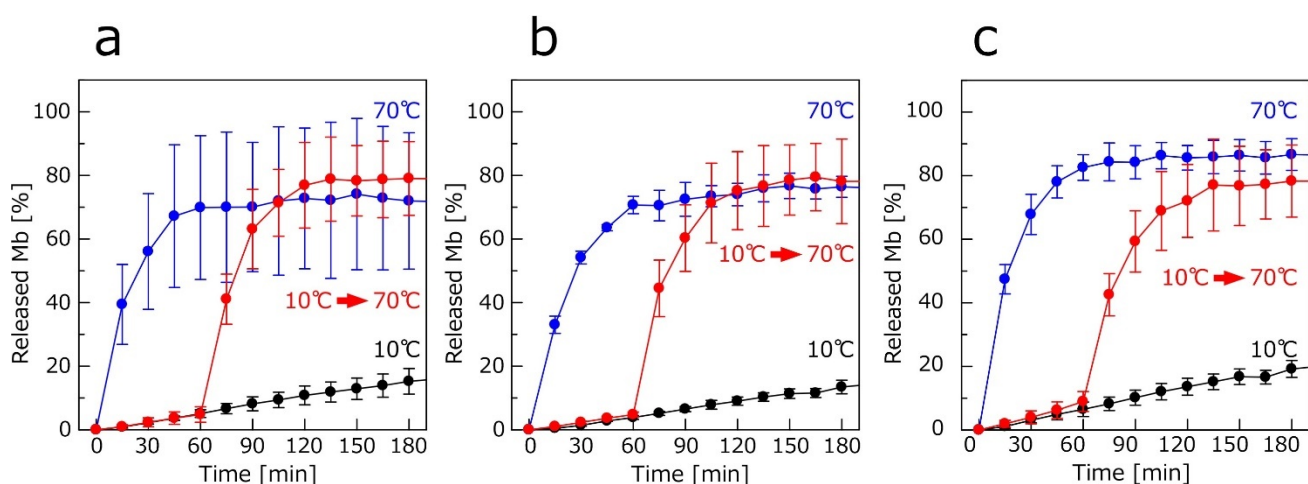


Fig. 3-10 Effect of temperature on the release behavior of κ -CRG particles containing Mb. The polymeric surfactants used were (a) PEG2100-PCL9700 (b) PEG3200-PCL8300, and (c) PEG3400-PCL4300.

Fig. 3-10 shows the effect of temperature on the release behavior of κ -CRG particles. At 10°C, approximately 20% of the inclusions were released from the particles 180 min after the start of release and at 70°C, 80% of the inclusions were released from the particles 60 min after the start of release. In contrast, when the temperature was shifted from 10 to 70°C, the particles exhibited a rapid release behavior 60 min after the start of release. All the particles showed almost the same release behavior which was independent of the molecular weight of PEG-PCL. However, the release behavior of the particles prepared with PEG2100-PCL9700 showed a larger deviation in multiple experiments when compared to the release behavior of the other particles. For PEG2100-PCL9700, the composition ratio of hydrophilic-hydrophobic blocks is different from that of the other block copolymers, and its ability to form emulsions is probably low. Therefore, PEG2100-PLA9700 is more likely to form particles with distorted surfaces than the other two block copolymers. As a result, the heterogeneity of the surface area of the obtained particles increased, which may have resulted in a larger deviation of the release properties in multiple experiments.

Table 3-4 Determination of parameters by fitting the release profiles of the κ -CRG particles to mathematical models.

Surfactants	Temperature [°C]	Models	R^2	k [min^{-1}] or	n
				k_H [$\text{min}^{-1/2}$]	
		Zero-order	0.999	0.0864	-
PEG2100-PCL9700	10	Higuchi	0.959	0.946	-
		Korsmeyer-Peppas	0.993	0.045	1.14

		Zero-order	0.851	0.569	-
	70	Higuchi	0.961	6.76	-
		Korsmeyer-Peppas	0.999	10.57	0.488
		Zero-order	0.997	0.0746	-
	10	Higuchi	0.941	0.81	-
		Korsmeyer-Peppas	0.989	0.0145	1.35
PEG3200-PCL8300		Zero-order	0.876	0.589	-
	70	Higuchi	0.973	6.955	-
		Korsmeyer-Peppas	0.981	6.49	0.608
		Zero-order	0.996	0.109	-
	10	Higuchi	0.962	1.19	-
		Korsmeyer-Peppas	0.987	0.0644	1.11
PEG3500-PCL4300		Zero-order	0.852	0.679	-
	70	Higuchi	0.962	8.07	-
		Korsmeyer-Peppas	0.991	13.77	0.461

Table 3-4 shows the results of the analysis of the release behavior of the particles using the following mathematical models: the zero-order, Higuchi, and Korsmeyer–Peppas models^[37,38]:

Zero-order model:

$$M_t = kt \quad (3)$$

where M_t is the amount of drug released in time t , and k is the rate constant of the drug release.

Higuchi model:

$$M_t = K_H t^{1/2} \quad (4)$$

where M_t is the amount of drug released in time t . Higuchi's release constant, K_H , is obtained by plotting the cumulative release rate of the released drug against the square root of time t .

Korsmeyer–Peppas model:

$$M_t/M_\infty = kt^n \quad (5)$$

where M_t and M_∞ are the amounts of drug released in time t and at equilibrium, respectively, and k is the rate constant. The release exponent n represents the drug release mechanism, that is, the mechanisms involved Fickian diffusion ($n < 0.43$, the drug release is governed by diffusion), non-Fickian diffusion ($0.43 < n < 0.85$, the drug release is governed by both diffusion and swelling of the polymer chains), and zero-order drug release ($n > 0.85$, the drug release is governed by the swelling or relaxation of the polymer chains).

At 10°C, the coefficient of determination (R^2) values for the zero-order and Korsmeyer–Peppas models are above 0.98 for all the systems, which indicate that these two models are applicable for the analysis of the experimental results. In addition, the n values for the Korsmeyer–Peppas model at 10°C exceeded 1 for all the systems. If the value of n is greater than 1 for the Korsmeyer–Peppas model, the drug release behavior can be approximated as zero-order release^[37], which implies that Mb is released at a constant rate which is independent of the concentration at 10°C. In contrast, at 70°C, the R^2 values for the Korsmeyer–Peppas model exceeded 0.98 for all the systems, which indicated that the release behavior could be satisfactorily described by this model. Because the n values were almost the same (0.461–0.608) in all the systems and were within the range of $0.43 < n < 0.85$, it was concluded that (1) the composition of PEG-PCL had little effect on the release behavior of the particles, and (2) diffusion (due to particle dissolution) and swelling-relaxation of the polymer chains occurred competitively. These analyses suggested that the κ -CRG particles dissolved rapidly at 70°C, and the Mb diffused into the PBS solution.

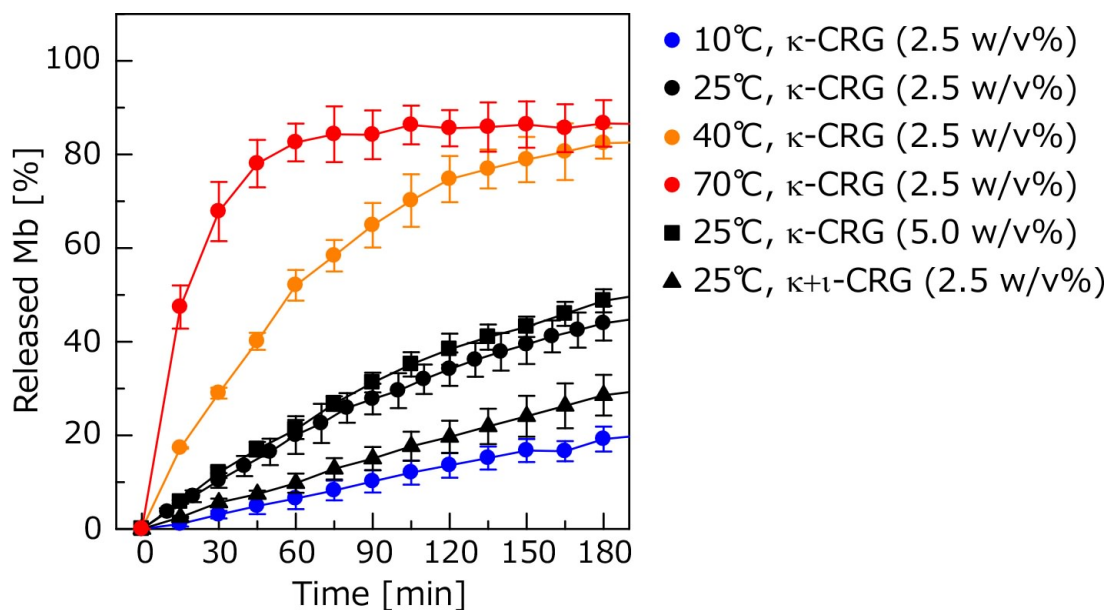


Fig. 3-11 Effect of temperature and polysaccharide concentration on the release behavior of κ -CRG and mixed κ,ι -CRG particles containing Mb.

The effects of the temperature of the developing solvent, CRG concentration, and CRG composition (κ -, ι -, and κ,ι -) on the release behavior of the particles were evaluated to investigate the factors affecting the temperature-dependent release behavior of the particles. As shown in Fig. 3-11, under the condition of constant κ -CRG concentration during particle preparation, the release rate was found to increase with increasing temperature. This

temperature dependence may be due to the change in the crystallinity of PEG-PCL and the mobility of both κ -CRG and PEG-PCL. PEG-PCL, a crystalline surfactant, shows an exothermic peak of crystallization at approximately 15–25°C in DSC measurements independent of the composition (data not shown), and similar results have been reported elsewhere^[28]. The diffusion-dependence of the zero-order drug release behavior at 10°C with increasing temperature may be due to a combination of the following factors: (1) at 10°C, the PEG-PCL oriented on the particle surface crystallizes and inhibits the solvent flow into the particles, (2) as the temperature increases, PEG-PCL becomes amorphous and the solvent flow into the particles is promoted, and (3) the increase in temperature increases the mobility of PEG-PCL and κ -CRG, which further accelerates the solvent flow into the particles. Fig. 3-11 also shows that increasing the CRG concentration has no effect on the release behavior of the particles, whereas the use of a mixture of κ -CRG and ι -CRG suppresses the release from the particles. ι -CRG has two sulfate groups in a molecule and has a higher negative charge than κ -CRG. Therefore, it is postulated that the use of ι -CRG in forming particles increases the electrostatic interaction between the positively charged Mb and negatively charged particles and suppresses the release via diffusion from the particles. I also considered preparing particles using only ι -CRG. However, this was difficult to achieve due to the following two reasons: (1) ι -CRG forms less rigid (more elastic) gels than κ -CRG^[17], and (2) the sol-gel transition rate of ι -CRG is slower than that of κ -CRG, which promotes the aggregation of the w/o emulsion.

3.5. Observation of the surface morphology of the mixed κ,ι -CRG particles containing Mb and evaluation of their release behavior

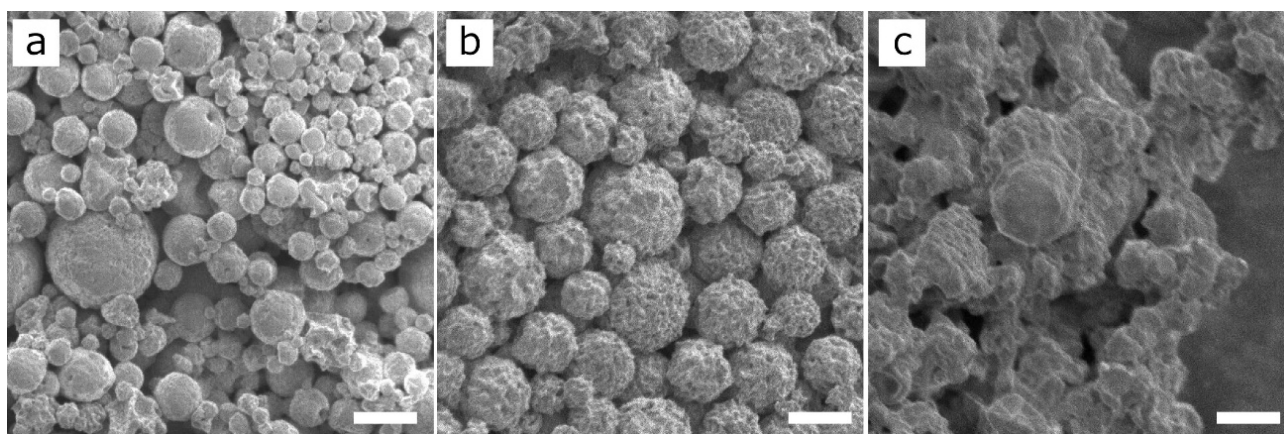


Fig. 3-12 Surface morphology of the mixed κ,ι -CRG particles prepared from various polymeric surfactants (bar: 5 μm). The polymeric surfactants used were (a) PEG3400-PCL4300 (b) PEG2000-PLA7300, and (c) PEG2100-PLA5200.

Because the release behavior of the particles was found to change upon the mixing of κ -CRG and ι -CRG, the surface morphology and release behavior of the mixed κ,ι -CRG particles were evaluated in detail. Fig. 3-12 shows the surface morphology of the mixed κ,ι -CRG particles prepared from the PEG2100-PCL9700, PEG3200-PCL8300, and PEG3200-PCL4300. As can be seen in the SEM images in Fig. 3-12, the encapsulation of the compound had

little effect on the formation and surface morphology of the mixed κ,ι -CRG particles.

Table 3-5 Encapsulation ratio and encapsulation efficiency of the Mb for the mixed κ,ι -CRG particles

Polymeric surfactants	Encapsulation ratio [%]	Encapsulation efficiency [%]
PEG3500-PCL4300	1.85 ± 0.82	64.3 ± 33.1
PEG2000-PLA7300	0.074 ± 0.054	21.9 ± 20.1
PEG2100-PLA5200	0.028 ± 0.013	12.5 ± 6.52

Table 3-5 shows the encapsulation ratio and encapsulation efficiency of Mb in the mixed κ,ι -CRG particles. The encapsulation ratio and encapsulation efficiency of Mb in the particles were 1.85 ± 0.82 and $64.3\% \pm 33.1\%$, 0.074 ± 0.054 and $21.9\% \pm 20.1\%$, and 0.028 ± 0.013 and $12.5\% \pm 6.52\%$ for the particles prepared from PEG3500-PCL4300, PEG2000-PLA7300, and PEG2100-PLA5200, respectively. When the mixed κ,ι -CRG particles were prepared using PEG3400-PCL4300, both the encapsulation rate and encapsulation efficiency increased compared to the corresponding values for the particles prepared using κ -CRG alone (Fig. 3-9). This may be due to the increase in the electrostatic interaction with the inclusion by mixing ι -CRG with κ -CRG, as described above. However, such a positive effect was not observed when the mixed κ,ι -CRG particles were prepared using PEG-PLA, and a decreasing trend was observed in both the encapsulation ratio and encapsulation efficiency. The low crystallinity of PEG-PLA is considered to be a major factor responsible for this decrease. Because the PEG-PLA oriented on the particle surface is amorphous, it has a low retention of inclusions during particle preparation. In other words, the composition of the polymeric surfactant and that of the particle-forming CRG were found to play an important role in increasing the retention of inclusions.

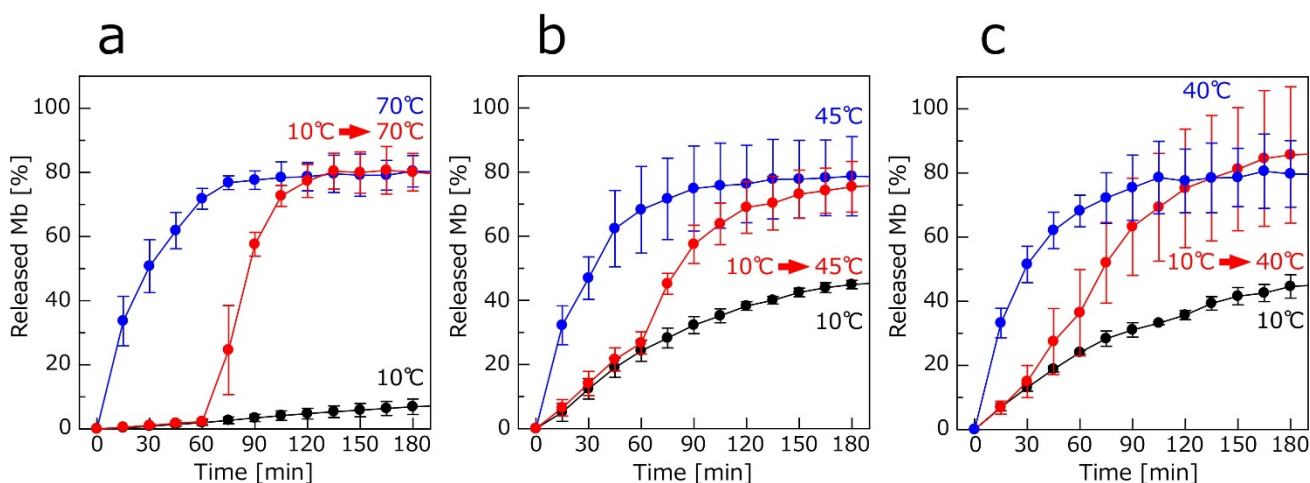


Fig. 3-13 Effect of temperature on the release behavior of κ -CRG particles containing Mb. The polymeric surfactants used were (a) PEG3400-PCL4300 (b) PEG2000-PLA7300, and (c) PEG2100-PLA5200.

Fig. 3-13 shows the effect of temperature on the release behavior of the mixed κ,ι -CRG particles. When PEG3500-PCL4300 was used as a polymeric surfactant (Fig. 3-13(a)), at 10°C , approximately 7% of the inclusions were released from the particles 180 min after the start of release, and at 70°C , 80% of the inclusions were released

from the particles 60 min after the start of release. In contrast, when the temperature was shifted from 10 to 70°C 60 min after the start of release, the particles showed a rapid release behavior.

The analysis of the release behavior of the mixed κ,ι -CRG particles using the zero-order, Higuchi, and Korsmeyer–Peppas models (Table 3-6) showed that, at 10°C, the R^2 values for the zero-order and Korsmeyer–Peppas models exceeded 0.99, which indicated that these two models were applicable to the analysis of the experimental results. In addition, the n values for the Korsmeyer–Peppas model at 10°C was greater than 1 and that at 70°C was 0.558, which indicated that the drug release behaviors of the κ -CRG and mixed κ,ι -CRG particles were identical. Furthermore, the release rate from the mixed κ,ι -CRG particles (Fig. 3-13(a)) was lower than that from the κ -CRG particles (Fig. 3-10(c)) 180 min after the start of release. Considering this experimental result and the aforementioned mathematical analysis, it was concluded that the mixed κ,ι -CRG particles inhibited the release of the inclusions without changing the release mechanism.

In contrast, when PEG2000-PLA7300 and PEG2100-PLA5200 were used as polymeric surfactants (Fig. 3-13(b), (c)), almost identical experimental results were obtained: (1) at 10°C, approximately 40% of the inclusions were released from the particles 180 min after the start of release, (2) at 45°C, 80% of the inclusions were released from the particles 90 min after the start of release, (3) compared to the case where PEG-PCL was used, the temperature at which the release behavior could be switched was lowered from 70 to 40–45°C because of the lower dissolution temperature of the particles prepared using PEG-PLA (Fig. 3-6), and (4) when the temperature was shifted from 10 to 40°C, 60 min after the start of release, the inclusions were released at a slightly slower rate than that from the particles prepared using PEG-PCL as the surfactant. Compared to the particles prepared using PEG-PCL, the temperature at which the release behavior could be switched was lowered from 70 to 40°C because of the lower dissolution temperature of the particles prepared using PEG-PLA. The n value at each temperature was $0.43 < n < 0.85$, indicating that the release behavior at these temperatures was competitively governed by Fickian diffusion and polymer chain swelling-relaxation. The n value at 10°C was almost 0.85, indicating that the release behavior at 10°C was predominantly derived from the swelling and relaxation of the polymer chains. These results suggest that, unlike PEG-PCL, PEG-PLA is amorphous on the particle surface, which facilitates solvent exchange between the interior and exterior of the particles and the release of inclusions.

Table 3-6 Determination of parameters by fitting the release profiles of the mixed κ,ι -CRG particles to mathematical models.

Surfactants	Temperature [°C]	Models	R^2	k [min^{-1}] or k_H [$\text{min}^{-1/2}$]	n
PEG3500-PCL4300	10	Zero-order	0.998	0.0385	-
		Higuchi	0.944	0.419	-
		Korsmeyer-Peppas	0.996	0.0119	1.24

		Zero-order	0.883	0.613	-
	70	Higuchi	0.977	7.21	-
		Korsmeyer-Peppas	0.998	7.46	0.558
		Zero-order	0.979	0.295	-
	10	Higuchi	0.991	3.32	-
		Korsmeyer-Peppas	0.962	0.675	0.839
PEG2000-PLA7300		Zero-order	0.89	0.601	-
	45	Higuchi	0.98	7.05	-
		Korsmeyer-Peppas	0.995	6.37	0.595
		Zero-order	0.978	0.288	-
	10	Higuchi	0.994	3.24	-
		Korsmeyer-Peppas	0.984	1.09	0.731
PEG2100-PLA5200		Zero-order	0.889	0.43	-
	40	Higuchi	0.98	7.12	-
		Korsmeyer-Peppas	0.994	4.94	0.577

4. Conclusions

In chapter 3, I aimed to develop polysaccharide microparticles that release their inclusions in response to temperature. I mainly investigated the effects of the type and composition of polymeric surfactants and particle-forming polysaccharides on the dissolution behavior of the particles. Although the composition of PEG-PCL did not affect its melting point, the melting point of PEG-PLA changed significantly depending on the molecular weight of PEG. The dissolution temperature of the particles prepared using PEG-PLA decreased depending on its melting point, indicating that the dissolution temperature of the particles could be arbitrarily controlled by controlling the hydrogen bonding forces between PEG-PLA and CRG. Furthermore, in the case of the particles prepared by mixing κ -CRG and ι -CRG, the diffusion-dependent release of inclusions was suppressed below the dissolution temperature of the particles, and the inclusions were rapidly released immediately after the temperature was increased. The results

indicate the possibility that the prepared particles can penetrate deep into lung tissues and release their inclusions at body temperature without the need for heating. These results suggest that the particles can be applied as drug carriers for pulmonary administration with high therapeutic efficacy for the urgent treatment of seizures and abnormal increases in blood glucose levels.

In chapter 3, I prepared CRG particles that showed temperature responsiveness at approximately 40–45°C. The major challenge for the future is to achieve temperature responsiveness at temperatures lower than 40–45°C (i.e., near body temperature). It is known that the triblock copolymer, PCL-PEG-PCL, has a melting point of approximately 40°C and is crystalline^[39]. By using such surfactants in particle preparation to control the dissolution temperature and release properties of the particles, a temperature response behaviors can be achieved near body temperature.

5. Reference

- [1] Patton, J. S., Byron, P. R., Inhaling medicines: Delivering drugs to the body through the lungs., *Nat. Rev. Drug Discov.*, **6**, 67–74, (2007)
- [2] Loira-Pastoriza, C., Todoroff, J., Vanbever, R., Delivery strategies for sustained drug release in the lungs., *Adv. Drug Deliv. Rev.*, **75**, 81–91, (2014)
- [3] Al-Qadi, S., Taboada, P., Remuñán-López, C., Micro/nanostructured inhalable formulation based on polysaccharides: Effect of a thermoprotectant on powder properties and protein integrity., *Int. J. Pharm.*, **551**, 23–33, (2018)
- [4] d'Angelo, I., Conte, C., La Rotonda, M. I., Miro, A., Quaglia, F., Ungaro, F., Improving the efficacy of inhaled drugs in cystic fibrosis: Challenges and emerging drug delivery strategies., *Adv. Drug Deliv. Rev.*, **75**, 92–111, (2014)
- [5] Bosquillon, C., Lombry, C., Pr at, V., Vanbever, R., Influence of formulation excipients and physical characteristics of inhalation dry powders on their aerosolization performance., *J. Control. Release*, **70**, 329–339, (2001)
- [6] Agu, R. U., Ugwoke, M. I., Armand, M., Kinget, R., Verbeke, N., The lung as a route for systemic delivery of therapeutic proteins and peptides., *Respir. Res.*, **2**, 198–209, (2001)
- [7] Labiris, N. R., Dolovich, M. B., Pulmonary drug delivery. Part I: Physiological factors affecting therapeutic effectiveness of aerosolized medications., *Br. J. Clin. Pharmacol.*, **56**, 588–599, (2003)
- [8] Parumasivam, T., Chang, R. Y. K., Abdelghany, S., Ye, T. T., Britton, W. J., Chan, H. K., Dry powder inhalable formulations for anti-tubercular therapy., *Adv. Drug Deliv. Rev.*, **102**, 83–101, (2016)
- [9] Feng, W., Zhou, X., He, C., Qiu, K., Nie, W., Chen, L., Wang, H., Mo, X., Zhang, Y., Polyelectrolyte multilayer functionalized mesoporous silica nanoparticles for pH-responsive drug delivery: Layer thickness-dependent release profiles and biocompatibility., *J. Mater. Chem. B*, **1**, 5886–5898, (2013)
- [10] Meng, H., Xue, M., Xia, T., Zhao, Y. L., Tamanoi, F., Stoddart, J. F., Zink, J. I., Nel, A. E., Autonomous in vitro

- anticancer drug release from mesoporous silica nanoparticles by pH-sensitive nanovalves., *J. Am. Chem. Soc.*, **132**, 12690–12697, (2010)
- [11] Nagasaki, T., Taniguchi, A., Tamagaki, S., Photoenhancement of transfection efficiency using novel cationic lipids having a photocleavable spacer., *Bioconjug. Chem.*, **14**, 513–516, (2003)
- [12] Kojima, C., Umeda, Y., Harada, A., Kono, K., Preparation of near-infrared light absorbing gold nanoparticles using polyethylene glycol-attached dendrimers., *Colloids Surfaces B Biointerfaces*, **81**, 648–651, (2010)
- [13] Nagasaki, T., Wada, K., Tamagaki, S., Photo-enhancement of transfection efficiency with a novel azobenzene-based cationic lipid., *Chem. Lett.*, **32**, 88–89, (2003)
- [14] Yu, F., Wu, H., Tang, Y., Xu, Y., Qian, X., Zhu, W., Temperature-sensitive copolymer-coated fluorescent mesoporous silica nanoparticles as a reactive oxygen species activated drug delivery system., *Int. J. Pharm.*, **536**, 11–20, (2018)
- [15] Kono, K., Nakashima, S., Kokuryo, D., Aoki, I., Shimomoto, H., Aoshima, S., Maruyama, K., Yuba, E., Kojima, C., Harada, A., *et al.*, Multi-functional liposomes having temperature-triggered release and magnetic resonance imaging for tumor-specific chemotherapy., *Biomaterials*, **32**, 1387–1395, (2011)
- [16] Pacheco-Quito, E. M., Ruiz-Caro, R., Veiga, M. D., Carrageenan: Drug Delivery Systems and Other Biomedical Applications., *Mar. Drugs*, **18**, (2020)
- [17] Li, L., Ni, R., Shao, Y., Mao, S., Carrageenan and its applications in drug delivery., *Carbohydr. Polym.*, **103**, 1–11, (2014)
- [18] Yegappan, R., Selvaprithiviraj, V., Amirthalingam, S., Jayakumar, R., Carrageenan based hydrogels for drug delivery, tissue engineering and wound healing., *Carbohydr. Polym.*, **198**, 385–400, (2018)
- [19] Anzai, R., Takami, T., Uchida, Y., Murakami, Y., Poly(ϵ -caprolactone) (PCL) hybrid sheets containing polymeric micelles: Effects of inner structures on the material properties of the sheets., *Mater. Sci. Eng. C*, **72**, 325–331, (2017)
- [20] Anzai, R., Murakami, Y., Poly(ϵ -caprolactone) (PCL)-polymeric micelle hybrid sheets for the incorporation and release of hydrophilic proteins., *Colloids Surfaces B Biointerfaces*, **127**, 292–299, (2015)
- [21] Moroishi, H., Yoshida, C., Murakami, Y., A free-standing, sheet-shaped, ‘hydrophobic’ biomaterial containing polymeric micelles formed from poly(ethylene glycol)-poly(lactic acid) block copolymer for possible incorporation/release of ‘hydrophilic’ compounds., *Colloids Surfaces B Biointerfaces*, **102**, 597–603, (2013)
- [22] Takami, T., Murakami, Y., Unexpected and successful ‘one-step’ formation of porous polymeric particles only by mixing organic solvent and water under ‘low-energy-input’ conditions., *Langmuir*, **30**, 3329–3336, (2014)
- [23] Uchida, Y., Murakami, Y., Successful preferential formation of a novel macromolecular assembly-Trilayered polymeric micelle-That can incorporate hydrophilic compounds: The optimization of factors affecting the micelle formation from amphiphilic block copolymers., *Colloids Surfaces B Biointerfaces*, **84**, 346–353, (2011)
- [24] Ito, T., Takami, T., Uchida, Y., Murakami, Y., Chitosan gel sheet containing drug carriers with controllable drug-release properties., *Colloids Surfaces B Biointerfaces*, **163**, 257–265, (2018)
- [25] Takeshita, H., Fukumoto, K., Ohnishi, T., Ohkubo, T., Miya, M., Takenaka, K., Shiomi, T., Formation of lamellar structure by competition in crystallization of both components for crystalline-crystalline block copolymers., *Polymer (Guildf)*, **47**, 8210–8218, (2006)

- [26] Gomes, M. L. S., da Silva Nascimento, N., Borsato, D. M., Pretes, A. P., Nadal, J. M., Novatski, A., Gomes, R. Z., Fernandes, D., Farago, P. V., Zanin, S. M. W., Long-lasting anti-platelet activity of cilostazol from poly(ϵ -caprolactone)-poly(ethylene glycol) blend nanocapsules., *Mater. Sci. Eng. C*, **94**, 694–702, (2019)
- [27] Zhang, Y., Lu, Y., Cao, M., Chen, P., Yang, B., Miao, J., Xia, R., Qian, J., Y-shaped copolymers of poly(ethylene glycol)-poly(ϵ -caprolactone) with ketal bond as the branchpoint for drug delivery., *Mater. Sci. Eng. C*, **93**, 554–564, (2018)
- [28] Zhang, Y., Lu, Y., Cao, M., Chen, P., Yang, B., Miao, J., Xia, R., Qian, J., Y-shaped copolymers of poly(ethylene glycol)-poly(ϵ -caprolactone) with ketal bond as the branchpoint for drug delivery., *Mater. Sci. Eng. C*, **93**, 554–564, (2018)
- [29] Wei, X. W., Gong, C. Y., Gou, M. L., Fu, S. Z., Guo, Q. F., Shi, S., Luo, F., Guo, G., Qiu, L. Y., Qian, Z. Y., Biodegradable poly(ϵ -caprolactone)-poly(ethylene glycol) copolymers as drug delivery system., *Int. J. Pharm.*, **381**, 1–18, (2009)
- [30] Behl, A., Parmar, V. S., Malhotra, S., Chhillar, A. K., Biodegradable diblock copolymeric PEG-PCL nanoparticles: Synthesis, characterization and applications as anticancer drug delivery agents., *Polymer (Guildf)*, **207**, 122901, (2020)
- [31] Essa, S., Rabanel, J. M., Hildgen, P., Effect of polyethylene glycol (PEG) chain organization on the physicochemical properties of poly(D, L-lactide) (PLA) based nanoparticles., *Eur. J. Pharm. Biopharm.*, **75**, 96–106, (2010)
- [32] Li, F., Li, S., El Ghzaoui, A., Nouailhas, H., Zhuo, R., Synthesis and gelation properties of PEG-PLA-PEG triblock copolymers obtained by coupling monohydroxylated PEG-PLA with adipoyl chloride., *Langmuir*, **23**, 2778–2783, (2007)
- [33] Danafar, H., Rostamizadeh, K., Davaran, S., Hamidi, M., Drug-conjugated PLA-PEG-PLA copolymers: a novel approach for controlled delivery of hydrophilic drugs by micelle formation., *Pharm. Dev. Technol.*, **22**, 947–957, (2017)
- [34] Chen, W. L., Peng, Y. F., Chiang, S. K., Huang, M. H., Thermal properties and physicochemical behavior in aqueous solution of pyrene-labeled poly(ethylene glycol)-polylactide conjugate., *Int. J. Nanomedicine*, **10**, 2815–2822, (2015)
- [35] Hossein Panahi, F., Peighambaroust, S. J., Davaran, S., Salehi, R., Development and characterization of PLA-mPEG copolymer containing iron nanoparticle-coated carbon nanotubes for controlled delivery of Docetaxel., *Polymer (Guildf)*, **117**, 117–131, (2017)
- [36] Kister, G., Cassanas, G., Bergounhon, M., Hoarau, D., Vert, M., Structural characterization and hydrolytic degradation of solid copolymers of D, L-lactide-co- ϵ -caprolactone by Raman spectroscopy., *Polymer (Guildf)*, **41**, 925–932, (2000)
- [37] Tamboli, V., Mishra, G. P., Mitra, A. K., Novel pentablock copolymer (PLA-PCL-PEG-PCL-PLA)-based nanoparticles for controlled drug delivery: effect of copolymer compositions on the crystallinity of copolymers and in vitro drug release profile from nanoparticles., *Colloid Polym. Sci.*, **291**, 1235–1245, (2013)
- [38] Bruschi, M., Mathematical models of drug release., in *Strategies to Modify the Drug Release from Pharmaceutical Systems*, 63–86, (Elsevier, 2015), doi:10.1016/B978-0-08-100092-2.00005-9

- [39] Huang, J., Yu, X., Zhou, Y., Zhang, R., Song, Q., Wang, Q., Li, X., Directing the nanoparticle formation by the combination with small molecular assembly and polymeric assembly for topical suppression of ocular inflammation., *Int. J. Pharm.*, **551**, 223–231, (2018)

Chapter 4

Temperature-Responsive Nanoparticle-Decorated Polysaccharide Microparticles for Pulmonary Drug Delivery: The Release of Multiple Cationic/Anionic Compounds

1. Introduction

As shown in chapter 1, a variety of nanoparticles have been developed to date, including inorganic nanoparticles formed from silica and titanium, and polysaccharide nanoparticles formed from alginate and chitosan (CS)^[1-8]. These nanoparticles have been used as drug carriers in various drug-dosage forms, including for oral and intravenous administration^[9-12]. Among these nanoparticles, cationic ones have been reported to exhibit antimicrobial activities and membrane permeabilities, and can be used as anticancer agents^[13-15]. Biologically derived polymers, such as CS and poly-L-lysine (PLL), are often used as cationic polymers to form cationic nanoparticles^[16-18]. CS is a linear polymer prepared by deacetylating natural chitin, which is obtained from crustaceans, such as shrimp and crab. PLL is a polymer produced by the fermentation of lysine by *Streptomyces albulus*^[18]. Nanoparticles formed from CS or PLL have been reported on several occasions^[18-21]. For example, mixing CS or PLL with tripolyphosphoric acid (TPP) has been reported to form nanoparticles through electrostatic interactions between the amino groups of the cationic polymer and the phosphate groups of TPP^[22-27]; such nanoparticles are easily formed by ultrasonication in the absence of surfactants.

Pulmonary administration^[28-32], in which drugs are inhaled and absorbed into the body through the lungs, is a medication method that has many advantages, including simplicity of administration, excellent immediate efficacy, and efficient treatment of lung diseases^[33-36]. However, the drug carriers used in pulmonary administration are mainly microparticles with diameters over 1 μm , with few examples of nanoparticles used; nanoparticles less than 1 μm in diameter are too small for pulmonary administration because they are expelled from the body through exhalation^[37-39].

In contrast, I previously developed temperature-responsive carrageenan (CRG) microparticles in chapter 2 and 3 that are efficiently delivered to the lungs. These particles, which are readily prepared by the sol-gel transition of CRG, are capable of rapidly releasing their inclusions by collapsing in response to temperature. CRG particles are formed from water-in-oil (w/o) emulsions and readily encapsulate compounds dissolved or dispersed in the CRG

solution. However, because CRG particles are negatively charged, encapsulating negatively charged compounds is difficult due to electrostatic repulsion. Therefore, developing CRG microparticles capable of encapsulating a wide range of compounds is important.

In chapter 4, I developed temperature-responsive microparticles by complexing cationic nanoparticles with anionic microparticles; this system efficiently delivers nanoparticles to the lungs where multiple drugs can be released. Dispersing these cationic nanoparticles in aqueous CRG solution during microparticle preparation facilitates their complexation with anionic microparticles through electrostatic interactions. Furthermore, these cationic nanoparticles can contain anionic compounds, also through electrostatic interactions. Therefore, the previously developed CRG microparticles can contain positively charged compounds, while the microparticles developed in chapter 4 facilitate the concurrent containment of negatively charged compounds through complexation with the cationic nanoparticles. The CRG microparticles designed on the basis of this idea should exhibit two-step release behavior; that is, the nanoparticles and the compound dispersed inside the microparticles are released in a temperature-responsive manner, followed by the release of another compound from within the nanoparticles (Fig. 4-1). In chapter 4, nanoparticles were first prepared using CS or PLL, after which I evaluated the release behavior of negatively charged compounds from these nanoparticles. I then investigated nanoparticle complexation within CRG microparticles based on the sol-gel transition of CRG. In addition, I prepared CRG microparticles containing both positively charged compounds and the aforementioned nanoparticles and evaluated the release behavior of the two compounds from the microparticles. To the best of my knowledge, the release of a wide range of compounds by combining polysaccharide microparticles and biopolymer nanoparticles based on technology that controls both the sol-gel transition and emulsion formation, has not been reported.

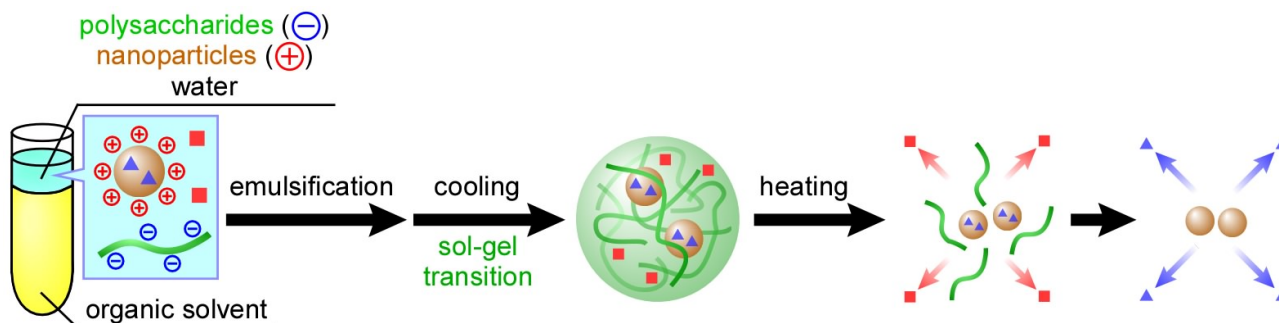


Fig. 4-1 Temperature-responsive nanoparticle-containing polysaccharide microparticles for the release of multiple compounds.

2. Material and Methods

2.1. Materials

κ -Carrageenan (κ -CRG), potassium chloride, methylene blue trihydrate (Mb), pentasodium triphosphate (TPP), acetic acid, hydrochloric acid (1N), sodium hydroxide solution (8N), and toluene were purchased from Wako Pure Chemical Industries (Osaka, Japan). ι -Carrageenan (ι -CRG) and PLL (405 kDa) were purchased from Sigma-

Aldrich (St. Louis MO, USA). Sodium 2-naphthalenesulfate (Ns) was purchased from Tokyo Chemical Industry Co., Ltd. (Tokyo, Japan). CS (100 kDa) was purchased from Dainishiseika Color & Chemicals Mfg. Co., Ltd. (Tokyo, Japan). Block copolymers, poly(ethylene glycol)-*b*-poly(ϵ -caprolactone) (PEG-PCL), were synthesized according to a previously reported method^[40,41] with a slight modification (PEG M_n : 3500, PCL M_n : 4300, M_w/M_n : 1.35). All the other reagents were of analytical grade and were used without further purification.

2.2. Preparing CS(Ns) and PLL(Ns) nanoparticles

CS(Ns) and PLL(Ns) nanoparticles were prepared according to previously reported methods^[22,24,26,42–44]. Here, $A(m)$ nanoparticles refer to nanoparticles A that contain m inside them. If a compound is contained within the nanoparticles, then m is the name of the compound, while m is simply written as “-” if the nanoparticle contains no compound. CS(Ns) nanoparticles were prepared by dropping an aqueous solution (5 mL, pH 5) of TPP (4.2 mg) into an acetate buffer solution (10 mL, pH 5) containing CS (20 mg) and Ns (20 mg) while being sonicated (20 kHz, 5 min) with an ultrasonic homogenizer (UH-50, SMT Co., Ltd., Japan). The solution was ultrasonicated for another 10 min, then stirred at 300 rpm for 30 min and centrifuged at 9200 rpm for 20 min to give CS(Ns) nanoparticles. In contrast, PLL(Ns) nanoparticles were prepared by dropping an aqueous solution (5 mL, pH 4) containing TPP (0.92 mg) into an aqueous solution (10 mL, pH 4) of PLL (10 mg) and Ns (20 mg) while being sonicated (20 kHz, 5 min) with an ultrasonic homogenizer. The pH was then adjusted to 7 with NaOH, and then ultrasonicated for another 10 min. PLL(Ns) nanoparticles were subsequently obtained following the same procedure used for the CS(Ns) nanoparticles.

2.3. Preparing CRG(CS(Ns), Mb) and CRG(PLL(Ns), Mb) microparticles

The CRG(CS(Ns), Mb) and CRG(PLL(Ns), Mb) microparticles were prepared according to a previously reported method in chapter 2 and 3. Here, $A(m, n)$ microparticles refers to microparticles A that contain m and n inside them. If a compound or nanoparticle is contained inside microparticles, then m and n are the names of the compound and nanoparticle; if the microparticle contains only one compounds or nanoparticle, then only m is indicated, while m is simply written as “-” if the microparticle contains no compound or nanoparticle. An aqueous polysaccharide solution was prepared by dissolving κ -CRG (2.5 w/v%), ι -CRG (2.5 w/v%), potassium chloride (32 mM), and Mb (7.3 mM) in Milli-Q water (70°C, 40 mL). A mixture of κ -CRG and ι -CRG was used instead of κ -CRG or ι -CRG alone because it can satisfy both fast gelation speed and moderate rigidity. The organic solvent was prepared by dissolving PEG-PCL (0.5 mM) in toluene (10 mL). The w/o emulsion was then prepared by emulsifying (70°C, 12000 rpm, 5 min) the polysaccharide solution (0.35 g), organic solvent, and nanoparticle dispersion (CS(Ns) (1.6 mg/mL) or PLL(Ns) (0.6 mg/ml) nanoparticles, 100 μ L) with a high-speed homogenizer (NS-51 K and NS-10, Microtec Co., Ltd., Japan). The emulsion was gradually cooled to 25°C in a water bath and the microparticles were washed three times by the repetitive addition of toluene and subsequent centrifugation to remove excess PEG-PCL. The CRG(CS(Ns), Mb) and CRG(PLL(Ns), Mb) microparticles were finally obtained after drying naturally in a perfluoroalkoxyalkane (PFA) beaker. For comparison, the formation of microparticles using only PLL(Ns)

nanoparticles (without CRG) was also investigated. The w/o emulsion was prepared by mixing a solution of PEG-PCL (0.5 mM) in toluene (10 mL), Milli-Q water (0.35 mL), and a nanoparticle dispersion (100 μ L) with a homogenizer (70°C, 12000 rpm, 5 min). The white solid was then collected by the same process used to prepare the CRG-containing microparticles.

2.4. Characterizing nanoparticles and microparticles

The diameters of the nanoparticles and microparticles were determined by dynamic light scattering (DLS). A particle dispersion (1 mg/mL) was placed in the DLS instrument (Zetasizer Nano-ZS; Malvern Instruments, UK) and the effects of temperature (70°C) and homogenization (12000 rpm, 5 min) on nanoparticle diameter were evaluated.

Nanoparticle morphologies were examined by transmission electron microscopy (TEM; JEM-1400, JEOL, Tokyo, Japan). A CS(Ns) or PLL(Ns) nanoparticle dispersion (5 μ L) was applied to a grid (Microgrid Cu200, JEOL, Tokyo) and the solution was removed using filter paper after 1 min. A drop of gadolinium acetate (2.5 w/w%, 5 μ L) was applied for 1 min to negatively stain the sample. Excess staining solution was removed using filter paper and the sample was dried for 15 min. An accelerator voltage of 120 kV was used for TEM.

Microparticles morphologies were examined by scanning electron microscopy (SEM; VE-9800, KEYENCE, Japan) with an accelerator voltage of 1.3 kV. Specimens were prepared by placing the microparticles on an aluminum plate and coating them with an \sim 10-nm-thick platinum thin film under reduced pressure using an MSP-1S ioncoater (Vacuum Device, Ibaraki, Japan).

Nanoparticle inclusions in microparticles were examined by differential scanning calorimetry (DSC). The CRG(CS(Ns), Mb) and CRG(PLL(Ns), Mb) microparticles (5 mg) were placed in a sealed aluminum pan and subjected to DSC at 10°C/min from 0 to 500°C using a differential scanning calorimeter (DSC-60A plus, SHIMADZU, Japan). To examine in detail whether or not nanoparticles are complexed inside the microparticles, I subjected the following samples to DSC: CS(Ns) and PLL(Ns) nanoparticles, CRG(Mb) microparticles, CS, PLL, Mb, Ns, TPP, PEG-*b*-PCL, and κ,ι -CRG (i.e., a physical mixture of κ -CRG and ι -CRG).

The following quantities were determined by spectrofluorometry (FP-6500, JASCO Co., Japan; $\lambda_{\text{ex}} = 273$ nm, $\lambda_{\text{em}} = 324$ nm for Ns $\lambda_{\text{ex}} = 640$ nm, $\lambda_{\text{em}} = 680$ nm for Mb): (1) The encapsulation ratios and encapsulation efficiencies of Ns in the CS(Ns) and PLL(Ns) nanoparticles; (2) the encapsulation ratios and encapsulation efficiencies of Mb in the CRG(CS(Ns), Mb) and CRG(PLL(Ns), Mb) microparticles; (3) the retention ratio and retention efficiency of the CS(Ns) nanoparticles in the CRG(CS(Ns), Mb) microparticles, and (4) the retention ratio and retention efficiency of the PLL(Ns) nanoparticles in the CRG(PLL(Ns), Mb) microparticles.

The encapsulation ratio and encapsulation efficiency were determined using the following equations:

$$\text{Encapsulation ratio [\%]}: \frac{\text{Weight of Ns or Mb in the nanoparticles or microparticles [mg]}}{\text{Weight of the nanoparticles or microparticles [mg]}} \times 100 \quad (1)$$

$$\text{Encapsulation efficiency [\%]}: \frac{\text{Weight of Ns or Mb in the nanoparticles or microparticles [mg]}}{\text{Weight of the Ns or Mb (mg)}} \times 100 \quad (2)$$

The retention ratio and retention efficiency were determined using the following equations:

$$\text{Retention ratio [\%]}: \frac{\text{Weight of the Ns in the microparticles [mg]}}{\text{Microparticle weight [mg]} \times (\text{encapsulation ratio of the Ns in the nanoparticles [\%]})/100} \times 100 \quad (3)$$

$$\text{Retention efficiency [\%]}: \frac{\text{Weight of the Ns in the microparticles [mg]}}{\text{Weight of the Ns [mg]} \times (\text{encapsulation ratio of the Ns in nanoparticles [\%]})/100} \times 100 \quad (4)$$

2.5. Nanoparticle and microparticle Ns- and Mb-release profiles

Profiles depicting the release of Ns and Mb from the nanoparticles and microparticles were constructed using a dialysis method ($n = 3$) according to a previous report^[45]. CS(Ns) or PLL(Ns) nanoparticles (1 mg) were dispersed in phosphate-buffered saline (PBS) solution (1 mL), whereas CRG(CS(Ns), Mb) or CRG(PLL(Ns), Mb) microparticles (3 mg) were dispersed in PBS solution (3 mL). The nanoparticle (1 mL) or microparticle (3 mL) dispersion was dialyzed against PBS solution (39 mL for the nanoparticles and 37 mL for the microparticles) through a Spectra/Por6 dialysis membrane (molecular weight cut-off: 10000; Spectrum Houston, TX, USA). Ns or Mb was released from the nanoparticles and the microparticles in a sustained manner with gentle stirring. Each sample was collected periodically (1 mL/15 min) from the exterior of the dialysis membrane, and the same amount of PBS (1 mL) was added to the solution. Particle-release behavior was evaluated using three temperature patterns: (1) constant at 10°C, (2) constant at 70°C, and (3) ramped from 10°C to 70°C at 1 h after the start of experiment. The following values were determined by spectrofluorometry: (1) the release ratio of the Ns from the CS(Ns) or PLL(Ns) nanoparticles, and (2) the release ratio of Mb from the CRG(CS(Ns), Mb) or CRG(PLL(Ns), Mb) microparticles.

3. Results and discussion

3.1. Preparing and characterizing the CS(Ns) and PLL(Ns) nanoparticles

Controlling the charge states of both molecules in solution is very important when forming CS(Ns) and PLL(Ns) nanoparticles through electrostatic interactions between cationic polymers and TPP. Most of the amino groups of CS are positively charged at around pH 4.43 because its pK_a is approximately 6.5^[23,46], whereas 80% of its amino groups are deprotonated at pH 7.14^[23].

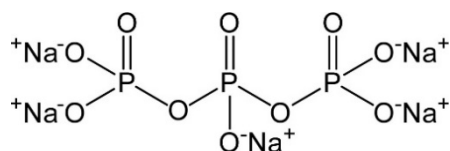


Fig. 4-2 Chemical structure of TPP.

On the other hand, as shown in Fig. 4-2, three of the five phosphate groups of TPP are negatively charged at pH 4–5^[23]. Therefore, CS nanoparticles are formed by electrostatic interactions in acetate buffer solution at pH 5.

In contrast, because PLL has a pK_a of $\sim 10^{[47-50]}$, most of its amino groups are positively charged, even at around pH 7. In addition, because four of the five phosphate groups of TPP are negatively charged at pH 7^[23], TPP interacts electrostatically more strongly with PLL than with CS, resulting in the formation of nanoparticles with stronger structures. However, strong electrostatic PLL/TPP interactions may also progress cross-linking reactions between nanoparticles to form nanoparticle aggregates. Therefore, the pH of the aqueous TPP solution was adjusted to four during particle formation to reduce electrostatic interactions between PLL and TPP and inhibit aggregate formation; the pH was shifted to seven after particle formation to facilitate crosslinking within each nanoparticle.

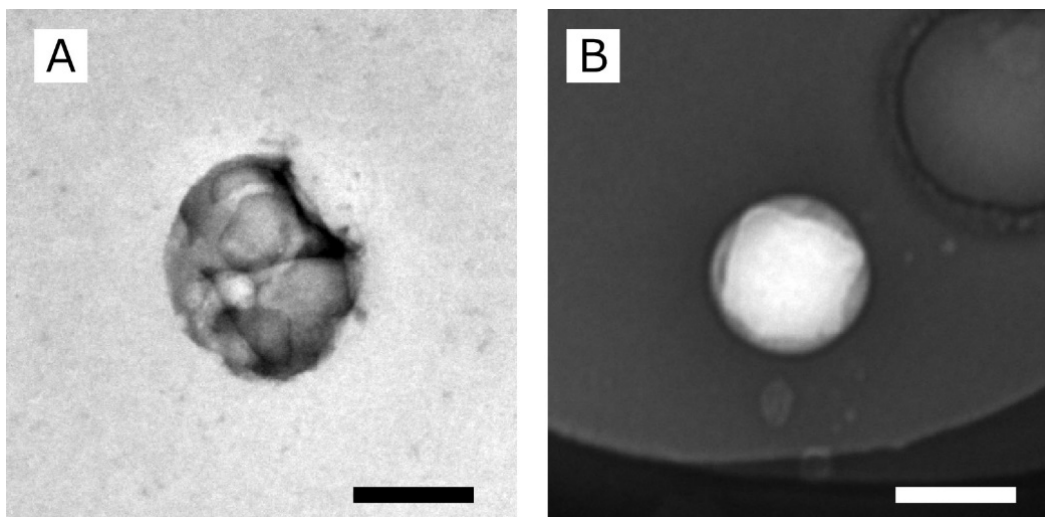


Fig. 4-3 TEM images of the (A) CS(Ns) nanoparticles and (B) PLL(Ns) nanoparticles (bar: 200 nm).

Fig. 4-3 shows TEM images of CS(Ns) and PLL(Ns) nanoparticles. Fig. 4-3 shows that spherical nanoparticles with diameters of 100–200 nm were formed. Aggregates of CS(Ns) nanoparticles were also formed, which is attributable to nanoparticle dialysis with Milli-Q water during nanoparticle preparation; i.e., the solution becomes almost neutral in pH during dialysis, which lowers the positive charge of CS through progressive deprotonation, with nanoparticles finally aggregated through hydrophobic interactions. In contrast, almost no aggregates were observed for the PLL(Ns) nanoparticles, which is possibly due to the fact that PLL is positively charged, even at near neutral pH, which prevents the formation of aggregates through electrostatic repulsion between nanoparticles.

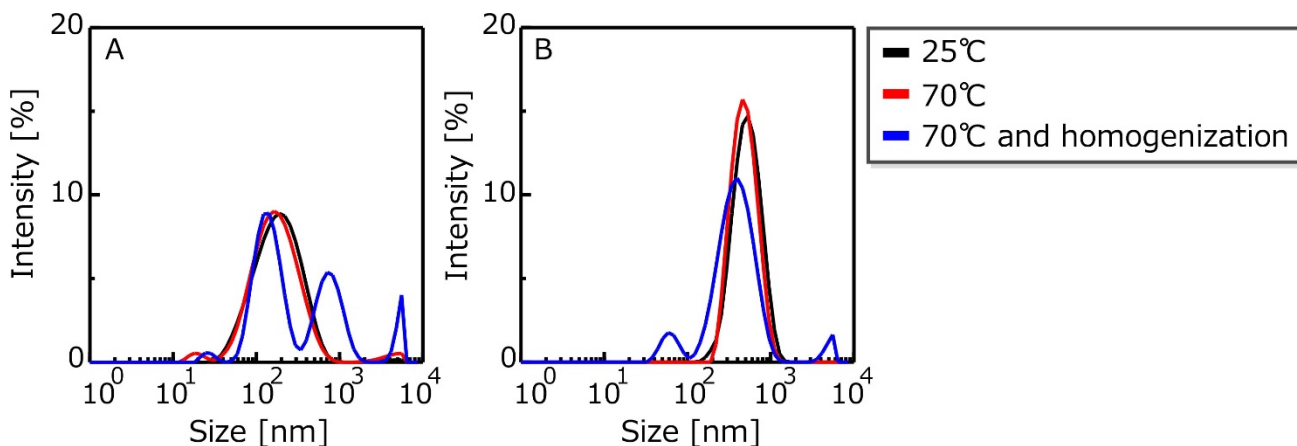


Fig. 4-4 DLS-determined diameter distributions of CS(Ns) and PLL(Ns) nanoparticles: (A) CS(Ns) and (B) PLL(Ns) nanoparticles. Measurement conditions: 25°C (black trace), 70°C (red trace), and 70°C after homogenization at 12,000 rpm for 5 min (blue trace).

Fig. 4-4 shows DLS-determined diameter distributions of CS(Ns) and PLL(Ns) nanoparticles. As shown by DLS, the CS(Ns) and PLL(Ns) nanoparticles are approximately 200 nm and 500 nm in diameter, respectively; both values are larger than those measured by TEM. This difference is attributable to nanoparticle swelling in water, consistent with previous reports that nanoparticles formed from water-soluble polymers swell and increase in size when dispersed in water^[51–53].

To evaluate the effects of temperature and homogenization on the particle state during nanoparticle/microparticle complexation, I also measured particle diameters after heating (70°C) and homogenization (12,000 rpm, 5 min), the results of which are shown in Fig. 4-4. CS(Ns) nanoparticles exhibited almost no change in particle diameter when heated alone, but became larger when heated and homogenized. On the other hand, the average particle diameter of the PLL(Ns) nanoparticles did not change significantly upon heating or homogenization. This difference is attributable to different CS/TPP and PLL/TPP electrostatic interaction strengths; i.e., the PLL(Ns) nanoparticles are more structurally stable than the CS(Ns) nanoparticles, as TPP interacts more strongly with PLL than with CS.

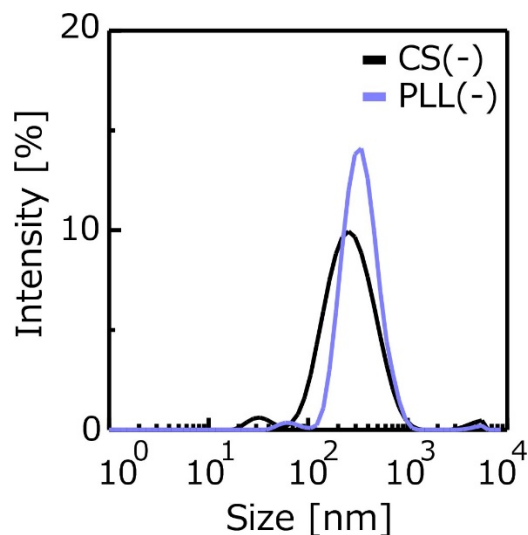


Fig. 4-5 DLS-determined diameter distributions of CS(-) and PLL(-) nanoparticles.

Fig. 4-5 shows DLS-determined diameter distributions of CS(-) and PLL(-) nanoparticles. In the absence of Ns encapsulation, the CS(-) and PLL(-) nanoparticles exhibited average diameters of 150 nm and 300 nm, respectively. As shown in Figs. 4-3 and 4-4, the diameters of the CS(-) nanoparticles increased from 150 nm to 200 nm, while those of the PLL(-) nanoparticles increased from 300 nm to 500 nm upon encapsulating Ns. Nanoparticle size has been reported to depend on the amount of TPP added; in addition, electrostatic interactions between cationic polymers and TPP decrease as the amount of added TPP decreases, resulting in an increase in nanoparticle diameter^[54]. I conclude that, in the present experimental system, the diameters of the obtained nanoparticles increase due to stronger electrostatic interactions between the positively charged polymers and Ns, and concurrent weaker electrostatic interactions with TPP resulting from the encapsulation of negatively charged Ns. In other words, I suggest that nanoparticle size can easily be adjusted by changing the amount of inclusion or TPP added.

3.2. Ns-release profiles for CS(Ns) and PLL(Ns) nanoparticles

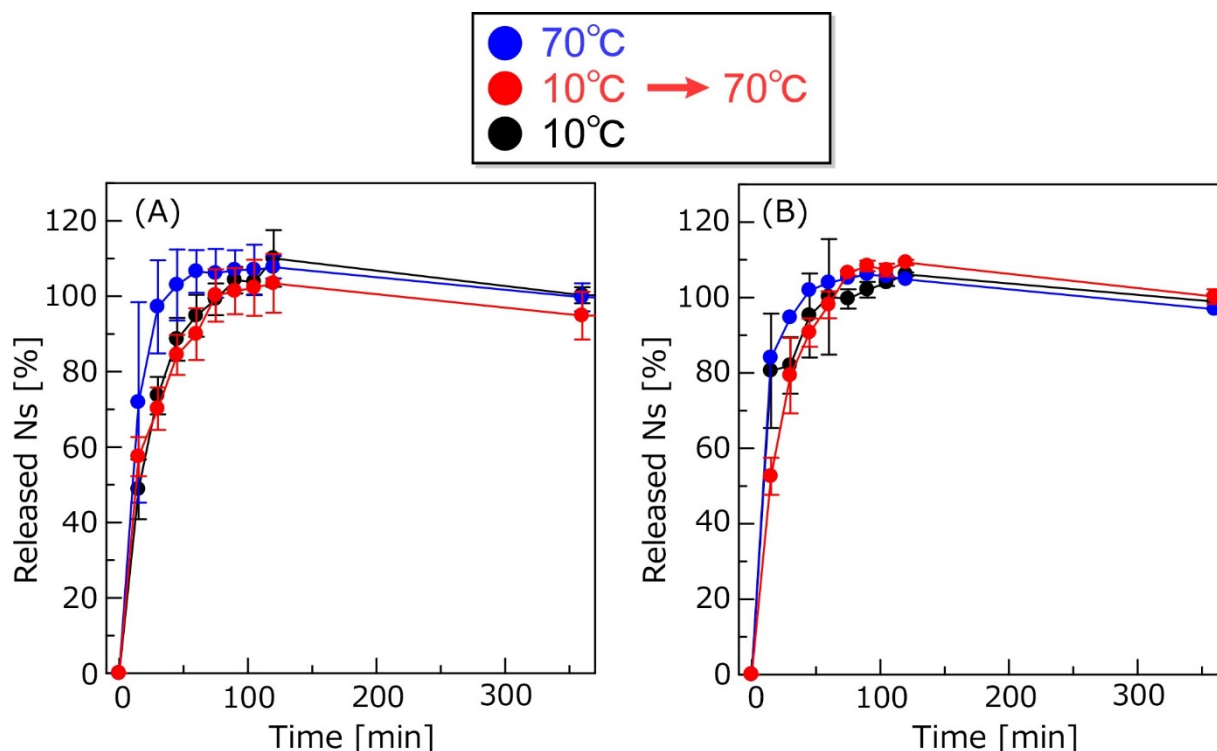


Fig. 4-6 Ns-release profiles of (A) CS(Ns) and (B) PLL(Ns) nanoparticles.

Fig. 4-6 shows Ns-release profiles for the CS(Ns) and PLL(Ns) nanoparticles, which reveals that Ns-release behavior does not significantly depend on the type of cationic polymer. As shown in Fig. 4-6, no significant difference in the release behavior of Ns was observed between cationic polymers; both the CS(Ns) and PLL(Ns) nanoparticles released almost 100% of their inclusions within 1 h, demonstrating that these nanoparticles rapidly release Ns. Furthermore, the CS(Ns) nanoparticle dialysis membrane dispersion became cloudy with further increases in time, while the analogous dispersion remained transparent for the PLL(Ns) nanoparticles.

Table 4-1 Encapsulation ratios and encapsulation efficiencies for Ns in CS(Ns) and PLL(Ns) nanoparticles.

nanoparticles	Encapsulation ratio [%]	Encapsulation efficiency [%]
CS(Ns)	19.6 ± 4.8	33.3 ± 8.1
PLL(Ns)	42.8 ± 5.9	37.2 ± 5.1

Next, I calculated the Ns-nanoparticle encapsulation ratios and encapsulation efficiencies of CS(Ns) and PLL(Ns) (Table 4-1), with encapsulation ratios of $19.6 \pm 4.8\%$ and $42.8 \pm 5.9\%$ obtained, respectively. These results show that the PLL(Ns) nanoparticles encapsulate more Ns than the CS(Ns) nanoparticles, which is attributable to the different cationic properties of CS and PLL; in former, the pH of the CS(Ns) nanoparticle dispersion is close to neutral due to dialysis during the preparation of the nanoparticles, and the amino groups of CS are partially

deprotonated. Therefore, CS and the negatively charged Ns interact weakly, which results in a lower internalization ratio. The encapsulation efficiency does not appear to depend on the type of cationic polymer used to form the nanoparticles, with values of $33.3 \pm 8.1\%$ and $37.2 \pm 5.1\%$ determined for the CS(Ns) and PLL(Ns) nanoparticles, respectively.

3.3. Evaluation of the profile depicting the release of the Ns from the CS(Ns) and PLL(Ns) nanoparticles

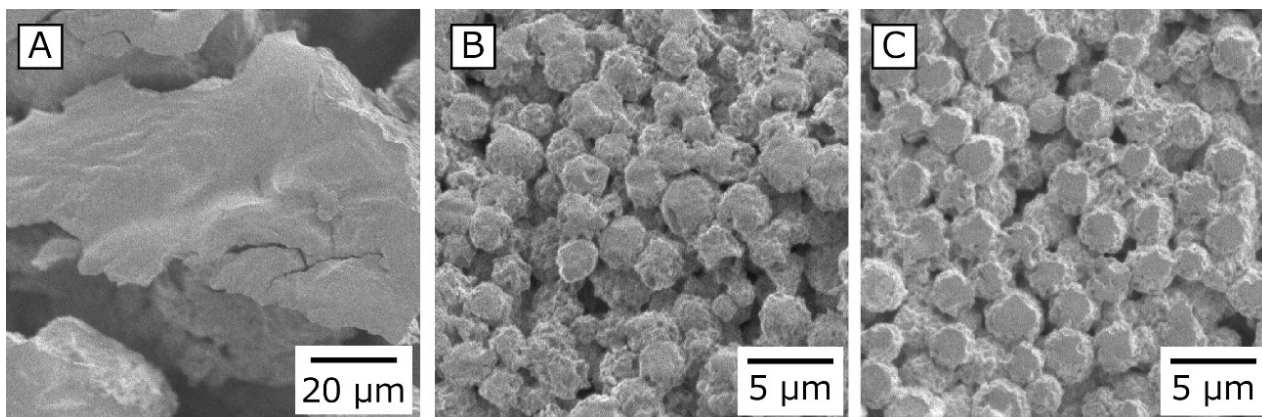


Fig. 4-7 SEM images of (A) the white solid formed from PLL(Ns) nanoparticles devoid of CRG, (B) CRG(CS(Ns), Mb) microparticles, and (C) CRG(PLL(Ns), Mb) microparticles.

Fig. 4-7 shows SEM images of the white solid formed from PLL(Ns) nanoparticles in the absence of CRG, CRG(CS(Ns), Mb) microparticles, and CRG(PLL(Ns), Mb) microparticles. No spherical structures were obtained by cooling the w/o emulsion formed from water in which only PLL(Ns) nanoparticles were dispersed (Fig. 4-4A). However, microparticles several micrometers in diameter were formed when the w/o emulsion prepared using a nanoparticle dispersion in a CRG solution was cooled (Figs. 4-7B and C). I confirmed that these particles were formed by the sol-gel transition of CRG by cooling the w/o emulsion only in the presence of CRG. In addition, the CRG microparticles obtained in chapter 4 exhibit a much rougher surface profile than previously reported CRG microparticles in chapter 2 and 3 formed using a similar emulsion technique, which suggests that the emulsion state in chapter 4 is different from previously reported ones used to prepare microparticles; this difference is possibly ascribable to the formation of a Pickering emulsion in my system.

The following has been reported for Pickering emulsions that coexist with nanoparticles^[55-60]: (1) Nanoparticles act as surfactants when present during the preparation of w/o or o/w emulsions and, in some cases, Pickering emulsions with nanoparticles oriented on the emulsion surface are formed^[55-59]; (2) Pickering emulsions several tens of micrometers in size are formed in the presence of 100–700-nm-diameter nanoparticles^[57,60]; and (3) the diameter of the Pickering emulsion depends on the amount of nanoparticles added, with diameter decreasing with increasing amount of added nanoparticles^[57,60]. Because the CS(Ns) and PLL(Ns) nanoparticles prepared in chapter 4 are 200–500 nm in size, these nanoparticles are possibly oriented near the surfaces of Pickering emulsions when w/o emulsions are formed from nanoparticle dispersions in aqueous CRG solution. In particular, the PEG-b-PCL (a

polymeric surfactant) used to form the emulsions in chapter 4 is likely to increase Pickering emulsion stability. The rough surfaces of the resulting particles are ascribable to nanoparticles present on the surfaces of the CRG particles formed from the Pickering emulsion. Particles with rough surfaces have been reported to be more easily delivered to deep lung sites (such as the alveoli) than smooth particles^[61-63]. The rough microparticles obtained in chapter 4 are expected to be useful drug carriers for pulmonary drug-delivery applications.

3.4. Inclusions of nanoparticles in microparticles

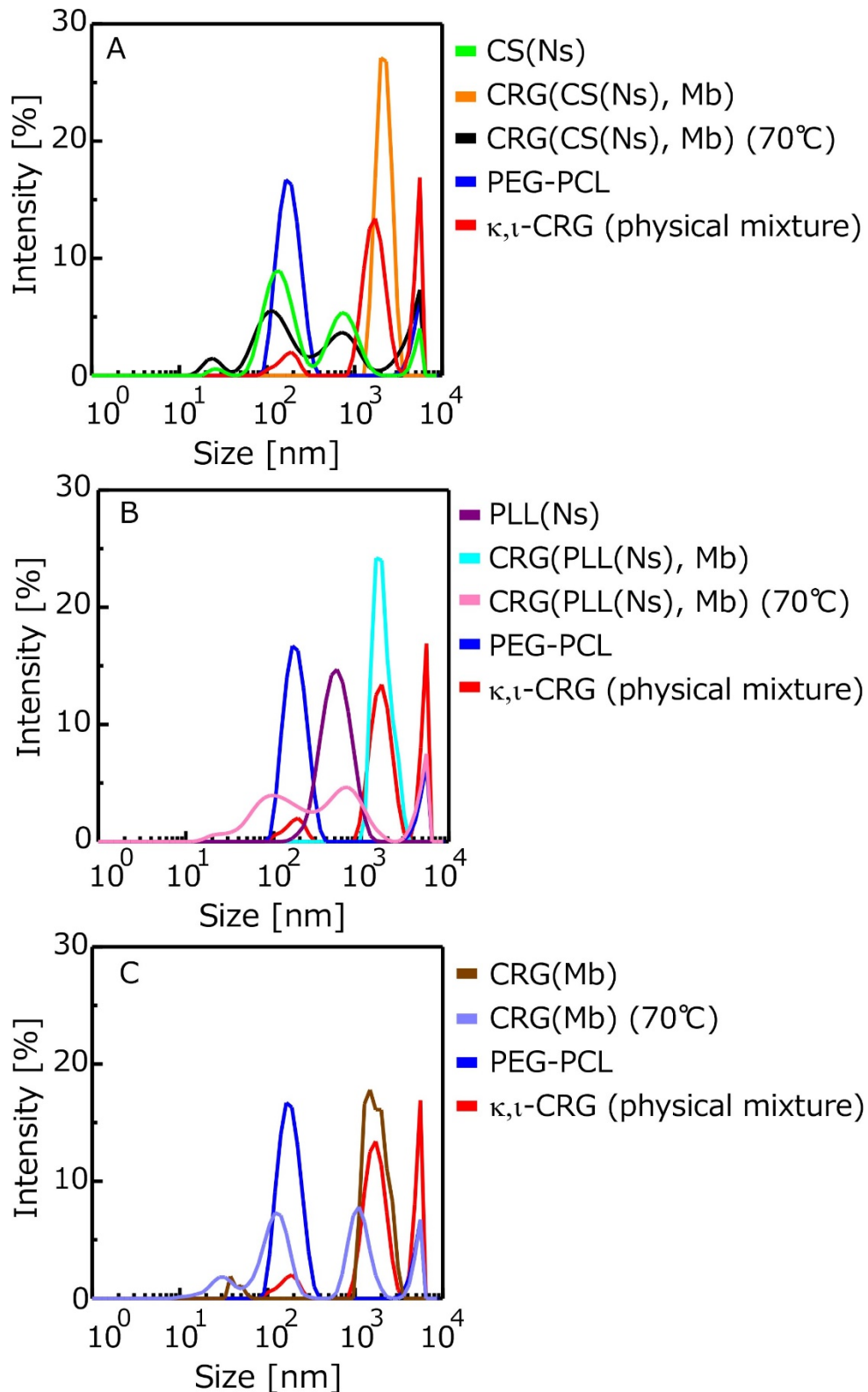


Fig. 4-8 DLS-determined diameter distributions of (A) CRG(CS(Ns), Mb) and (B) CRG(PLL(Ns), Mb) (C) CRG(Mb) microparticles. DLS data for CS (Ns) and PLL(Ns) nanoparticles, PEG-PCL, and a κ,ι-CRG (physical mixture of κ-CRG and ι-CRG) are also shown for comparison.

Fig. 4-8 shows DLS data for microparticle dispersions prior to heating, after heating (70°C), a PEG-PCL dispersion, an aqueous κ,ι -CRG (i.e., a physical mixture of κ -CRG and ι -CRG) solution, and a nanoparticle dispersion, which reveals that the microparticles have significantly different diameters before and after heating. The CRG(CS(Ns), Mb) microparticles (Fig. 4-8A) show a unimodal peak at 2 μm (orange trace), whereas three peaks at 100 nm, 600 nm, and 9 μm are observed after heating (black trace). Three situations are depicted in Fig. 4-8A: (1) PEG-PCL does not completely dissolve when dispersed in water and forms structures 100–200 nm in diameter (blue trace); (2) CS(Ns) nanoparticles form aggregates with diameters of approximately 600 nm when heated and homogenized (green trace), as shown in Fig. 4-4A; and (3) CRG precipitates and forms structures several micrometers in diameter after the particles are collapsed by heat, since CRG is insoluble in water at 25°C (red trace). Based on these three situations, multiple peaks, which are not observed for the pre-heated CRG(CS(Ns), Mb) microparticles, are obtained after heating, and are attributable to PEG-PCL, CS(Ns) nanoparticles (and their aggregates), and CRG. I conclude that, despite the lack of homogenization after heating, the CS(Ns) nanoparticles aggregate due to the presence of anionic polysaccharides. These results strongly suggest that CS(Ns) nanoparticles are complexed inside the CRG(CS(Ns), Mb) microparticles because a peak corresponding to the CS(Ns) nanoparticles was observed for the heated CRG(CS(Ns), Mb) microparticles.

In comparison, the PLL(CS(Ns), Mb) microparticles (Fig. 4-8B) exhibit a unimodal peak at approximately 2 μm (light blue trace), and three peaks at 100 nm, 500 nm, and 9 μm (pink trace) in a similar manner to the CRG(CS(Ns), Mb) microparticles. The peaks near 100 nm and above 9 μm are believed to be derived from structures formed by PEG-PCL and CRG precipitates, while the peak at around 500 nm agrees well with the particle-size distribution of the PLL(Ns) nanoparticles (purple trace). These results strongly suggest that PLL(Ns) nanoparticles are complexed inside the CRG(PLL(Ns), Mb) microparticles.

Furthermore, the CRG(Mb) microparticles (Fig. 4-8C) exhibit a unimodal peak at approximately 2 μm (brown trace) at approximately 2 μm , and three peaks at 100 nm, 1 μm , and 9 μm (ultramarine trace). The peaks near 100 nm, 1 μm , and above 9 μm are believed to be derived from structures formed by PEG-PCL and CRG precipitates. The diameter distribution of the nanoparticles was obtained only when the nanoparticles were contained in the microparticles. This result will assist that the nanoparticles are complexed inside microparticles.

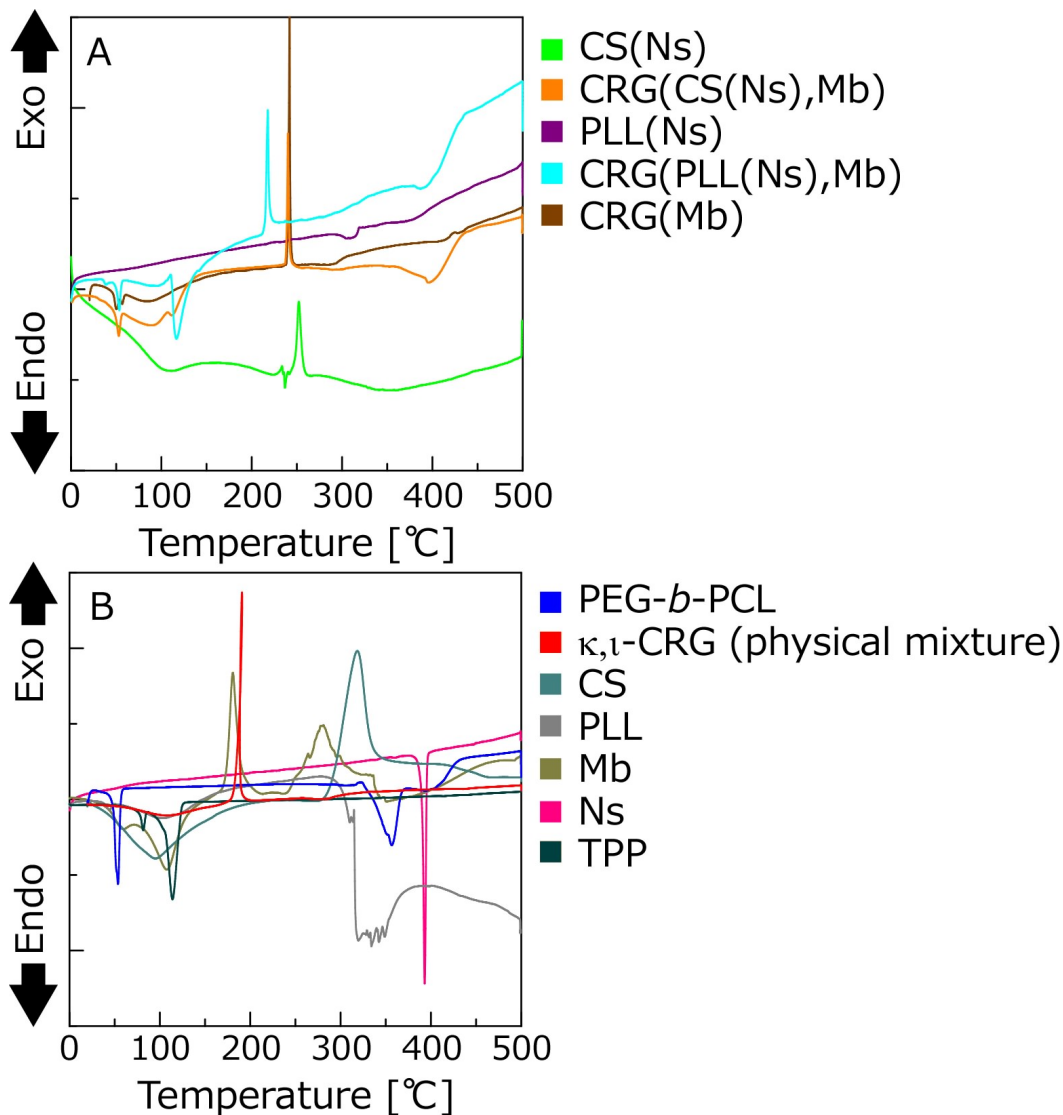


Fig. 4-9 DSC thermograms (0–500°C) of (A) particles and (B) molecules that form particles and molecules encapsulated in particles.

Fig. 4-9 shows the thermal behavior of the particles, particle-forming agents, and inclusions evaluated by DSC, with nanoparticle and microparticle data summarized in Fig. 4-9A, while those of the other molecules are shown in Fig. 4-9B. Fig. 4-9A reveals that the CRG(CS(Ns), Mb), CRG(PLL(Ns), Mb), and CRG(Mb) microparticles exhibit endothermic peaks at ~55°C and exothermic peaks at 220°C or 240°C. Furthermore, the CRG(CS(Ns), Mb) and CRG(PLL(Ns), Mb) microparticles show minor endothermic peaks at approximately 400°C. On the other hand, the CS(Ns) nanoparticles exhibit an exothermic peak at 250°C, while PLL(Ns) nanoparticles show a minor endothermic peak at approximately 300°C. Fig. 4-9B also shows that PEG-PCL is associated with endothermic peaks at 55°C and 350°C, κ, ι -CRG shows an exothermic peak at 200°C, CS has an exothermic peak at 300°C, PLL exhibits an endothermic peak at ~300°C, Mb has exothermic peaks at 200°C and 300°C, Ns has an endothermic peak at 400°C, and TPP is associated with endothermic peaks at 90°C and 120°C.

The CS(Ns) and PLL(Ns) nanoparticles do not exhibit endothermic peaks derived from Ns (~400°C),

suggesting that Ns is uniformly dispersed inside the nanoparticles; however, the microparticles composited with these nanoparticles exhibit a minor endothermic peak around 400°C, which suggests that a small amount of Ns is released from the nanoparticles and form local microcrystals during microparticle preparation.

The exothermic peak corresponding to the CRG particles is shifted to a higher temperature than that of the physical mixture of CRGs, indicating that CRG is more thermally stabilized by particle formation, which is ascribable nanoparticle internalization and the Mb inside the CRG microparticles. Pure CS has been reported to have an exothermic peak at approximately 300°C, while pure PLL has an endothermic peak at approximately 300°C^[64]. The exothermic peak reportedly shifts to a higher temperature when CS and PLL are mixed with CRG, which is ascribable to electrostatic interactions between the cationic polymers and CRG^[65,66]. Furthermore, Mb exhibits an exothermic peak at approximately 280°C and is more thermally stable than CRG. Therefore, both nanoparticle complexation and electrostatic interactions between Mb and CRG possibly reduce the free volume of CRG and limit polymer-chain mobility, thereby improving the thermal stability of CRG. Furthermore, an endothermic peak associated with the evaporation of the water retained by each material was observed at approximately 100°C. Taken together, the data in Figs. 4-8 and 4-9 show that microparticles several micrometers in diameter can be prepared by the emulsion technique while controlling the sol-gel transition of CRG.

3.5. *Ns- and Mb-release profiles of CRG(CS(Ns), Mb) and CRG(PLL(Ns), Mb) microparticles*

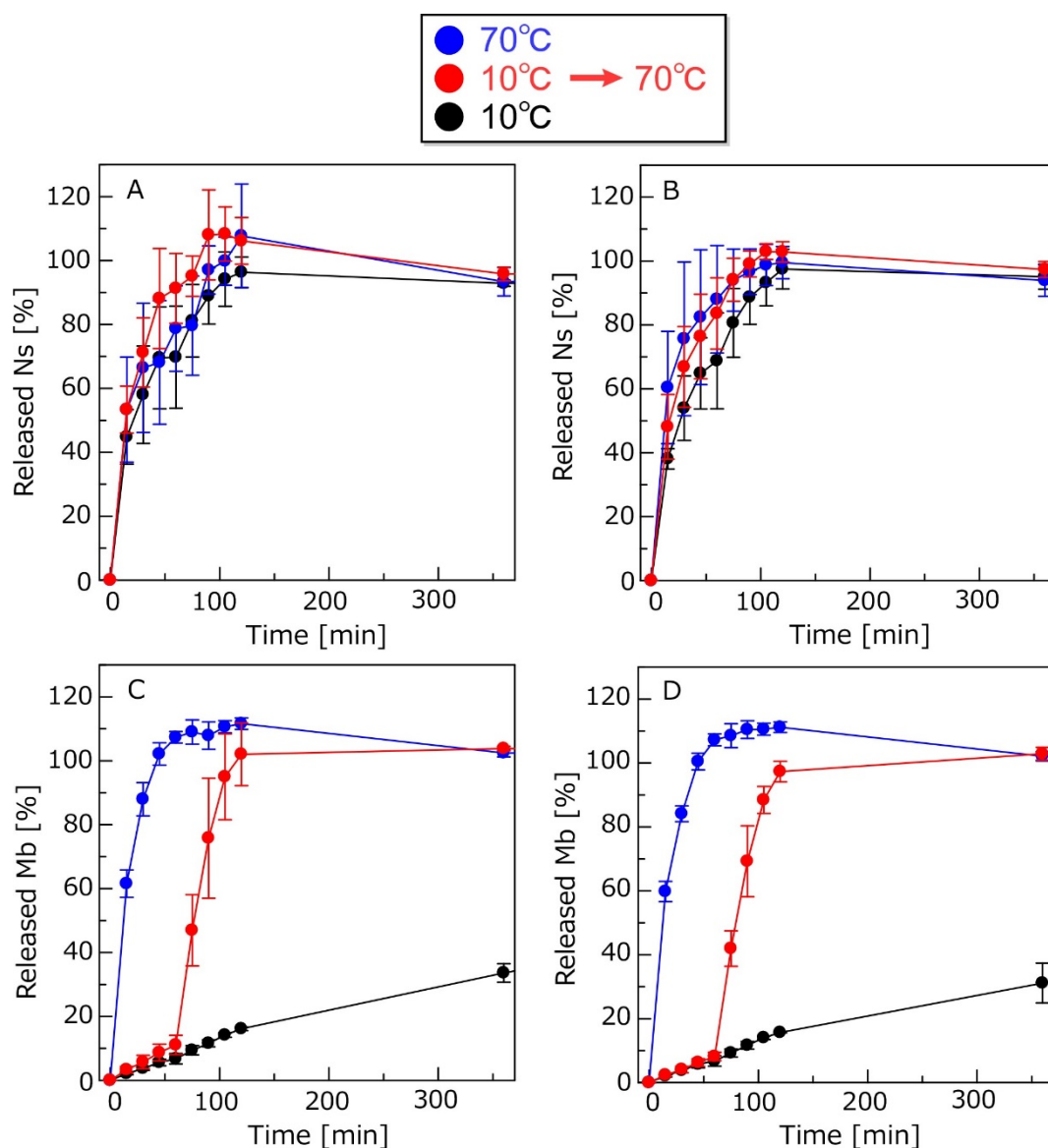


Fig. 4-10 (A, B) Ns- and (C, D) Mb-release profiles of (A, C) CRG(CS(Ns), Mb) and (B, D) CRG(PLL(Ns), Mb) microparticles.

Fig. 4-10 shows profiles depicting the release of Ns and Mb from the CRG(CS(Ns), Mb) and CRG(PLL(Ns), Mb) microparticles. Approximately 80% of its Ns was released by the CRG(CS(Ns), Mb) microparticles at 60 min, while the CRG(PLL(Ns), Mb) microparticles released almost 100% at 120 min; both release profiles were found to be temperature-independent (Figs. 4-10A and B). Nanoparticle complexation within the microparticles results in a slightly reduced Ns-release ratio because the nanoparticles release almost all of their Ns in 60 min (Fig. 4-6). Consistent with the data in Fig. 4-7, it is highly likely that the nanoparticles act as surfactants to form Pickering emulsions during microparticle preparation. The frequency of contact between the expanded solvent and the

nanoparticles is higher because many nanoparticles are present at the microparticle surfaces in a Pickering emulsion; hence, Ns is released from the microparticles by diffusion in a temperature-independent manner (Fig. 4-6) and both types of microparticle show almost the same release behavior (Figs. 4-10A and B). On the other hand, the release of Mb dispersed within the microparticles was temperature-responsive (Figs. 4-10C and D), which suggests that Mb is uniformly distributed inside the CRG particles and interacts electrostatically with the sulfate groups of CRG, thereby suppressing its release by diffusion.

Table 4-2 Retention ratios and retention efficiencies for CS(Ns) and PLL(Ns) nanoparticles inside CRG(CS(Ns), Mb) and CRG(PLL(Ns), Mb) microparticles

Microparticle	Nanoparticle	Retention ratio [%]	Retention efficiency [%]
CRG(CS(Ns), Mb)	CS(Ns)	0.31 ± 0.03	51.6 ± 10.1
CRG(PLL(Ns), Mb)	PLL(Ns)	0.087 ± 0.04	60.8 ± 11.0

Table 4-3 Encapsulation ratios and encapsulation efficiencies of the Mb inside CRG(CS(Ns), Mb) and CRG(PLL(Ns), Mb) microparticles

Microparticle	Encapsulation ratio [%]	Encapsulation efficiency [%]
CRG(CS(Ns), Mb)	0.49 ± 0.04	15.6 ± 2.5
CRG(PLL(Ns), Mb)	0.44 ± 0.01	13.7 ± 0.69

Next, I determined the retention ratios and retention efficiencies of CS(Ns) and PLL(Ns) nanoparticles within the CRG(CS(Ns), Mb) and CRG(PLL(Ns), Mb) microparticles (Table 4-2), as well as the encapsulation ratios and encapsulation efficiencies of Mb within the microparticles (Table 4-3). The type of encapsulated nanoparticle was found to have little effect on the retention ratios and retention efficiencies of the nanoparticles within the microparticles, nor did it affect the retention ratios and retention efficiencies of the compounds within the microparticles. The nanoparticles were also found to complex more efficiently with the negatively charged microparticles, despite the nanoparticles and Mb both being positively charged, which is attributable to the formation of Pickering emulsions, polymer-chain entanglement, and electrostatic interactions during microparticle complexation. In other words, interactions between the cationic nanoparticles and the anionic CRG, the formation of Pickering emulsions (i.e., nanoparticle accumulation on the emulsion surface layers), and the entanglement of CRS chains resulting from the sol-gel transition inhibit nanoparticle release from the microparticles that, consequently, result in highly efficient nanoparticle/microparticle complexation.

These results reveal that the nanoparticle-“decorated” polysaccharide microparticles prepared in chapter 4 are capable of releasing two differently charged compounds in a stepwise manner (Fig. 4-11), although the observed release behavior is different from that assumed at the start of chapter 4 (Fig. 4-1).

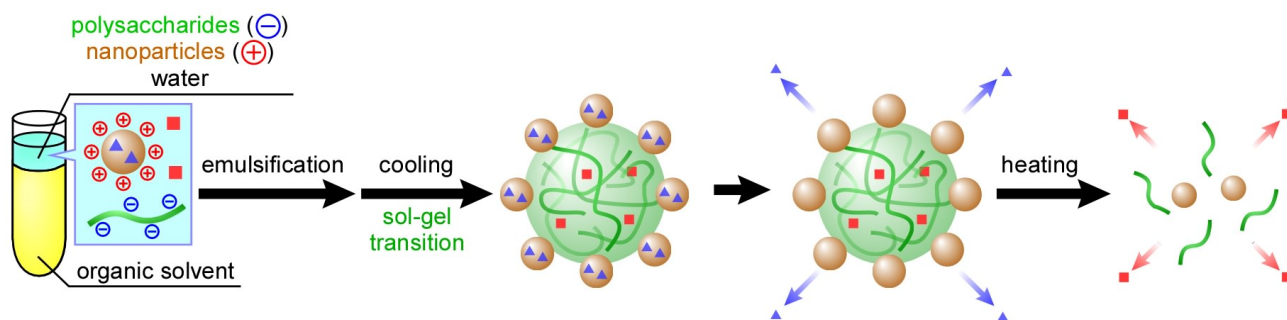


Fig. 4-11 Release behavior of temperature-responsive nanoparticle-decorated polysaccharide microparticles based on the experimental results of chapter 4.

4. Conclusion

In chapter 4, I developed nanoparticle-containing polysaccharide microparticles for the temperature-responsive and two-step release of inclusions. CS nanoparticles, PLL nanoparticles, and CRG microparticles separately complexed with both nanoparticles were prepared and evaluated mainly for the abilities of the nanoparticles to be included in the microparticles, and the effect of the type of cationic polymer on nanoparticle and microparticle release behavior. Nanoparticle/microparticle complexation was confirmed by DSL and DSC. The nanoparticles release their inclusions rapidly in a manner that is independent of the type of cationic polymer and temperature. On the other hand, inclusions within the nanoparticles on the microparticle surfaces are released first, after which microparticle inclusions are released through microparticle collapse, which reveals that the microparticles prepared by this method are capable of releasing two differently charged compounds in two steps, although the release behavior is different from that originally assumed. Because the microparticles developed in chapter 4 have rough surfaces that are suitable for delivery to the lungs, they are expected to efficiently deliver nanoparticles deep into the lungs and release a wide range of compounds in a charge-independent manner. In other words, these particles are expected to be used as temperature-responsive drug carriers for pulmonary administration and the controlled release of multiple drugs.

The major challenge for the future involves including nanoparticles within microparticles rather than on their surfaces. The same process as that used in chapter 4 is expected to result in the formation of nanoparticles, even when various other polymers are used, such as polyethyleneimine (pK_a : 7.0) and polyarginine (pK_a : 12.0). Nanoparticle hydrophilicity in solution can be adjusted significantly by judiciously choosing a polymer with the required pK_a [67–69]. Increasing nanoparticle hydrophilicity or increasing the amount of nanoparticles and surfactants is expected to disperse the nanoparticles into the emulsion; this approach should afford microparticles that exhibit two-step release behavior, in which the microparticles collapse in response to temperature, followed by nanoparticle release and subsequent release of their inclusions. In addition, there are few reports on the formation of Pickering emulsions that use mixtures of polymeric surfactants and nanoparticles. However, highly structurally stable few-micrometer-diameter emulsions are easily prepared using polymeric surfactants together with nanoparticles, as described in chapter 4. These results are expected to be useful for future material designs that use emulsions as the base technology.

5. Refelence

- [1] Cho, H., Lai, T. C., Tomoda, K., Kwon, G. S., Polymeric Micelles for Multi-Drug Delivery in Cancer., *AAPS PharmSciTech*, **16**, 10–20, (2014)
- [2] Kanakubo, Y., Ito, F., Murakami, Y., Novel one-pot facile technique for preparing nanoparticles modified with hydrophilic polymers on the surface via block polymer-assisted emulsification/evaporation process., *Colloids Surfaces B Biointerfaces*, **78**, 85–91, (2010)
- [3] Subramanian, S. B., Francis, A. P., Devasena, T., Chitosan-starch nanocomposite particles as a drug carrier for the delivery of bis-desmethoxy curcumin analog., *Carbohydr. Polym.*, **114**, 170–178, (2014)
- [4] Yuan, Q., Shah, J., Hein, S., Misra, R. D. K., Controlled and extended drug release behavior of chitosan-based nanoparticle carrier., *Acta Biomater.*, **6**, 1140–1148, (2010)
- [5] Ikem, V. O., Menner, A., Bismarck, A., High internal phase emulsions stabilized solely by functionalized silica particles., *Angew. Chemie - Int. Ed.*, **47**, 8277–8279, (2008)
- [6] Frelichowska, J., Bolzinger, M. A., Valour, J. P., Mouaziz, H., Pelletier, J., Chevalier, Y., Pickering w/o emulsions: Drug release and topical delivery., *Int. J. Pharm.*, **368**, 7–15, (2009)
- [7] Caprifico, A. E., Foot, P. J. S., Polycarpou, E., Calabrese, G., Overcoming the protein corona in chitosan-based nanoparticles., *Drug Discov. Today*, **26**, 1825–1840, (2021)
- [8] Zohri, M., Arefian, E., Akbari Javar, H., Gazori, T., Aghae-Bakhtiari, S. H., Taheri, M., Fatahi, Y., Azadi, A., Khoshayand, M. R., Ghahremani, M. H., Potential of chitosan/alginate nanoparticles as a non-viral vector for gene delivery: Formulation and optimization using D-optimal design., *Mater. Sci. Eng. C*, **128**, 112262, (2021)
- [9] Zhang, Y., Huang, Y., Li, S., Polymeric micelles: Nanocarriers for cancer-targeted drug delivery., *AAPS PharmSciTech*, **15**, 862–871, (2014)
- [10] Tam, Y. Y. C., Chen, S., Cullis, P. R., Advances in lipid nanoparticles for siRNA delivery., *Pharmaceutics*, **5**, 498–507, (2013)
- [11] Mukhopadhyay, P., Mishra, R., Rana, D., Kundu, P. P., Strategies for effective oral insulin delivery with modified chitosan nanoparticles: A review., *Prog. Polym. Sci.*, **37**, 1457–1475, (2012)
- [12] Cheng, H., Cui, Z., Guo, S., Zhang, X., Huo, Y., Mao, S., Mucoadhesive versus Mucopenetrating nanoparticles for oral delivery of insulin., *Acta Biomater.*, (2021), doi:10.1016/j.actbio.2021.08.046
- [13] Chen, J., Hessler, J. A., Putchakayala, K., Panama, B. K., Khan, D. P., Hong, S., Mullen, D. G., DiMaggio, S. C., Som, A., Tew, G. N., *et al.*, Cationic nanoparticles induce nanoscale disruption in living cell plasma membranes., *J. Phys. Chem. B*, **113**, 11179–11185, (2009)
- [14] Yim, H., Park, S. jung, Bae, Y. H., Na, K., Biodegradable cationic nanoparticles loaded with an anticancer drug for deep penetration of heterogeneous tumours., *Biomaterials*, **34**, 7674–7682, (2013)
- [15] Bilensoy, E., Cationic nanoparticles for cancer therapy., *Expert Opin. Drug Deliv.*, **7**, 795–809, (2010)
- [16] Samal, S. K., Dash, M., Vlierberghe, S. Van, Kaplan, D. L., Chiellini, E., Blitterswijk, C. van, Moroni, L., Dubruel, P., Cationic polymers and their therapeutic potential., *Chem. Soc. Rev.*, **41**, 7147–7194, (2012)
- [17] Patil, N. A., Kandasubramanian, B., Functionalized polylysine biomaterials for advanced medical applications: A review., *Eur. Polym. J.*, **146**, 110248, (2021)

- [18] Yuan, J., Guo, L., Wang, S., Liu, D., Qin, X., Zheng, L., Tian, C., Han, X., Chen, R., Yin, R., Preparation of self-assembled nanoparticles of ϵ -polylysine-sodium alginate: A sustained-release carrier for antigen delivery., *Colloids Surfaces B Biointerfaces*, **171**, 406–412, (2018)
- [19] Divya, K., Jisha, M. S., Chitosan nanoparticles preparation and applications., *Environ. Chem. Lett.*, **16**, 101–112, (2018)
- [20] Zargar, V., Asghari, M., Dashti, A., A Review on Chitin and Chitosan Polymers: Structure, Chemistry, Solubility, Derivatives, and Applications., *ChemBioEng Rev.*, **2**, 204–226, (2015)
- [21] Jin, H., Yu, Y., Chrisler, W. B., Xiong, Y., Hu, D., Lei, C., Delivery of microRNA-10b with polylysine nanoparticles for inhibition of breast cancer cell wound healing., *Breast Cancer Basic Clin. Res.*, **5**, 9–19, (2011)
- [22] Fàbregas, A., Miñarro, M., García-Montoya, E., Pérez-Lozano, P., Carrillo, C., Sarrate, R., Sánchez, N., Ticó, J. R., Suñé-Negre, J. M., Impact of physical parameters on particle size and reaction yield when using the ionic gelation method to obtain cationic polymeric chitosan-tripolyphosphate nanoparticles., *Int. J. Pharm.*, **446**, 199–204, (2013)
- [23] Mazancová, P., Némethová, V., Trešová, D., Kleščíková, L., Lacík, I., Rázga, F., Dissociation of chitosan/tripolyphosphate complexes into separate components upon pH elevation., *Carbohydr. Polym.*, **192**, 104–110, (2018)
- [24] Antoniou, J., Liu, F., Majeed, H., Qi, J., Yokoyama, W., Zhong, F., Physicochemical and morphological properties of size-controlled chitosan-tripolyphosphate nanoparticles., *Colloids Surfaces A Physicochem. Eng. Asp.*, **465**, 137–146, (2015)
- [25] Rashidipour, M., Rasoulían, B., Maleki, A., Davari, B., Pajouhi, N., Mohammadi, E., Pectin/chitosan/tripolyphosphate encapsulation protects the rat lung from fibrosis and apoptosis induced by paraquat inhalation., *Pestic. Biochem. Physiol.*, **178**, 104919, (2021)
- [26] Agazzi, M. L., Herrera, S. E., Cortez, M. L., Marmisollé, W. A., Azzaroni, O., Self-assembled peptide dendrigraft supraparticles with potential application in pH/enzyme-triggered multistage drug release., *Colloids Surfaces B Biointerfaces*, **190**, 110895, (2020)
- [27] KOSURI, B. S., Study of Polylysine and Chitosan nanoparticles synthesized using various cross-linkers and their applications for heavy metal ion recovery., (2016)
- [28] Loira-Pastoriza, C., Todoroff, J., Vanbever, R., Delivery strategies for sustained drug release in the lungs., *Adv. Drug Deliv. Rev.*, **75**, 81–91, (2014)
- [29] d'Angelo, I., Conte, C., La Rotonda, M. I., Miro, A., Quaglia, F., Ungaro, F., Improving the efficacy of inhaled drugs in cystic fibrosis: Challenges and emerging drug delivery strategies., *Adv. Drug Deliv. Rev.*, **75**, 92–111, (2014)
- [30] Takeuchi, I., Tetsuka, Y., Nii, T., Shinogase, M., Makino, K., Inhalable nanocomposite particles using amino acids with improved drug content and humidity resistance., *Colloids Surfaces A Physicochem. Eng. Asp.*, **529**, 387–393, (2017)
- [31] Al-Qadi, S., Taboada, P., Remuñán-López, C., Micro/nanostructured inhalable formulation based on polysaccharides: Effect of a thermoprotectant on powder properties and protein integrity., *Int. J. Pharm.*, **551**, 23–33, (2018)

- [32] Okuda, T., Okamoto, H., Present situation and future progress of inhaled lung cancer therapy: Necessity of inhaled formulations with drug delivery functions., *Chem. Pharm. Bull.*, **68**, 589–602, (2020)
- [33] Seo, J., Lee, C., Hwang, H. S., Kim, B., Thao, L. Q., Lee, E. S., Oh, K. T., Lim, J. L., Choi, H. G., Youn, Y. S., Therapeutic advantage of inhaled tacrolimus-bound albumin nanoparticles in a bleomycin-induced pulmonary fibrosis mouse model., *Pulm. Pharmacol. Ther.*, **36**, 53–61, (2016)
- [34] Wall, D. A., Pulmonary absorption of peptides and proteins., *Drug Deliv.*, **2**, 1–20, (1995)
- [35] Pilcer, G., Amighi, K., Formulation strategy and use of excipients in pulmonary drug delivery., *Int. J. Pharm.*, **392**, 1–19, (2010)
- [36] Agu, R. U., Ugwoke, M. I., Armand, M., Kinget, R., Verbeke, N., The lung as a route for systemic delivery of therapeutic proteins and peptides., *Respir. Res.*, **2**, 198–209, (2001)
- [37] Patton, J. S., Byron, P. R., Inhaling medicines: Delivering drugs to the body through the lungs., *Nat. Rev. Drug Discov.*, **6**, 67–74, (2007)
- [38] Yang, Y., Bajaj, N., Xu, P., Ohn, K., Tsifansky, M. D., Yeo, Y., Development of highly porous large PLGA microparticles for pulmonary drug delivery., *Biomaterials*, **30**, 1947–1953, (2009)
- [39] Ou, C., Hang, J., Deng, Q., Particle deposition in human lung airways: Effects of airflow, particle size, and mechanisms., *Aerosol Air Qual. Res.*, **20**, 2846–2858, (2020)
- [40] Anzai, R., Takami, T., Uchida, Y., Murakami, Y., Poly(ϵ -caprolactone) (PCL) hybrid sheets containing polymeric micelles: Effects of inner structures on the material properties of the sheets., *Mater. Sci. Eng. C*, **72**, 325–331, (2017)
- [41] Anzai, R., Murakami, Y., Poly(ϵ -caprolactone) (PCL)-polymeric micelle hybrid sheets for the incorporation and release of hydrophilic proteins., *Colloids Surfaces B Biointerfaces*, **127**, 292–299, (2015)
- [42] Anandhakumar, S., Krishnamoorthy, G., Ramkumar, K. M., Raichur, A. M., Preparation of collagen peptide functionalized chitosan nanoparticles by ionic gelation method: An effective carrier system for encapsulation and release of doxorubicin for cancer drug delivery., *Mater. Sci. Eng. C*, **70**, 378–385, (2017)
- [43] Dyer, A. M., Hinchcliffe, M., Watts, P., Castile, J., Jabbal-Gill, I., Nankervis, R., Smith, A., Illum, L., Nasal delivery of insulin using novel chitosan based formulations: A comparative study in two animal models between simple chitosan formulations and chitosan nanoparticles., *Pharm. Res.*, **19**, 998–1008, (2002)
- [44] Morris, G. A., Castile, J., Smith, A., Adams, G. G., Harding, S. E., The effect of prolonged storage at different temperatures on the particle size distribution of tripolyphosphate (TPP)-chitosan nanoparticles., *Carbohydr. Polym.*, **84**, 1430–1434, (2011)
- [45] Ito, T., Takami, T., Uchida, Y., Murakami, Y., Chitosan gel sheet containing drug carriers with controllable drug-release properties., *Colloids Surfaces B Biointerfaces*, **163**, 257–265, (2018)
- [46] Wang, Q. Z., Chen, X. G., Liu, N., Wang, S. X., Liu, C. S., Meng, X. H., Liu, C. G., Protonation constants of chitosan with different molecular weight and degree of deacetylation., *Carbohydr. Polym.*, **65**, 194–201, (2006)
- [47] Eckenrode, H. M., Dai, H. L., Nonlinear optical probe of biopolymer adsorption on colloidal particle surface: Poly-L-lysine on polystyrene sulfate microspheres., *Langmuir*, **20**, 9202–9209, (2004)
- [48] Dos, A., Schimming, V., Tosoni, S., Limbach, H., Acid-Base Interactions and Secondary Structures of Poly-L-Lysine Probed by ^{15}N and ^{13}C Solid State NMR and., 15604–15615, (2008)

- [49] Volodkin, D., Ball, V., Schaaf, P., Voegel, J. C., Mohwald, H., Complexation of phosphocholine liposomes with polylysine. Stabilization by surface coverage versus aggregation., *Biochim. Biophys. Acta - Biomembr.*, **1768**, 280–290, (2007)
- [50] Grigsby, J. J., Blanch, H. W., Prausnitz, J. M., Effect of secondary structure on the potential of mean force for poly-L-lysine in the α -helix and β -sheet conformations., *Biophys. Chem.*, **99**, 107–116, (2002)
- [51] Akrami-Hasan-Kohal, M., Eskandari, M., Solouk, A., Silk fibroin hydrogel/dexamethasone sodium phosphate loaded chitosan nanoparticles as a potential drug delivery system., *Colloids Surfaces B Biointerfaces*, **205**, 111892, (2021)
- [52] Mahobia, S., Bajpai, J., Bajpai, A. K., An in-vitro investigation of swelling controlled delivery of insulin from egg albumin nanocarriers., *Iran. J. Pharm. Res.*, **15**, 695–711, (2016)
- [53] Bajpai, A. K., Choubey, J., Design of gelatin nanoparticles as swelling controlled delivery system for chloroquine phosphate., *J. Mater. Sci. Mater. Med.*, **17**, 345–358, (2006)
- [54] Pan, C., Qian, J., Zhao, C., Yang, H., Zhao, X., Guo, H., Study on the relationship between crosslinking degree and properties of TPP crosslinked chitosan nanoparticles., *Carbohydr. Polym.*, **241**, 116349, (2020)
- [55] Aveyard, R., Binks, B. P., Clint, J. H., Emulsions stabilised solely by colloidal particles Robert., *Adv. Colloid Interface Sci.*, **100–102**, 503–546, (2003)
- [56] Larson-Smith, K., Pozzo, D. C., Pickering emulsions stabilized by nanoparticle surfactants., *Langmuir*, **28**, 11725–11732, (2012)
- [57] Mao, Q., Li, M., Zhang, S., Zhang, X., He, G., Zhang, W., Chitosan-hydrophobic alginate nanocomposites stabilized pH-triggered Pickering emulsion for drug controlled-release., *Int. J. Biol. Macromol.*, **162**, 1888–1896, (2020)
- [58] Alison, L., Rühls, P. A., Tervoort, E., Teleki, A., Zanini, M., Isa, L., Studart, A. R., Pickering and Network Stabilization of Biocompatible Emulsions Using Chitosan-Modified Silica Nanoparticles., *Langmuir*, **32**, 13446–13457, (2016)
- [59] Ikem, V. O., Menner, A., Bismarck, A., Norman, L. R., Liquid screen: A novel method to produce an in-situ gravel pack., *SPE J.*, **19**, 437–442, (2014)
- [60] Ge, S., Xiong, L., Li, M., Liu, J., Yang, J., Chang, R., Liang, C., Sun, Q., Characterizations of Pickering emulsions stabilized by starch nanoparticles: Influence of starch variety and particle size., *Food Chem.*, **234**, 339–347, (2017)
- [61] Nishimura, S., Takami, T., Murakami, Y., Porous PLGA microparticles formed by “one-step” emulsification for pulmonary drug delivery: The surface morphology and the aerodynamic properties., *Colloids Surfaces B Biointerfaces*, **159**, 318–326, (2017)
- [62] Kawashima, Y., Serigano, T., Hino, T., Yamamoto, H., Takeuchi, H., Effect of surface morphology of carrier lactose on dry powder inhalation property of pranlukast hydrate., *Int. J. Pharm.*, **172**, 179–188, (1998)
- [63] Hassan, M. S., Lau, R., Inhalation performance of pollen-shape carrier in dry powder formulation: Effect of size and surface morphology., *Int. J. Pharm.*, **413**, 93–102, (2011)
- [64] Liang, C., Yuan, F., Liu, F., Wang, Y., Gao, Y., Structure and antimicrobial mechanism of ϵ -polylysine-chitosan conjugates through Maillard reaction., *Int. J. Biol. Macromol.*, **70**, 427–434, (2014)

- [65] Li, T., Wen, C., Dong, Y., Li, D., Liu, M., Wang, Z., Janaswamy, S., Zhu, B., Song, S., Effect of ϵ -polylysine addition on κ -carrageenan gel properties: Rheology, water mobility, thermal stability and microstructure., *Food Hydrocoll.*, **95**, 212–218, (2019)
- [66] Deka, C., Dutta, M., Deka, D., Jha, D. K., Kakati, K., Study of olive oil-loaded chitosan / carrageenan coacervate and its antibacterial property., **6**, 1524–1533, (2016)
- [67] Fitch, C. A., Platzer, G., Okon, M., Garcia-Moreno, B. E., McIntosh, L. P., Arginine: Its pKa value revisited., *Protein Sci.*, **24**, 752–761, (2015)
- [68] Curtis, K. A., Miller, D., Millard, P., Basu, S., Horkay, F., Chandran, P. L., Unusual salt and pH induced changes in polyethylenimine solutions., *PLoS One*, **11**, 1–20, (2016)
- [69] Von Harpe, A., Petersen, H., Li, Y., Kissel, T., Characterization of commercially available and synthesized polyethylenimines for gene delivery., *J. Control. Release*, **69**, 309–322, (2000)

Chapter 5

General conclusion of this thesis

This doctoral thesis is a study to develop temperature-responsive particles for pulmonary administration. The pulmonary administration method has been focused as the next generation of administration method with high therapeutic efficacy at home. In chapter 1, drug administration methods and drug carriers are introduced, and a novel drug carrier is proposed.

There are a variety of drug-administration methods, including oral, intravenous, and transdermal administrations, and it is important to select methods that are appropriate for the patient's condition and situation. In recent years, much attention has been paid to pulmonary administration, i.e., the administration method by which drugs are delivered to the lungs. The method has many advantages, three of which are highly prominent: (1) a simple administration (inhalation), (2) highly efficient absorption due to both an enormous surface area (100 m²) and a highly permeable membrane (0.1–1 μm in thickness) in alveoli, and (3) no denaturation owing to the absence of digestive enzymes in the alveoli. Despite these advantages of pulmonary administration, it is difficult to deliver only drugs to the deep lungs. In all medications, administration of only the drugs causes side effects due to drug denaturation, rapid increase in local concentration, and inability to deliver the drug to the target site. Recent studies have tried to encapsulate the drug in a polymeric drug carrier for delivery. The drug carriers used in the pulmonary administration need to satisfy the following four conditions for the delivery of drugs to alveoli: (1) an aerodynamic ability to reach alveoli, (2) biocompatibility and ability to avoid the immune system, (3) proper control of the size of the carriers (1–5 μm in an aerodynamic diameter), and (4) rapid release of drugs. Among drug carriers, stimuli-responsive carriers rapidly change the microstructure of the carrier in response to stimuli from the external environment, releasing the drug. To date, drug carriers that respond to stimuli such as pH, light, and temperature have been developed. Carrageenan (CRG), a linear sulfated polysaccharide that is extracted from red algae seaweed, is an anionic natural polymer in which 3,6-anhydro-D-galactose alternately repeats α-1,3 and β-1,4 glycosidic linkages. Depending on the number of sulfone groups and the presence or absence of an anhydro bond, CRG falls into one of three classes: κ, ι, and λ. Co-existing metal salts and proteins greatly affect the physical properties of CRG. Furthermore, novel physical properties of CRG become manifest when the polymer is mixed with other polysaccharides. These properties have made CRG a widely popular component of gelling, thickening, and stabilizing agents in the food and medical industries. In addition, aqueous solutions of polysaccharides form a gel at appropriate temperatures (sol-gel transition), where a coil-helix transition occurs and a subsequent aggregation of helices forms physically crosslinked domains.

I propose to develop "temperature-responsive microparticles" that rapidly release drugs in the body by an emulsion technique utilizing the sol-gel transition phenomenon of polysaccharide. By emulsifying an organic solvent

in which a surfactant is dissolved and an aqueous polysaccharide solution, a w/o emulsion is formed. When the resulted w/o emulsion is cooled, the polysaccharide performs the sol-gel transition and gel particles are formed. The resulted gel particles are then dried to form microparticles. Thus, the CRG microparticles to be developed (1) are simple to administer, (2) are fast-acting drug carriers that respond to body temperature and release drugs, and (3) have a high potential advantage in urgent diseases such as seizures and abnormal increases of blood glucose levels. As aging populations around the world grow, the CRG microparticles will be the next generation of drug carriers that can be administered by patients themselves to provide highly effective home treatment.

In chapter 2, I have prepared temperature-responsive polysaccharide particles for pulmonary administration. I found that highly stable s/o suspensions were formed regardless of the HLB value, structure, and composition of the surfactants when high-molecular-weight surfactants were used. There are two possible important factors affecting the formation of spherical κ -CRG particles: (1) the formation of physically crosslinked domains inside the particle by means of the increase of concentrations of polysaccharides and cations and (2) the formation of a stable solid-liquid interfaces by using high-molecular-weight surfactants. I obtained stable polysaccharide particles with dimpled surfaces. In addition, the diameter of the microparticles depends on the emulsification rate and emulsification time, so the microparticles with diameters suitable for pulmonary administration are prepared. From the results of my DLS measurement, laser diffraction measurements, and optical microscope observations, the κ -CRG particles in chapter 2 exhibited temperature responsiveness to collapse at 52°C. Furthermore, as a result of the *in vitro* aerosol dispersion performance of the κ -CRG particles with the cascade impactor, I identified the characteristic delivery behavior of κ -CRG particles: the particles delivered more to the alveoli than to the pharynx and bronchi, despite their high density. From the perspective of material design, the present study shows that the “dimpled” κ -CRG particles can likely stay in the alveoli so that high therapeutic effects will likely occur in pulmonary administration.

In chapter 3, I aimed to develop polysaccharide microparticles that release their inclusions in response to temperature. I mainly investigated the effects of the type and composition of polymeric surfactants and particle-forming polysaccharides on the dissolution behavior of the particles. Although the composition of PEG-PCL did not affect its melting point, the melting point of PEG-PLA changed significantly depending on the molecular weight of PEG. The dissolution temperature of the particles prepared using PEG-PLA decreased depending on its melting point, indicating that the dissolution temperature of the particles could be arbitrarily controlled by controlling the hydrogen bonding forces between PEG-PLA and CRG. Furthermore, in the case of the particles prepared by mixing κ -CRG and ι -CRG, the diffusion-dependent release of inclusions was suppressed below the dissolution temperature of the particles, and the inclusions were rapidly released immediately after the temperature was increased. The results indicate the possibility that the prepared particles can penetrate deep into lung tissues and release their inclusions at body temperature without the need for heating. These results suggest that the particles can be applied as drug carriers for pulmonary administration with high therapeutic efficacy for the urgent treatment of seizures and abnormal increases in blood glucose levels.

In chapter 4, I developed nanoparticle-containing polysaccharide microparticles for the temperature-responsive and two-step release of inclusions. CS nanoparticles, PLL nanoparticles, and CRG microparticles separately complexed with both nanoparticles were prepared and evaluated mainly for the abilities of the nanoparticles to be included in the microparticles, and the effect of the type of cationic polymer on nanoparticle and

microparticle release behavior. Nanoparticle/microparticle complexation was confirmed by DSL and DSC. The nanoparticles release their inclusions rapidly in a manner that is independent of the type of cationic polymer and temperature. On the other hand, inclusions within the nanoparticles on the microparticle surfaces are released first, after which microparticle inclusions are released through microparticle collapse, which reveals that the microparticles prepared by this method are capable of releasing two differently charged compounds in two steps, although the release behavior is different from that originally assumed. Because the microparticles developed in chapter 4 have rough surfaces that are suitable for delivery to the lungs, they are expected to efficiently deliver nanoparticles deep into the lungs and release a wide range of compounds in a charge-independent manner. In other words, these particles are expected to be used as temperature-responsive drug carriers for pulmonary administration and the controlled release of multiple drugs.

The major challenge for the future involves including nanoparticles within microparticles rather than on their surfaces. The same process as that used in chapter 4 is expected to result in the formation of nanoparticles, even when various other polymers are used, such as polyethyleneimine (pK_a : 7.0) and polyarginine (pK_a : 12.0). Nanoparticle hydrophilicity in solution can be adjusted significantly by judiciously choosing a polymer with the required pK_a . Increasing nanoparticle hydrophilicity or increasing the amount of nanoparticles and surfactants is expected to disperse the nanoparticles into the emulsion; this approach should afford microparticles that exhibit two-step release behavior, in which the microparticles collapse in response to temperature, followed by nanoparticle release and subsequent release of their inclusions. In addition, there are few reports on the formation of Pickering emulsions that use mixtures of polymeric surfactants and nanoparticles. However, highly structurally stable few-micrometer-diameter emulsions are easily prepared using polymeric surfactants together with nanoparticles, as described in this paper. These results are expected to be useful for future material designs that use emulsions as the base technology.

Acknowledgement

I would like to express my gratitude to many people for their help in conducting this research and writing this doctoral dissertation.

I would like to express my gratitude to my main supervisor, Professor Yoshihiko Murakami, for his guidance in all aspects of my research, including the concept of this study, experimental design, and basic experimental techniques. Thanks to his ardent guidance, I was able to write this doctoral thesis and academic paper. I would like to express my deepest gratitude to him.

I would also like to express my gratitude to Professor Hiromu Saito for lending me experimental equipment and advising me on the results of my research, and also for being an associate referee for my doctoral thesis. I would like to express my deepest gratitude to him.

In writing this doctoral thesis, I would also like to thank my associate referees, Prof. Toshiyuki Watanabe, Prof. Takeshi Shimomura, and Associate Prof. Koji Nakano, for their many comments and suggestions for further development of this research. I would like to express my gratitude to all of them

I would like to express my gratitude to all the members of Murakami Laboratory. I am grateful to all the members, including my seniors who gave me advice on my experiments and befriended me not only in my experiments but also in my private life, and my classmates and juniors who worked hard together to improve our research. I would like to express my gratitude to all of them. I am especially grateful to Dr. Nishimura. He gave me advice on experiments, experimental techniques, and taught me not only experiments but also how to write texts and make presentations, as we worked on the same genre of "particles". I would like to express my deepest gratitude to him for his kindness and support.

I would like to thank my family. I have received financial and living support for my research life. Thanks to their support, I was able to lead a fruitful research life. I would like to express my deepest gratitude.

Finally, I would like to express my gratitude again to all the people who have helped me in carrying out this research.

December 2022

Takumi SATO